

LA-4307-MS

CIC-14 REPORT COLLECTION  
**REPRODUCTION  
COPY**

C-3

**LOS ALAMOS SCIENTIFIC LABORATORY**  
of the  
**University of California**  
LOS ALAMOS • NEW MEXICO

Quarterly Status Report on the  
**Advanced Plutonium Fuels Program**  
July 1 to September 30, 1969



UNITED STATES  
ATOMIC ENERGY COMMISSION  
CONTRACT W-7405-ENG 36

## LEGAL NOTICE

This report was prepared as an account of Government sponsored work. Neither the United States, nor the Commission, nor any person acting on behalf of the Commission:

A. Makes any warranty or representation, expressed or implied, with respect to the accuracy, completeness, or usefulness of the information contained in this report, or that the use of any information, apparatus, method, or process disclosed in this report may not infringe privately owned rights; or

B. Assumes any liabilities with respect to the use of, or for damages resulting from the use of any information, apparatus, method, or process disclosed in this report.

As used in the above, "person acting on behalf of the Commission" includes any employee or contractor of the Commission, or employee of such contractor, to the extent that such employee or contractor of the Commission, or employee of such contractor prepares, disseminates, or provides access to, any information pursuant to his employment or contract with the Commission, or his employment with such contractor.

This LA. . MS report presents the status of the LASL Advanced Plutonium Fuels Program. Previous Quarterly Status Reports in this series, all unclassified, are:

LA-3607-MS	LA-3760-MS*	LA-4073-MS
LA-3650-MS	LA-3820-MS	LA-4114-MS
LA-3686-MS	LA-3880-MS	LA-4193-MS
LA-3708-MS*	LA-3933-MS	LA-4284-MS
LA-3745-MS	LA-3993-MS	

This report, like other special-purpose documents in the LA. . MS series, has not been reviewed or verified for accuracy in the interest of prompt distribution.

Distributed: November 12, 1969

LA-4307-MS  
SPECIAL DISTRIBUTION

**LOS ALAMOS SCIENTIFIC LABORATORY**  
of the  
**University of California**  
LOS ALAMOS • NEW MEXICO

Quarterly Status Report on the  
**Advanced Plutonium Fuels Program**  
July 1 to September 30, 1969



## FOREWORD

This is the thirteenth quarterly report on the Advanced Plutonium Fuels Program at the Los Alamos Scientific Laboratory.

Studies on Fast Reactor Metallic Fuels, formerly reported as Project 461 in this series of documents, have been discontinued except for phase-out effort. Any results from the final work will be described under Project 467, a new work category covering all irradiation experiments [chiefly those concerned with (U,Pu)C fuels].

Most of the investigations discussed here are of the continuing type. Results and conclusions described may therefore be changed or augmented as the work continues. Published reference to results cited in this report should not be made without obtaining explicit permission to do so from the person in charge of the work.

TABLE OF CONTENTS

<u>PROJECT</u>	<u>PAGE</u>
401 EXAMINATION OF FAST REACTOR FUELS	5
I. Introduction	5
II. Equipment Development	5
III. DP West Facility	8
IV. Methods of Analysis	9
V. Examination of Unirradiated Fuels	10
VI. Requests from DRDT	10
VII. Papers Presented	11
462 SODIUM TECHNOLOGY	12
I. Introduction	12
II. Study and Design of Precipitation Devices	12
III. Sampling and Analysis	15
IV. Projects Being Phased Out	16
References	19
463 CERAMIC PLUTONIUM FUEL MATERIALS	20
I. Introduction	20
II. Synthesis and Fabrication	20
III. Properties	20
IV. Analytical Chemistry	28
V. References	29
464 STUDIES OF Na-BONDED (U,Pu)C LMFBR FUELS	30
I. Introduction	30
II. Synthesis and Fabrication of Fuel Pellets	30
III. Loading Facility for Test Capsules	31
IV. Carbide Fuel Compatibility Studies	32
V. Sodium-Bond Heat Transfer Studies	36
VI. Analytical Chemistry	38
VII. References	39
465 REACTOR PHYSICS	40
I. Introduction	40
II. Cross-Section Procurement, Evaluation, and Testing	40
III. Reactor Analysis Methods and Concept Evaluation	42
References	51
467 FUEL IRRADIATION EXPERIMENTS	52
I. Introduction	52
II. EBR-II Irradiation Testing	52
III. Thermal Irradiations of Sodium-Bonded Mixed Carbides	53
IV. Thermal Irradiations of Sodium-Bonded U-Pu-Zr	53
V. References	56
471 OTHER ADVANCED SYSTEMS - RESEARCH AND DEVELOPMENT	58
I. Measurement of Delayed Gamma-Ray Yields	58
II. Codes	58
References	60

TABLE OF CONTENTS  
(continued)

<u>PROJECT</u>	<u>PAGE</u>
501 STANDARDS, QUALITY CONTROL, AND INSPECTION OF PRODUCTS	62
I. Introduction	62
II. FFTF Analytical Chemistry Program	62
III. Investigation of Methods	62
IV. References	65
SPECIAL DISTRIBUTION	66

## PROJECT 401

### EXAMINATION OF FAST REACTOR FUELS

Person in Charge: R. D. Baker  
Principal Investigators: J. W. Schulte  
J. A. Leary  
C. F. Metz

---

#### I. INTRODUCTION

This project is directed toward the examination and comparison of the effects of neutron irradiation on LMFBR Program fuel materials. Unirradiated and irradiated materials will be examined as requested by the Fuels and Materials Branch of DRDT. Capabilities are established for providing conventional pre-irradiation and post-irradiation examinations. Additional capabilities include less conventional properties measurements which are needed to provide a sound basis for steady-state operation of fast reactor fuel elements, and for safety analysis under transient conditions.

Analytical chemistry methods that have been modified and mechanized for hot cell manipulators will continue to be applied to the characterization of irradiated fuels. The shielded electron microprobe and emission spectrographic facilities will be used in macro and micro examinations of various fuels and clads. In addition, new capabilities will be developed with emphasis on gamma scanning and analyses to assess spatial distribution of fuel and fission products.

High temperature properties of unirradiated LMFBR fuel materials are now being determined by Contractor in an associated project (ident. no. 07463). Equipment designs and interpretive experience gained in this project are being extended to provide unique capabilities such as differential thermal analysis, melting point determination, high temperature dilatometry, and high temperature heat content and heat of fusion for use on irradiated materials.

#### II. EQUIPMENT DEVELOPMENT

##### A. Inert Atmosphere Systems (C. E. Frantz, J. M. Ledbetter, R. F. Velkinburg)

###### System for Metallography Cells

A recirculating Ar purification system was installed to provide high purity atmosphere for the two alpha boxes (where metallographic specimens are prepared) and the blister (where the metallograph is located). This work included installation of the plumbing, wiring, absolute filters, pressure control system, manifold system for Ar-H<sub>2</sub> regenerant gas, sampling system for moisture and O<sub>2</sub>, and connections for the Ar purge system. Special seals were made around the metallograph in the blister to provide this area with three options: recirculating Ar when the alpha seal window is in place; single pass Ar without the alpha seal window; and regular room air without the alpha seal window.

Difficulty with the second set of solenoid control valves has required that the purification system be shut down until a more reliable type is procured and installed. During this period a single pass Ar supply is being used.

Initial, short-duration tests with the purifier indicated that it is possible to attain atmospheres with < 50 ppm O<sub>2</sub> and < 20 ppm H<sub>2</sub>O.

###### System for Disassembly Box

The absorbent chemicals in the purifier for the disassembly box were replaced when it was apparent that they could not be regenerated. It is suspected that the

absorbents were poisoned by oil from the pressure relief safety device. This device has been replaced to obviate recurrence of this problem.

Performance tests on this system will be continued in the near future. It was necessary to use a single pass Ar atmosphere in the disassembly box to maintain the schedule set for preparing the tube burst test specimens for BNWL.

#### Installation of High Pressure Tank System

A design was started to provide a high pressure Ar supply by installing a tank-trailer adjacent to the Hot Cell Facility. Argon from this source would be used for purging, as a back-up for the two recirculating systems, and as a single pass system when it was suspected that fumes from chemical etchants or solvents might be deleterious to chemical absorbents.

#### B. In-Cell Equipment

(J. H. Bender, G. R. Brewer, D. B. Court, E. L. Ekberg, F. J. Fitzgibbon, C. E. Frantz, D. D. Jeffries, M. E. Lazarus, J. M. Ledbetter, C. D. Montgomery, T. Romanik, T. J. Romero, A. E. Tafoya, J. R. Trujillo, R. F. Velkinburg, L. A. Waldschmidt)

The majority of effort during this quarter was directed toward completing the new metallography facility. In addition to installing the capability for an inert atmosphere, many other improvements have been added which should lead to the preparation and examination of specimens at an increased rate. Hot operations were begun on September 25.

Some of the specialized equipment which has been installed in the new boxes is listed below.

Material Transfer Systems: In addition to the transfer systems employing the 7-in. and 18-in. diam ports, other systems were devised and installed which also do not violate the "alpha seal" principle. Improvements were made in the transfer methods between the metallographic cells and blister.

Sphincter Pass-Throughs: These pass-throughs permit the transfer of cold material into the box from the operating area, and the discharge of empty containers and other materials with low beta-gamma contamination levels into a plastic bag located in the basement. The sealing mechanisms rely on 12 tapered neoprene washers

in series and spaced 1/4 in. apart. Plastic containers, which are 10 in. long and slightly larger in diameter than the inside diameter of the neoprene washers, are used to introduce supplies to the box. These containers serve as not only the carrier but also as the seal plug within the washers. A means has been provided for filling the containers with Ar prior to being passed into the box, thus minimizing the introduction of O<sub>2</sub> and H<sub>2</sub>O impurities.

Bag-Out Port: The blister, housing the metallograph, was provided with a conventional bag-out port system and removable shield. This device permits the rapid removal of alpha and beta-gamma autoradiographs, replicas, and other samples having a low radiation level. The radiation from the samples is first surveyed through the port hole before removing the samples.

Intercell Transfer Systems: For transfers between the two metallographic cells and between these cells and the blister, a newly designed system was installed. This system employs large vacuum-tight valves for isolating the three boxes for inert atmosphere control. Motorized conveyors are used for movement of material between boxes. The system is also equipped with controls and safety interlocks.

Grinding-Polishing Equipment: A modified Unipol grinder-polisher is the basic component of this system. Custom designed hold-down clamps, with adjustable loading force, are incorporated along with special fluid delivery lines and an effluent collector system (see Figure 401-1). There are three of these units in each of the two metallographic preparation boxes. Two Syntron vibratory polishers are installed in the polishing box (see Figure 401-2). This equipment can be removed remotely from the alpha box for maintenance or modification utilizing the master-slave manipulators, a small overhead mono-rail hoist within the alpha box, and the 18-in. transfer system.

Specimen Loading-Unloading Fixture: A tool has been designed, fabricated, tested and is in use for loading and unloading the metallography specimens from the three multiple-hole (4, 5 and 6) specimen holders used in grinding and polishing (see Figure 401-3). This fixture is readily operable using the manipulators and can either be

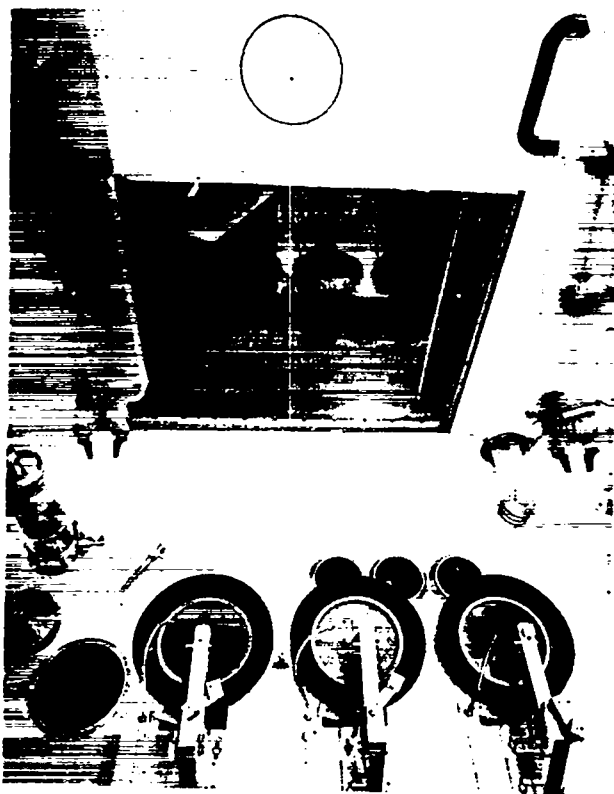


Fig. 401-1. View of Unipol Machines and Other Equipment in Metallographic Preparation (Grinding) Box.

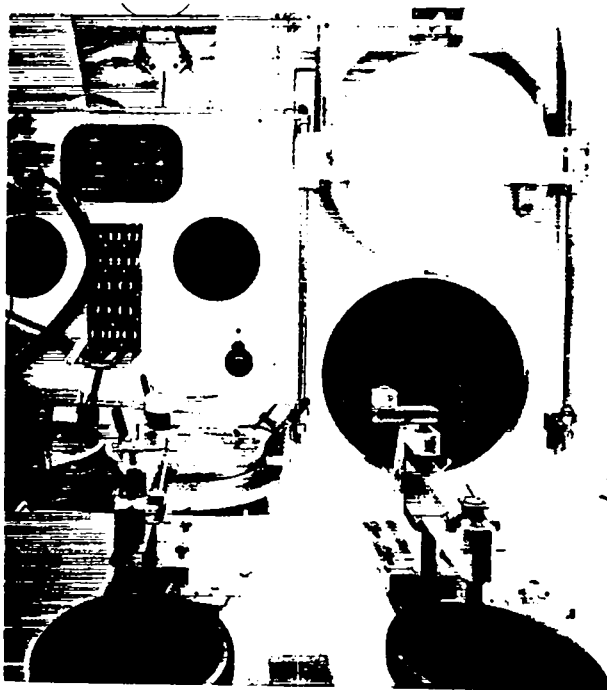


Fig. 401-2. View of Unipol and Synttron Units in Metallographic Preparation (Polishing) Box.

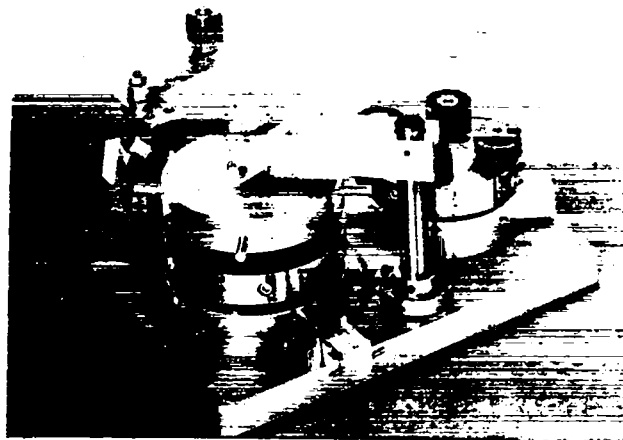


Fig. 401-3. Loading-Unloading Fixture for Metallographic Specimens.

set aside in the alpha box when not in use or removed from the box for maintenance using the 18-in. transfer system. Special components to accommodate the hole configurations of the holders are filed on wall racks within the box.

Camera System for Macro-Photography: A special camera system was designed and built incorporating a through-the-shield-wall camera, Pb shield, viewing port, reflector, specimen positioner, strobe light and an optical data block method for identification of negatives. This system is in use to provide high resolution photographs of metallographic specimens still in the multiple-specimen holders.

Other Equipment: A device has been built to compact into one-gallon cans the cell waste materials, such as grinding-polishing cloths and papers. The purpose of the compactor system is to decrease the number of time-consuming transfer and bagging operations on waste material from the metallographic cells.

Equipment for vacuum mounting of metallographic specimens was re-installed and found to be operationally acceptable.

Equipment for the "dismounting" of specimens from epoxy using the hot oil technique was also provided in the new boxes.

A device for the remote encapsulation in an inert atmosphere of fuel segments (or other material) which are

intended for shipment or long-term storage has been installed and successfully used. The device, as shown in Figure 401-4, relies on mechanically crimping a pre-formed and "tinned" stainless steel tube around a "tinned" oap. A resistance heating element is then used to melt the Aladdin 450 soft silver solder to effect a vacuum-tight seal. This equipment has been used in preparing 35 closures thus far.

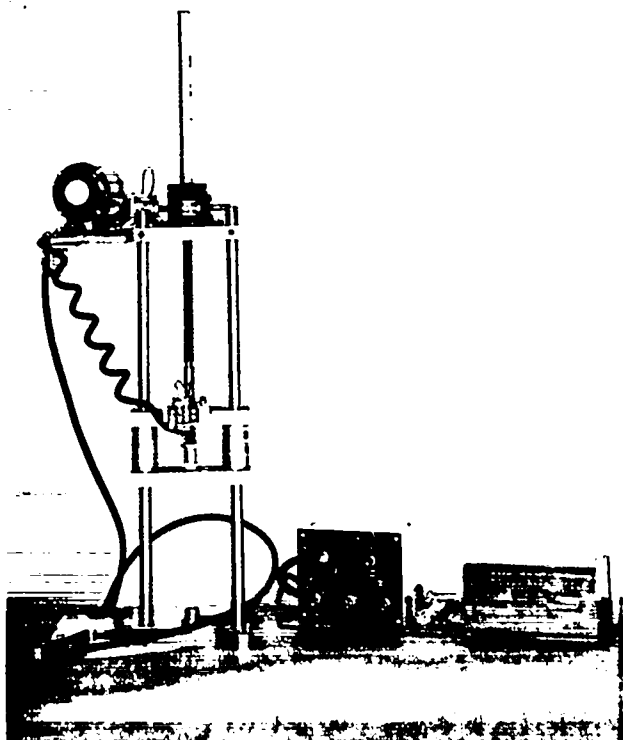


Fig. 401-4. Remote Encapsulator.

C. Shipping Cask

(C. D. Montgomery, J. W. Schulte, A. E. Tafoya)

The approved cask, designated as DOT SP-5885, was received on September 12, 1969. Results of an integrity test, using an 1800 Ci  $^{60}\text{Co}$  source, indicated that no serious voids existed.

The cask has a cavity 6 in. diam by 42 in. long. It has sufficient shielding (6.5 in. of depleted U) to accommodate 19 fuel elements, each containing 150 g fissile material (80% U and 20% Pu), which have been irradiated to 100,000 MWD/T burnup and cooled for 30 days. The cask weighs 12,200 lb and is equipped with a removable

insert which can be designed to accommodate a variety of element types. A view of the cask is shown in Figure 401-5.

On September 30, the cask was shipped to BNWL with the tube burst test specimens and other fuel element components. Seven other shipments have been scheduled over the next few months.

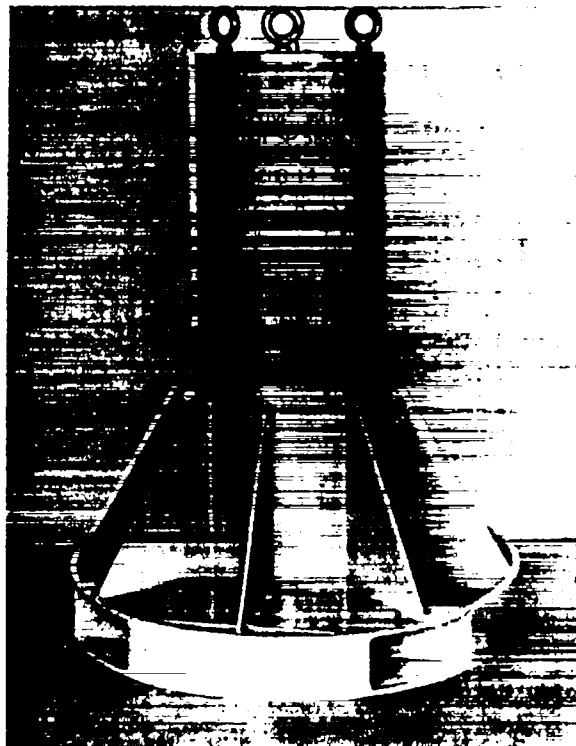


Fig. 401-5. Cask for Shipping Irradiated Fuel Elements.

III. DP WEST FACILITY

(D. B. Court, F. J. Fitzgibbon, C. D. Montgomery, G. H. Mottaz, M. E. Lazarus, J. R. Phillips, T. Romanik)

Building modifications and equipment design, fabrication and procurement are in progress to provide a working complex of hot cells which will complement the Wing 9 cells and permit a higher through-put of fast reactor fuel elements. It is expected that the equipment necessary to attain a rate of 150 fuel elements per year will be operational on July 1, 1970.

These cells are being equipped to accommodate various measurements of physical size, weight, temperature, contamination, and gross radiation. In addition,

precision analytical equipment is in design and fabrication to provide detailed gamma scan, detailed profilometry, photography, determination of void volume, and removal of capsule cladding and Na.

#### Building Modifications

Work scope and criteria drawings have been reviewed and submitted to the AEC for approval. This work includes minimal building changes to provide for unloading shipping casks (up to 25 tons) and transferring them into the cell corridor. Holes in the wall, floor, and ceiling will have to be provided to accommodate gamma scanning, profilometry, transfers, storage, and periscopes.

#### Gamma Scanning

A gamma scan shield has been fabricated using lead of low antimony and low activity content. The vertical transport and handling mechanism to accommodate fuel elements up to 61 in. long is being designed.

The Ge-Li detector has been delivered and checked out. Data processing and storage items are on order. Encoder systems will be ordered as soon as the basic design is approved.

#### Profilometry System

A Physitech Corporation electro-optical sensor has been ordered for the new profilometer. The pin transport mechanism is in initial design stages. When design is completed, an encoder system will be ordered to provide precise positioning information. This electro-optical profilometer is expected to provide much greater detailed information of anomalies observed on pins and capsules.

### IV. METHODS OF ANALYSIS

#### Measurement of U and Pu (J. W. Dahlby)

Controlled-potential coulometric equipment for titrating U and Pu, as part of the chemical characterization of irradiated mixed oxide or carbide fuels, was modified for remote operation and tested in-cell by repeated analyses of known amounts of each metal. The relative precision ( $1\sigma$ ) was 0.07 to 0.08 for a single determination of U or Pu. In the measurement of U, the titration current was integrated as U(VI) was coulo-

metrically reduced at a Hg electrode to U(IV) following a preliminary reduction of more-easily reduced impurities. The current for the coulometric oxidation of Pu(III) to Pu(IV) at a Pt electrode was integrated in determining Pu.

The method was unbiased if the equipment was calibrated using a chemical standard, but a small positive bias of 0.4 relative percent existed if electrical calibration was used. This bias increased to 0.3 to 0.4 relative percent for titrations of U in the presence of Pu using the titration cells modified for remote operation. Minor variations in the cell design, changes in titration potentials, and better control of potential while the sample was loaded into the titration cell were unsuccessful in reducing the bias. Changes in electrolyte composition and in the position of the electrical connection to the Hg electrode are being tried.

#### Shielded Electron Microprobe

(W. V. Cummings, D. B. Court, and C. D. Montgomery)

Detailed examination of areas as small as  $0.5\mu$  in diameter to determine the chemical compositions of various features in irradiated reactor fuels and cladding is a capability unique to the shielded electron microprobe. Information from these examinations is essential in determining the chemical behavior of the fuel element components. Following the recent installation and testing of a MAC shielded electron microprobe, a program of examinations was started to aid in the evaluation of fuels. Goals of this program include investigations of (a) fission product distributions and migrations, (b) redistribution of fuel components, (c) fuel-cladding interactions, (d) fission product precipitates and inclusions, (e) reactions of fission product elements with the fuel and with the cladding, (f) unusual features found metallographically or by other techniques, such as gamma scanning, and (g) variations in burnup relative to position. Selection of samples to be examined will be based upon metallography, gamma scanning, or other test results showing features in the sample that should provide desired information about fuel element behavior.

Proper functioning of the electron microprobe and associated equipment was demonstrated in the initial

testing and in the recently completed examinations of samples from an irradiated EBR-II driver fuel element. The initial samples selected for the program of examinations are being prepared for analysis.

Gross Gamma Scanning  
(J. Phillips and J. Deal)

An important use of gross gamma scanning is in locating anomalies and areas of interest for further analyses in irradiated fuel elements. To be of most value, the results must be obtained quickly to prevent delays in cutting and destructive sampling of the fuel element. A simple system is advantageous for this purpose because it generally is fast, reliable, and easily maintained. A system of this type is being assembled to complement the more complex capability for detailed gamma scanning. The scanning mechanism, slit, and lithium-drifted germanium-detector of the detailed gamma scanner will be used to obtain accurate resolution of scan position and reliable results. Other components are an amplifier, single channel analyzer set to accept all gamma energies above a preset background or noise level, a scaler timer, and a printer or an x-y recorder. The electronic components provide signals to advance the scanning mechanism a preset distance and stop it for recording of data at each point. Installation of this simple system is in progress. It is not anticipated that the gross gamma scanner will interfere significantly with scheduled work for the complex system for detailed gamma scanning.

V. EXAMINATION OF UNIRRADIATED FUELS

(J. A. Leary, M. W. Shupe, E. A. Hakala,  
R. T. Phelps, G. R. Waterbury, K. A. Johnson)

United Nuclear Corp. Oxides

The following tests and analyses were performed on pellets from UNC mixed-oxide fuel batches, UN-OX-14, -18, and -19; metallography, alpha-autoradiography, spectrochemical, U, Pu, and O analyses, electron microprobe, weights, dimensions, mechanical and immersion densities, and powder x-ray diffraction.

These results have been reported in full.

Battelle Northwest Laboratory

The following tests and analyses were performed on pellets from BNWL mixed-oxide fuel batches ME-20

and ME-21 (representing fuel elements PNL-X-1, -3, -4); metallography, alpha-autoradiography, spectrochemical, U, Pu, and O analyses, electron microprobe, weights, measurements, mechanical and immersion densities and powder x-ray diffraction.

The final report on these results is in process.

Westinghouse Advanced Reactor Division

Work is in progress on the metallography and electron microprobe analyses of mixed carbide samples S-6 and X-6.

Argonne National Laboratory (Idaho)

The following tests and analyses were performed on samples from ANL produced EBR-II driver fuel and on AGN produced EBR-II driver fuel; x-ray texture, spectrochemical, U, Mo and Zr analyses, electron microprobe, hot hardness, differential thermal analyses, metallography, hardness, beta-x-radiography, immersion density, and thermal expansion.

These results were reported in weekly reports to DRDT.

VI. REQUESTS FROM DRDT

A. Examination of Irradiated Material  
(D. M. Holm (K-1), K. A. Johnson, J. W. Schulte,  
G. R. Waterbury)

Battelle Northwest Laboratory Pins

From pins PNL-X-1, 3, 4, 6 and 7 and PNL-1-16, -18, the following types of samples were removed (in an inert atmosphere) from each pin:

1. Tube Burst Test\* - 5
2. Metallography - 4
3. Burnup - 1
4. Depleted UO<sub>2</sub> - 2
5. Ni Reflectors - 1
6. Miscellaneous Hardware

\*These samples were also packaged in an inert atmosphere in Swagelok fittings provided by BNWL personnel.

Most of the above items were shipped to BNWL on September 29.

Metallographic preparation of one sample from each of the seven pins referenced above was started on September 25.

Examination of EBR-II Driver Fuel Elements  
Containing AGN Fuel

The types of examinations conducted on five fuel elements (two irradiated and three unirradiated) received from ANL are mentioned here. Results of these examinations were provided to DRDT in Weekly Reports.

1. Nondestructive Tests on Fuel Elements:

Element 2249 from batch 100 was radiographed. Other determinations made were length, diameter, and eddy current tests for Na level and voids.

2. Chemical Analyses of Fuel Elements: Fuel:

Concentrations of U, Mo, Ru, Rh, Pd, Fe, and Nb in samples from unirradiated fuel pins 1136 and 3481, and of U, Mo, Ru, and Pd in irradiated fuel pin 1682 were determined by spectrophotometric methods. Determinations were made on solutions prepared by dissolving 0.1 to 1.0-g samples taken from the top, middle, and bottom of each pin. Emission spectrographic analyses for impurities were made on samples taken from the top and bottom halves of the fuel pins, and O<sub>2</sub> was determined by an inert-gas-fusion method in samples from the top and bottom of pin 3481. Three metallographically polished sections each from pins 1136 and 1682 were examined with a shielded and an unshielded electron microprobe.

Sodium: Concentrations of metallic impurities in Na taken from the top portion of fuel elements 1136 (unirrad.) and 1682 (irrad.) were determined by a semi-quantitative emission spectrographic method.

3. Atomics International Fuel and Flux Monitoring Wires:

Specific examinations were made on samples selected from 4 flux monitoring wires and from 120 UC pellets doped with W from EXP-NRX-9-101 Irradiation Experiment. Gamma scans were completed on the four flux monitor wires, and seven 0.25-in. sections from each of the two Al-Co wires were analyzed radiochemically to measure the absolute specific activity of each section.

Seven of the UC pellets were examined metallographically, and replicas were prepared for evaluation by Atomics International. Four of the pellets were shipped to Idaho Nuclear Corporation for burnup analyses.

All four monitoring wires have been gamma scanned, and the data are being evaluated.

4. Westinghouse Capsules: All three WARD capsules (W-1-G, W-2-G, W-3-G) were gamma scanned and the results are being studied.

5. LASL OWREX Experiment: An experimental capsule, irradiated in the Omega West Reactor at LASL, was disassembled in an inert atmosphere for examination of a suspected weld joint.

VII. PAPERS PRESENTED

1. "X-Ray Fluorescence Spectrometric Determination of Plutonium and Zirconium in Uranium Base Alloys," R. G. Hurley, E. A. Hakala, and G. R. Waterbury, 13th Conference on Analytical Chemistry in Nuclear Technology, September 30 to October 2, 1969, Gatlinburg, Tennessee.
2. "X-Ray Spectrometric Determination of Rhodium and Palladium in Uranium Base 'Fission' Alloys," E. A. Hakala, R. G. Hurley, and G. R. Waterbury, 13th Conference on Analytical Chemistry in Nuclear Technology, September 30 to October 2, 1969, Gatlinburg, Tennessee.

PROJECT 462

SODIUM TECHNOLOGY

Person in Charge: D. B. Hall  
Principal Investigator: J. C. Biery

---

I. INTRODUCTION

For the successful operation of high temperature sodium systems contemplated for use in fast, central station reactor concepts, impurities in the sodium must be monitored and controlled. Nonradioactive impurities such as oxygen must be maintained at low concentration levels to limit corrosion processes. To control the levels of these impurities, a knowledge of their behavior and interactions in sodium must be developed.

The sodium technology program at LASL has projects directed toward acquiring information about and designing equipment for the control and monitoring of impurities with precipitation processes. Also, equipment is being designed to sample sodium cover gas at operating temperatures with a quadrupole mass spectrometer. The current LASL projects are summarized below.

- A. Study and Design of Precipitation Devices
  - 1. Analysis of Dynamic Cold Trap Performance
  - 2. Study of Plugging Meter Kinetics
- B. Sampling and Analysis
  - 1. Development of a High Temperature Quadrupole Mass Spectrometer for Cover Gas Analysis
  - 2. Total Carbon Analysis Development

The following projects are being phased out because of funding reduction and will be reported here as the final data are generated and analyzed.

- C. Phaseout Programs
  - 1. Study of Carbon Transport in Thermal Convection Loop
  - 2. Study of Gas Diffusion Through Metals
  - 3. Study of Soluble Getters in Sodium

- 4. Study of Sodium Leaks
- 5. Development of Remotely Operated Distillation Sampler for EBR-II

II. STUDY AND DESIGN OF PRECIPITATION DEVICES

- A. Analysis of Dynamic Cold Trap Performance  
(C. C. McPheeters, J. C. Biery, W. W. Schertz, D. N. Rodgers, R. Martinez)

1. General

In sodium coolant systems for future LMFBR's it will be necessary to use cold traps for removal and control of oxygen and other contaminants. These cold traps should be designed to handle adequately the impurity loads and to maintain the impurity concentration level below some specified upper limit. For economic reasons, cold traps must be the smallest and simplest designs which can meet the above requirements.

Knowledge of the mechanism of impurity deposition in cold traps is necessary to reach the optimum design for a given sodium coolant system. The rate of mass transfer of impurity species to cold trap surfaces must be measured and the effect of various flow patterns, surface conditions, and temperature on the mass transfer rates must be determined. The purpose of this study is to determine the effect of the above variables on the mass transfer coefficient for removal of oxygen from sodium systems. Knowledge of the mechanisms involved and the mass transfer coefficients will allow calculation of the rate of oxygen removal and the location of deposited oxides in the cold trap for any given system size and cold trap geometry. Proposed cold trap designs could be evaluated in terms of total oxide capacity and expected system cleanup rates.

Cold trap tests are being conducted with a 60-gal sodium system which has analytical capabilities including a vacuum distillation sampler, a plugging indicator, and two UNC oxygen meters. The cold trap tests consist of measurement of the rates of change of oxygen concentration in the system. Various cold trapping conditions of temperature and flow rates are tested to determine the effect of these variables on the oxygen removal rates. When the rate of change of oxygen concentration, the cold trap temperatures and the deposition surface area is known an overall mass transfer coefficient can be calculated.

## 2. Current Results

### a. Operations of Cold Trap Loop with a Packed Trap

Due to the presence of impurities other than oxygen in the cold trap test loop, an auxiliary cold trap was installed to clean up the system. The auxiliary cold trap was operated for five days at a minimum temperature of  $\sim 115^{\circ}\text{C}$ . After the five days of operation, no plug could be formed on the plugging indicator even when it was held at  $105^{\circ}\text{C}$  for extended periods of time.

Oxygen was added to the system in the form of pure gas at the distillation sampling port. A total amount, equivalent to 45.3 ppm in the total sodium volume, was added; however, only enough oxygen was found in solution to maintain the saturation temperature at  $235^{\circ}\text{C}$  (24 ppm). The missing 20 ppm were probably gettered by the stainless steel walls. The operating temperature of the system was  $310^{\circ}\text{C}$ .

A series of cold trapping runs was started in which the minimum cold trap temperatures were  $200^{\circ}\text{C}$  in the precipitation runs and  $230^{\circ}\text{C}$  in the dissolution runs. Flow rates of 1.0, 0.75, 0.5, 0.25 and 0.1 gpm were selected for this series. These runs were made with Cold Trap No. 3 which is a packed cold trap. The packing was 0.004-in. diam wire mesh which was wound around the NaK-cooled insert in the annular sodium flow channel. All of the runs except those at 0.1 gpm have been completed. However, the mass transfer coefficient calculations have not been made as yet.

For the data analysis the cold trap simulation computer code will have to be modified to accommodate the packed trap condition. Not only must the cold trap area be modified, but a mechanism must be provided in the code to allow the amount of surface

area to increase as the amount of oxide precipitated on the mesh increases. As the oxide precipitates on the wire mesh, the effective wire diameter increases which in turn increases the precipitation surface area.

### b. Design and Fabrication of the High Reynold's Number Cold Trap Loop

All work on designing a High Reynold's Number Cold Trap Loop has been terminated due to loss of funds. Parts that were fabricated but were not suitable for other uses have been salvaged.

### c. Acquisition of Cold Trap Data from the Liquid Metals Engineering Center

LASL personnel visited Liquid Metals Engineering Center (LMEC) and Atomics International on July 23 & 24, 1969, to obtain detailed information on the design and performance of Sodium Reactor Experiment (SRE) and Hallam Nuclear Power Facility (HNPF) cold traps. Data on the SRE cold traps were obtained from Mr. Robert Hinze. These data pertain to Atomics International Report No. NAA-SR-3638 and serve as a detailed backup to that report. Additional data were obtained from J. Nicholson on a modified SRE cold trap design. These data were taken over a period of three months in 1966 and include cold trap temperature, flow rate, inlet plugging temperature, bulk sodium temperature and some indication of oxide distribution in the cold trap. Atomics International Report No. NAA-SR-5348 (Rev.) contains a description of the system and cold traps.

Mr. Roman Cygan provided detailed information relating to evaluation of HNPF cold traps done by MSA Research. The information consisted of copies of the daily log and data sheets recorded by MSA Research in conjunction with the HNPF cold trap evaluation study. The semimonthly progress reports written by MSA Research covering this work located in the Liquid Metals Information Center. Pertinent parts of these reports were copied in order to help locate useful data in the daily log.

### d. Analysis of Data from EBR-II and LMEC

In order to reduce the data on EBR-II, SRE, and Hallam cold traps so that the performance of the different traps could be compared, mass transfer coefficients were calculated for the cold traps based on the isothermal cold trap model. Unfortunately, the mass transfer coefficients calculated thus far from the EBR-II, SRE, and Hallam data with

this approach do not give a good indication of a particular cold trap's performance.

B. Study of Plugging Indicator Kinetics  
(J. C. Biery, D. N. Rodgers, W. W. Schertz,  
J. L. Bacastow)

1 General

Plugging meters have been used on sodium systems for many years. They are relatively simple to design, install, and operate; however, the meaning of the data obtained from these instruments has not always been clear, and, as a result, the value of the instrument has sometimes been questioned in the past. Previously reported LASL work<sup>1</sup> indicates, however, that the plugging meter is a valuable instrument and that it can be used with confidence. The three areas of investigation indicated below are continuing in order to better understand and use the meter.

- (a) Characterization of the plugging indicator's dynamic behavior with type of impurity.
- (b) Studies of orifice configurations and materials to improve nucleation and dynamic characteristics at low concentrations (~1 ppm or less range).
- (c) Development of a prototype plugging indicator system incorporating the research results of (a) and (b).

2. Current Results

The Plugging Indicator Loop (PIL-1), formerly called Analytical Loop No. 2, was started up during the report period. The loop has the following physical characteristics.

Expansion Tank:

2-ft diam; 3 ft high; 45 gal of sodium; helium cover gas.

Mixing Side Loop:

5.8 gpm maximum flow; the return flow is forced upward from the bottom into a core piece designed for mixing.

Cold Trap - Distillation Sampler Side Loop:

Maximum flow rate - 1.4 gpm. The valving allows the sampler to remove samples from the inlet or outlet of the cold trap. Cold trap volume - 1 gal.

Plugging Indicator Side Loop:

At present the standard LASL regenerative plugging indicator is installed in a side loop of PIL-1. Throttle valves and a bypass are available. Maximum flow rate - 1.4 gpm.

Oxygen Meter Side Loop:

Provision was made for the installation of two UNC oxygen meters. These are as yet not installed. Maximum flow rate will be 1.4 gpm.

Removable Orifice Plugging Indicator Side Loop:

The removable orifice meter is not as yet installed. Maximum flow rate will be 1.4 gpm.

Special Equipment:

A solids charging mechanism is fitted to PIL-1.

a. Impurities in PIL-1 After Startup

Since startup, the loop has been operated isothermally. The temperature has been raised in 25°C increments to its present level of 350°C from 225°C. At each temperature of operation, samples have been taken to determine if the change in temperature has any effect on impurity levels in a new loop. Also, a series of plugging meter runs were made after each change in temperature. The results of the distillation samples are recorded in Table 462-I. As the operating temperature was increased, a decrease was noted in the "ppm oxygen" which may possibly be due to the slow in-loop decomposition of impurities other than Na<sub>2</sub>O.

The oscillating plugging indicator gave saturation temperatures of 190°C ± 2°C during the total temperature escalation. The semi-log linear Rutkauskas solubility curve<sup>1</sup> indicates a saturation of 4.9 ppm of oxygen at 190°C. As indicated in Table 462-I, the average distillation results decreased from 10.2 ppm oxygen at 225°C to 9.1 ppm oxygen at 250°C then to 4.8 ppm at 300°C and 6.0, 6.8, 6.0 ppm oxygen for sample averages at 350°C. Thus, the second impurity appears to have nearly disappeared at the 300°C and 350°C. The extra 4.2 ppm "oxygen" is equivalent to 0.53 ppm H as NaH.

b. Stability of Electromagnetic Flowmeters on PIL-1

Since installation of the flowmeters in the plugging meter side loop of PIL, the outputs of the meters have exhibited much noise and drift. It was suggested that the noise might be due to the thermocouple effect where the Type 304 stainless steel leads are silver soldered into the copper cable. Since one junction projected into the airspace above the magnet of the flowmeter and the other was protected from the air currents, the exposed junction could vary in temperature with air movements in the room while the other junction remained at a constant temperature. When a wet tissue was used to cool the upper lead, an immediate change of ~50% was noticed in the flowmeter output.

Table 462-I

## Impurity Levels in PIL-1 Since Startup

Date	Sample No.	Loop Temp. °C	ppm Oxygen*	Average ppm Oxygen
7/3	1	225	11.4	
7/9	2	225	11.0	10.2
7/10	3	225	8.5	
7/11	4	225	10.0	
7/17	5	250	11.7	
7/18	6	250	9.5	9.1
7/22	7	250	9.2	
7/24	8	250	6.2	
7/30	9	300	6.6	
7/31	10	300	4.8	
8/1	11	300	5.2	4.8
8/5	12	300	4.1	
8/6	13	300	3.5	
8/7	14	300	4.1	
8/8	15	300	6.5	6.0
8/12	16	350	7.1	
8/13	17	350	6.5	
8/14	18	350	7.5	
8/18	19	350	8.8	6.8
8/20	20	350	7.6	
8/22	21	350	3.3	
9/3	22	350	4.8	
9/10	23	350	6.7	6.0
9/17	24	350	6.0	
9/24	25	350	6.5	

\* As determined from residual Na in distillation residues.

An attempt to solve the noise problem by thermally insulating the flowmeter and junctions failed because the insulation produced a permanent (but stable) temperature difference across the two junctions which depressed the flowmeter output ~30%. The problem was successfully solved by welding a 1/16-in. Type 304 stainless steel rod to each flowmeter lead and bringing these lead extensions out next to each other. The two stainless steel-to-copper junctions were then close enough together to be at the same temperature and therefore did not generate an EMF. Both flowmeter outputs now have signal to noise ratios of  $\geq 50$  at ordinary bare orifice flow rates (0.5 to 1.0 mv).

c. Removable Orifice Plugging Indicator for PIL-1

Two importance aspects of the LASL plugging meter program will be the testing of various orifice configurations and determining the type and form the precipitate that deposits in the orifice. To obtain these types of data, a removable-orifice plugging meter has been designed and will be installed on one of the side loops on PIL-1. At present, the parts for the removable orifice plugging indicator have been completed and are ready for assembly. The side loop for the plugging indicator has been designed and is now being drawn.

d. Modifications to Plugging Indicator Loop No. 2 (PIL-2), Formerly Called Cold Trap Loop (CTL)

The Cold Trap Loop is to be used exclusively in plugging meter research as soon as the present series of cold trap runs are completed. The loop will be used to study multi-impurity (mainly oxygen and hydrogen) interactions and behavior on plugging meter dynamic performance. Methods of identifying the two impurities from their dynamic behavior will be developed with the use of this loop. The loop has the following physical characteristics.

Volume:

60 gal

Flow Rate:

Up to 2 gpm

Instrumentation:

1 plugging meter (regenerative type) on 0.7 gpm side loop.

2 UNC EMF cells

1 Vacuum distillation unit

Special Equipment:

Two cold traps: (1) Removable core trap, NaK cooled for impurity identification.

(2) Auxiliary cold trap for total impurity removal.

Gaseous Impurity Addition System:

Soluble impurity metered into recirculating side loop to vacuum distillation station.

## III. SAMPLING AND ANALYSIS

A. Development of a High Temperature Quadrupole Mass Spectrometer for Cover Gas Analysis  
(J. P. Brainard, C. R. Winkelmann)1. General

The purpose of this research is to develop a method for continuous on-line analysis of high temperature (up to 650°C) cover gas in an LMFBR. The

analyzer must be capable of detecting impurities such as nitrogen, oxygen, hydrogen, carbon dioxide, methane, and fission products in the cover gas with a sensitivity varying from the part-per-million range to the percent range. A response time of about 1 min is necessary if the analytical data are to serve as an error signal for activating devices for continuous control of cover gas composition.

A quadrupole mass spectrometer was obtained in order to meet the above requirements. It is believed that reasonably representative sampling can be accomplished by transporting the sample gas in sodium loop containment materials and at sodium loop temperatures until it has passed through the spectrometer for analysis.

## 2. Current Results

The design of the vacuum envelope, introductory system, gas beam, and quadrupole alignment is now complete. A schedule is now being set up with the shops for its fabrication.

Chopping the gas beam would be a distinct advantage to this instrument. Not only would sensitivity be increased, but the background gases would be suppressed. Thought is now directed to the design of a mechanical chopper (about 500 cps) which would be compatible with the existing high temperature gas analyzer design.

## B. Analysis Development (K. S. Bergstresser)

### 1. General

The low temperature combustion technique for analysis of total carbon of sodium is being refined. By using a high sensitivity gas chromatograph for quantitative measurement of the CO<sub>2</sub> produced, it is hoped that carbon concentrations in the 1-ppm range can be determined.

### 2. Current Results

Several equipment modifications were made and various operating parameters investigated in the gas chromatographic measurement system used in a proposed method for determining carbon at concentrations between 1 and 10 ppm in metallic sodium. The main operations in the method were based on the Kallman and Liu<sup>2</sup> principle of low-temperature ignition followed by quantitative separation of the CO<sub>2</sub> formed by acidification of the sodium oxide. The CO<sub>2</sub> was determined using a gas chromatograph, but the base-line of the instrument was unstable and

results for CO<sub>2</sub> were erratic. A thorough examination of the measuring system showed that moisture in the CO<sub>2</sub> and in the "high-purity" He sweep gas caused most of the difficulty. The chromatograph was thoroughly serviced, and faulty couplings and other components were repaired or replaced. A short chromatographic column and valving system was installed to remove moisture from the samples and to vent the moisture to atmosphere by flushing the column with dried He between sample analyses. A molecular sieve trap was installed to purify the He sweep gas.

The instrument was then tested by measuring small quantities of moist CO<sub>2</sub> introduced into the inlet system. Satisfactory results were obtained. As the detector system seemed reliable, investigation was resumed of other operations in the proposed method.

## IV. PROJECTS BEING PHASED OUT

(Status of programs which are being phased out because of funding cuts are discussed. No new work will be started in these areas. Results obtained during the orderly conclusion of these tasks will be given in this section of the Project 462 report.)

### A. Study of Carbon Transport in Thermal Convection Loops (J. C. Biery, C. R. Cushing)

#### 1. General

Studies have indicated that the use of carbon beds may be useful in the gettering of <sup>137</sup>Cs in sodium systems. Carbon, however, is slightly soluble in sodium and can carburize austenitic stainless steels and refractory metals. Therefore, the purpose of this study is to determine the conditions, if any, under which carbon mass transfer rates are sufficiently low to allow the use of carbon beds in a sodium system.

The carbon transfer rates from carbon rods are being studied in thermal convection loops. The Type 304 stainless steel loop itself is serving as the carbon sink.

#### 2. Current Results

As of September 30, 1969, 4,992 h of run time have been accumulated on the thermal harp. A summary of the times at various temperatures is presented in Table 462-II.

Table 462-II

Temperature - Time Summary - Thermal Convection Harp

<u>No. of Hours</u>	<u>Temperature - °C</u>	
	<u>Hot Leg</u>	<u>Cold Leg</u>
336	485	455
1608	520	480
2688	510	450
360	330	130

This experiment will be continued until 8,000 h of run time are accumulated. The loop will be destructively examined to determine the extent of the carbon mass transfer.

B. Study of Gas Diffusion Through Metals  
(J. P. Brainard)

1. General

Very little quantitative information is available on the diffusion of gases in reactor system containment materials, although the phenomenon has been observed in several high temperature, liquid-metal-cooled systems. Diffusion of nitrogen through stainless steel in such systems may be misinterpreted as evidence of an air leak in the plumbing. If quantitative information on diffusion were available, the expected rate of nitrogen influx could be estimated, and the existence of small hard-to-find leaks might be substantiated or dismissed by comparing the expected and observed rates of nitrogen accumulation in the system.

A program for determining the diffusion rate of nitrogen in stainless steels has therefore been undertaken. In later phases of the program the diffusion of oxygen and hydrogen in stainless steels will be studied.

2. Current Results

The apparatus for nitrogen diffusion through Type 304 stainless steel tubing is complete. The automatic liquid nitrogen filling is in operation. The diffusion cell and thermocouples have been installed. The system has been made leak tight and ultra-high vacuum has been obtained. Initial data have been taken, i.e., pumping speed, time response to pressure changes, and calibration of the mass spectrometer.

The first significant experiment that was attempted was the determination of thermal desorption rates, i.e., measurement of pressure with

increasing temperature. Thermal desorption spectra indicate the energy of the nitrogen states on the stainless steel and the relative surface coverages. The spectra also indicate whether the state is atomic or molecular. It is believed that only the atomic states play an important role in the permeation of gas since diffusion occurs atomically. However, large amounts of nitrogen were removed above 300°C (several monolayers), and this outgassing has not decayed significantly with time. Possibly, the observed nitrogen is coming out of the bulk stainless steel having been trapped there in its manufacture; this outgassing masks surface effects. However, this observation does give preliminary evidence that the nitrogen permeation is bulk rather than surface controlled.

A copper gasket broke its seal when the vacuum oven was heated to 600°C. Air oxidized the interior surfaces of the stainless steel. Large quantities of carbon monoxide were subsequently released from the system; apparently the oxygen in the air combined with carbon on the surface of the steel.

The permeation and diffusion experiments have now been started. A mixture of 80% N<sub>2</sub> and 20% helium has been introduced into the diffusion cell. The first temperature run will be at 275°C. This run is to be considered a control run since the nitrogen permeation will probably be below the sensitivity of the instruments at this low temperature. Runs at high temperatures are planned.

C. Study of Soluble Getters in Sodium  
(D. N. Rodgers, J. C. Biery)

1. General

For large sodium-cooled reactor systems, it may be desirable to use soluble getters for control of oxygen and other dissolved impurities in lieu of the more conventional hot and cold trapping techniques. The soluble getters of interest occur in the sodium coolant either naturally, as an impurity (calcium), or are produced during reactor operation (as with magnesium). The techniques for the controlled additions of these getters, maintenance of fixed getter levels, and the selective removal of depleted getter metals and other impurities from dynamic sodium systems must be developed if their usefulness is to be evaluated. The significant chemical reactions occurring in a sodium system containing these

soluble getters must be understood and controlled. This mode of purity control has the potential for effectively controlling not only oxygen, but also carbon, hydrogen, nitrogen, and possible metallic impurities.

## 2. Current Results

The soluble getter data from the first experiment are being analyzed and a report is being prepared. Some interesting results have come out of the analysis. These are summarized below.

- (a) Calcium metal in solution in sodium can be detected and its concentration determined by adsorption on a nickel surface. The distribution coefficient observed at 350°C is  $7.8 \times 10^{-7}$  g Ca/(cm<sup>2</sup>-ppm Ca).
- (b) Na<sub>2</sub>O was dissolved into the system at 350°C. A rate constant for dissolution in 1.4 cm/sec velocity sodium flowing past a 1-in. diam hemispherical oxide container was determined to be  $4.0 \times 10^{-7}$  g(O)/(cm<sup>2</sup>h ppm O).
- (c) Estimations of the product [Ca(ppm)] · [O(ppm)] were made at 350 and 125°C. The values at these temperatures were 0.23 and 0.13 ppm<sup>2</sup>.
- (d) When oxygen was added to the system containing dissolved calcium, particulate CaO appeared to precipitate. At the 1.2 cm/sec velocity in the hold tank, 14 days were required for the level to drop from 6 ppm CaO to the 1-ppm level. The flow velocity implied particle sizes less than 70μ in diam.
- (e) Calcium metal appeared to adsorb on stainless steel as well as on nickel surfaces. A surface concentration of  $9.7 \times 10^{-3}$  mg Ca/cm<sup>2</sup> was observed over the entire stainless steel loop system at 350°C. This quantity was available for gettering of oxygen. Larger quantities of calcium were permanently lost in the system and may have alloyed with the wall and were not available for gettering.

## D. Study of Sodium Leaks (J. P. Brainard)

### 1. General

The correlation of sodium leak development with measured helium leak rates observed during acceptance testing provides information on the degree of component integrity which must be attained for safe, long-term sodium plant operation. No firm criteria now exist that establish acceptable levels of leak-tightness for various situations.

This study uses fabricated stainless steel leaks and leaks that occur naturally in stainless steel bar stock. Selected samples having a range

of helium leak rates are incorporated into small sodium systems (cells) which are held at a predetermined temperature until sodium leakage occurs. From these observations it may be possible to establish, for mass spectrometer acceptance tests on sodium system components, the maximum tolerable helium rate which is consistent with adequate long-term containment of sodium by that component.

An interesting side effect from this work has been observation of the elusiveness of what are considered to be large leaks ( $10^{-5}$  to  $10^{-6}$  atm cm<sup>3</sup>/sec). Normal containments such as grease, water and some solvents can completely mask leaks of this size and invalidate a leak test, unless proper pretreatment of the component is performed; and in some cases this can involve firing of the component in a hydrogen atmosphere. If meaningful helium leak tests are to be performed on LMFBR components, procedures must be developed for treating and handling of the part prior to leak test.

## 2. Current Results

Cells 1, 2, and 3 remain leak tight after 12,240 h at 400°C. Two interesting phenomena are occurring in Cells 4 and 8 which are leaking sodium. Cell 4 (400°C) has increased in its leak rate about 100-fold in the last quarter. This increase in rate may indicate that corrosion is occurring in the leak passage. Cell 8 (650°C) is losing its nitrogen in the reaction chamber in some way. Nitrogen leakage, diffusion into stainless, or diffusion through the sodium leak are possibilities. Because of this phenomena the sodium leak rate during the quarter could not be measured.

## E. Development of a Remotely Operated Distillation Sampler for EBR-II (E. O. Swickard, J. R. Phillips)

### 1. General

The original objective of the project was to produce three remotely-operated distillation samplers: one as a prototype, one for installation on the EBR-II primary loop, and one for installation on the EBR-II secondary. Because of program funding reductions, the objective has been curtailed to the production of the prototype unit only.

The sampler is an engineering loop version of a laboratory model in use on Sodium Analytical Loop No. 1 and Plugging Indicator Loop No. 2 at LASL. Samples are taken from a continuously flowing

bypass stream. The sampler is fabricated from Type 304 stainless steel, and energy for sodium evaporation is supplied by induction heating.

## 2. Current Results

Because of additional personnel reductions, very little work was done on the remote sampler prototype in the report period. The transfer machine control chassis was completed, and the wiring was checked out. The control unit has been temporarily installed on the transfer machine assembly and is operating satisfactorily.

## REFERENCES

1. V. J. Rutkauskas, "Determination of the Solubility of Oxygen in Sodium Using the Vacuum Distillation Analytical Technique," Report LA-3879, Los Alamos Scientific Laboratory, 1968.
2. S. Kallmann and R. Liu, "The Determination of Total Carbon and Sodium Carbonate in Sodium Metal," Anal. Chem. 36, 590 (1964).

PROJECT 463  
CERAMIC PLUTONIUM FUEL MATERIALS

Person in Charge: R.D. Baker  
Principal Investigator: J.A. Leary

I. INTRODUCTION

The principal goals of this project are to prepare pure, well characterized plutonium fuel materials, and to determine their high temperature properties. Properties of interest are (1) thermal stability, (2) thermal expansion, (3) thermal conductivity, (4) phase relationships by differential thermal analysis, (5) structure and phase relationships by X-ray diffraction, high temperature X-ray diffraction, neutron diffraction and high-temperature neutron diffraction, (6) density, (7) hardness and its temperature dependence, (8) compatibility, including electron microprobe analysis, (9) compressive creep (deformation).

II. SYNTHESIS AND FABRICATION

(R. Honnell, S. McClanahan, H. G. Moore, R. Walker)

To meet the material needs of the physical property measurement program, a number of different carbide compositions were synthesized and fabricated into useful forms for testing. For hot hardness measurements, 1.0 dia x 0.375 in. discs were sintered and characterized with the following nominal compositions:  $\text{PuC}_x$  ( $x = 0.66, 0.82, \text{ and } 1.0$ ),  $(\text{U}_{0.8}\text{Pu}_{0.2})\text{C}_y$  ( $y = 0.92, 1.0, \text{ and } 1.003$ ), and  $(\text{U}_{0.5}\text{Pu}_{0.5})\text{C}_{1.0}$ . For mechanical property measurements, 0.358 dia x 0.5 in. cylinders with a nominal composition of  $(\text{U}_{0.8}\text{Pu}_{0.2})\text{C}_{1.0}$  were sintered and characterized.

A cursory investigation was initiated to determine the effectiveness of Ni and PuC as sintering aids for (U, Pu)C. Pellets containing 1.36 to 3.03 w/o nickel and 4.8 to 11.7 w/o PuC were prepared and sintered at

1800°C for 8 hr in Ar. The sintered pellets were examined metallographically and their microstructures compared with a control pellet. The pellets containing Ni additives had a noticeable decrease in porosity by point count analysis, relative to the control material, amounting to as much as 50% for specimens with 1.36 w/o Ni. However, a metallic appearing grain boundary phase was present (assumed to be nickel rich) which indicates that excessive nickel was added.

III. PROPERTIES

1. Differential Thermal Analysis  
(J. G. Reavis, L. Reese)

Additional differential thermal analysis observations have been made to investigate the melting behavior of (U, Pu) monocarbides in the composition range 0-50 m/o PuC. Melting behavior of Pu-C compositions in the range  $\text{PuC}_{1.08}$  to  $\text{PuC}_{1.48}$  has also been studied.

Melting Behavior of (U, Pu) Monocarbides: The melting behavior of (U, Pu)C compositions containing 0-50 m/o PuC was previously reported.<sup>(1)</sup> Solidus and liquidus temperatures were determined by application of differential thermal analysis and metallographic techniques and by macro observation of samples quenched from temperatures near the expected liquidus. The samples used in this work included arc melted material which may have been inhomogeneous and powder metallurgy products which may have contained traces of a second phase (either metal or  $\text{M}_2\text{C}_2$ ).

Single phase pellets of selected (U, Pu)C compositions

Table 463-I  
Solidus and Liquidus Temperatures of (U, Pu) Monocarbides

Composition	Solidus, °C	Liquidus, °C
U <sub>0.85</sub> Pu <sub>0.05</sub> C <sub>0.17</sub>	2450	2515
U <sub>0.84</sub> Pu <sub>0.06</sub> C <sub>0.18</sub>	2445	2535
U <sub>0.77</sub> Pu <sub>0.23</sub> C <sub>0.28</sub>	2250	2440
U <sub>0.88</sub> Pu <sub>0.12</sub> C <sub>0.18</sub>	2190	2380
U <sub>0.53</sub> Pu <sub>0.47</sub> C <sub>0.24</sub>	2050	2315

have recently been observed in this same manner and the solidus and liquidus temperatures listed in Table 463-I were determined. These data generally give a better fit of theoretical solidus and liquidus curves previously drawn, but indicate some modification may be desirable at the higher PuC concentrations. No changes of previously determined solidus and liquidus temperatures of U<sub>0.8</sub>Pu<sub>0.2</sub>C are needed.

Transformations in the Pu-C System: A series of Pu-C samples having C/M atomic ratios in the range 1.08 to 1.48 were investigated by DTA and by macro examination after quenching from temperatures near the liquidus. The results of this investigation are listed in Table 463-II. The thermal arrests at about 1605° were weak and were observed only on heating, but were reproducible for compositions having C/M atomic ratios up to 1.26. Irregularities were seen in DTA curves at various temperatures for the other compositions of Table 463-II, but these were not reproducible. The appearance of the 1605° arrests indicated a process involving small amounts of energy beginning at this temperature and continuing at higher temperatures.

It was not possible to detect the onset of liquid phase formation and it was not possible to determine whether or not liquid phase formation began in these samples with the heating arrests at about 1605°. It was possible, however, to determine unequivocally that

Table 463-II

Transformation Temperatures of Pu-C Samples

Nominal Composition	Thermal Arrest Temp., °C	Liquidus, °C
PuC <sub>1.08</sub>	1610	1840
PuC <sub>1.18</sub>	1605	1885
PuC <sub>1.26</sub>	1605	1915
PuC <sub>1.32</sub>	?	1985
PuC <sub>1.45</sub>	?	2030
PuC <sub>1.48</sub>	?	2050

macro liquid phase formation began more than 100° below the liquidus in some compositions.

The liquidus temperature was taken as the temperature at which the sample formed a smooth meniscus. It was not always possible to determine from DTA curves exactly the temperature at which this occurred, nor was it possible to ascertain that no solid particles remained after a smooth meniscus formed. The uncertainty in liquidus temperatures is estimated as ± 25° C.

## 2. Room Temperature X-ray Diffraction (C. W. Bjorklund)

The characterization of plutonium ceramics by X-ray powder diffraction techniques has been incorporated in other sections of this report. Studies of self-irradiation damage in plutonium compounds have been continued on a routine basis. Very little deviation from the results reported previously has been observed; the lattices of compounds of normal isotopic composition still continued to expand very slowly, and the lattice dimensions of the plutonium compounds slightly enriched with <sup>238</sup>Pu remain constant within limits of experimental error. No change in the quality of the X-ray patterns of any of the compounds has been observed.

## 3. High Temperature X-ray Diffraction (J. L. Green)

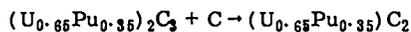
Investigation of the high temperature crystallographic properties of materials associated with the carbon-rich fields of the U-Pu-C phase diagram is continuing. Phase identification and thermal expansion data for the carbon-rich plutonium carbides have been reported previously. Studies of the mixed uranium-plutonium carbides were begun with the composition (U<sub>0.65</sub>Pu<sub>0.35</sub>)<sub>2</sub>C<sub>2.1</sub>. Samples of this material were prepared using the techniques described earlier for PuC<sub>2.2</sub>.

Thermal expansion data for carbon rich (U<sub>0.65</sub>Pu<sub>0.35</sub>)<sub>2</sub>C<sub>3</sub> have been obtained in the temperature interval from 800° to 1700° C. The fractional expansion of this phase as a function of temperature can be represented by the equation

$$\frac{\Delta a}{a_0} = 9.5 \times 10^{-6} (T - 20) + 1.7 \times 10^{-9} (T - 20)^2$$

where "a" is the lattice dimension and T is the temperature in °C. This corresponds to an average thermal expansion coefficient of  $12.3 \times 10^{-6}/^{\circ}\text{C}$  over the temperature range from 20° to 1700°C, which is somewhat smaller than the value of  $15.6 \times 10^{-6}/^{\circ}\text{C}$  reported earlier for carbon-saturated  $\text{Pu}_2\text{C}_3$ . No single set of data has been published for  $\text{U}_2\text{C}_3$  that covers this particular temperature interval. However, using high temperature data reported by Bowman<sup>(2)</sup> and a lattice parameter of 8.088 Å for  $\text{U}_2\text{C}_3$  at 20°C, the average expansion for  $\text{U}_2\text{C}_3$  over the temperature interval of interest is estimated to be  $10.3 \times 10^{-6}/^{\circ}\text{C}$ . These particular expansion values are essentially a linear function for the Pu/U + Pu ratio. A small amount of high temperature data for the composition  $(\text{U}_{0.65}\text{Pu}_{0.35})_2\text{C}_3$  has been published by Dalton, et al.<sup>(3)</sup> Thermal expansion coefficients, per se, were not presented in that work, but a value of  $12.0 \times 10^{-6}/^{\circ}\text{C}$  can be estimated from the data that was reported. This is in good agreement with the results of the present study. Possibly, this correspondence with Dalton's results should be considered somewhat fortuitous. The lattice parameters reported for this compound by Dalton agreed well with those from the present study for higher temperatures. However, those reported for lower temperatures were considerably smaller than those from the present study. Agreement between expansion coefficients computed for lower temperatures would, therefore, be somewhat poorer than that indicated above.

As in the case of  $\text{Pu}_2\text{C}_3$ , the kinetics of the transformation

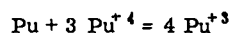


appear to be very slow near the transformation temperature. The only stable structure observed above the transformation temperature is the cubic modification of  $\text{MC}_2$ . During transformations from the sesquicarbide to the dicarbide, some interesting intensity effects have been noted. At temperatures below approximately 1900°C, the  $\text{MC}_2$  reflections have a distinct asymmetry on the low angle side. Most often, this effect is simply a low angle tail on the peak, but under some conditions

weak low angle satellite peaks are present. These low angle peaks have never been observed to grow relative to the reflections due to the major phase. In addition, homogenization of the sample at high temperatures, e.g., 1900°C, results in the disappearance of the asymmetry which does not reappear on slow cooling. An alternate statement of the latter observation is that the asymmetric features are not observed for samples that contain no residual  $\text{M}_2\text{C}_3$ . It has been reported by Dalton<sup>(3)</sup> that two face centered cubic  $\text{MC}_2$  structures exist at high temperatures as stable species for this composition and that a transition between the two occurs at approximately 1850°C. The above observations do not seem to be consistent with this interpretation. It would appear reasonable to associate these effects with metastable composition changes occurring during the transition; however, further work in this area will be necessary before positive conclusions can be drawn. Thermal expansion data was gathered for  $(\text{U}_{0.65}\text{Pu}_{0.35})\text{C}_2$  during cooling cycles after high temperature homogenization, i.e., for samples containing only one  $\text{MC}_2$  phase and graphite. The average expansion coefficient for the temperature range 1775° to 1900°C is  $20 \times 10^{-6}/^{\circ}\text{C}$ . Within experimental accuracy, this value is essentially the same as that reported previously ( $21 \times 10^{-6}/^{\circ}\text{C}$ ) for  $\text{PuC}_2$ .

#### 4. Thermodynamic Properties of Pu Compounds by High Temperature Electrochemistry (G.M. Campbell)

In order to use  $\text{PuCl}_3$ , LiCl-KCl electrolytes in determining thermodynamic properties of Pu alloys, the equilibrium



was studied by microelectrode techniques. Various techniques have been used by other workers to measure the free energy of similar reactions,<sup>(4)</sup> but agreement between different workers is poor. The reaction involving Pu ions in LiCl-KCl has not previously been studied. Since the microelectrode studies have indicated that the reaction is involved in equilibria with Pu ceramics, this type of equilibrium must be known. In this regard, isotype  $\text{Pu}_2\text{C}_3 + \text{C}$  electrodes have already indicated the stability of such equilibria and a

PuN electrode is currently being studied. Although PuN has already been investigated electrochemically<sup>(5)</sup> pure Pu metal electrodes were used as counter electrodes and cells were terminated when the residual current increased. Even so it is now believed that the rapid rise in emf at lower temperatures may have been the result of Pu<sup>3+</sup>/Pu<sup>4+</sup> equilibria. A cell with isotope PuN electrodes is still very stable after 35 days operation. Chronopotentiograms and voltammetric curves indicate that the Pu<sup>3+</sup>/Pu<sup>4+</sup> equilibrium is present. Potentials measured from this cell are slightly smaller than those which included the Pu counter electrode above the melting point of Pu (913°K). Low temperature measurements are currently in progress. These data and those of Pu<sub>2</sub>C<sub>3</sub> + C will be correlated with information from the micro electrode studies to determine the free energies of interest.

5. Mass Spectrometric Studies of the Vaporization of Pu Compounds  
(R. A. Kent)

The mass spectrometer-Knudsen cell assembly described previously<sup>(6)</sup> has been employed to study the vaporization behavior of a number of Pu-containing systems. The vaporization studies of Pu metal and PuN have been completed and the results published.<sup>(7, 8)</sup>

As a first step in the study of the Pu-U-C ternary system, the vaporization behavior of the Pu-C binary system is being investigated as a function of the C/Pu composition ratio. To date, a large number of experiments have been performed which indicate that there are three regions to the Pu-C phase diagram which give rise to invariant but not congruent vaporization:

1. Pu<sub>2</sub>C<sub>3</sub> + C
2. PuC<sub>2</sub> + C
3. PuC + Pu<sub>2</sub>C<sub>3</sub>

Sesquicarbide plus Carbon and Dicarbide plus

Carbon: A series of samples were prepared having initial stoichiometries ranging from single phase PuC<sub>1.50</sub> to PuC<sub>2.07</sub> (Pu<sub>2</sub>C<sub>3</sub> + C). These samples were effused from W Knudsen cells and/or from graphite cups contained in W Knudsen cells over the range 1745-2140°K.

The results indicate the following. Below the transition temperature of 1660°K the condensate consists

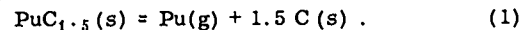
of sesquicarbide and carbon and the only vapor species observed was Pu(g). Above the transition temperature, the condensate consists of dicarbide plus carbon and again, the predominate vapor species is Pu(g).

The Pu<sup>+</sup> ion current was monitored as a function of temperature and the ion current data were converted to absolute pressure values using a National Bureau of Standards gold standard sample and the ionization cross sections calculated by Mann.<sup>(9)</sup>

Both above and below the transition temperature, the decomposition process is invariant, i. e., the Pu(g) pressure is independent of composition so long as the condensate consists of both carbon and either sesquicarbide or dicarbide.

The Pu(g) vapor pressure data above the sesquicarbide and dicarbide are presented in Fig. 463-1.

The sesquicarbide decomposes according to the reaction



The Pu(g) pressure in the range 1745-1928°K is given by

$$\log_{10} P_{\text{Pu}}(\text{atm}) = (4.385 \pm 0.072) - \frac{20450 \pm 134}{T^{\circ}\text{K}} \quad (2)$$

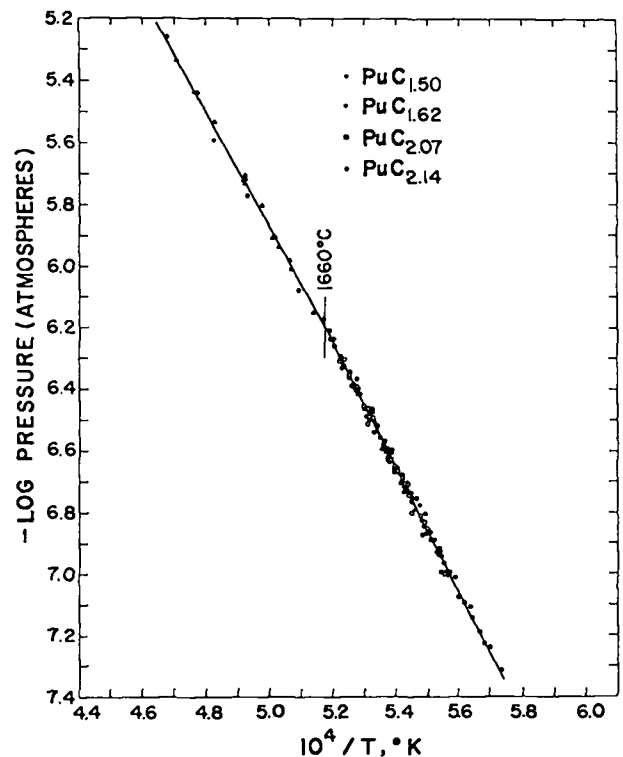
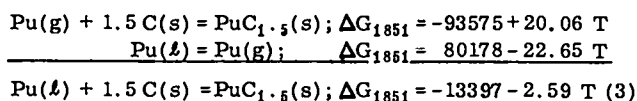


Figure 463-1. Plutonium Gas Pressure above Plutonium Sesquicarbide and Plutonium Dicarbide

When the free energy expression for the decomposition process is combined with known data for Pu(l) vaporizing to Pu(g)<sup>(7)</sup> the following expression for the free energy of formation for the sesquicarbide is obtained:



No high temperature heat capacity data exist for the sesquicarbide. Values may be estimated from known values for the monocarbide<sup>(10)</sup> and graphite.<sup>(11)</sup> From this the second law heat and entropy of formation are calculated to be

$$\Delta H_{f298}^{\circ} = -12.8 \pm 2.5 \text{ kcal/mole and } \Delta S_{f298}^{\circ} = +4.9 \pm 2.0 \text{ eu.}$$

The value of  $S_{298}^{\circ}$  is calculated to be +20.2 eu.

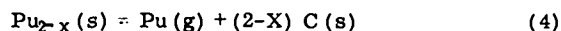
The actual precision in the heat and entropy values was plus or minus 5%. The listed uncertainties take into account possible errors in temperature measurement and the fact that estimated functions were used for the sesquicarbide.

In Table 463-III are listed values for the Pu(g) pressure at various temperatures. The value  $S_{298}^{\circ} = 20.2$  eu was employed to calculate the free energy functions for the sesquicarbide and the third law heats for the decomposition reaction. The third law heat of formation for the sesquicarbide is listed in the last column.

Table 463-III  
Third Law Results for the Decomposition of PuC<sub>1.5</sub>(s)

T, °K	P <sub>Pu</sub> (atm)	-Δ <sub>f</sub> f <sub>298</sub> cu	ΔH <sub>f298</sub> <sup>o</sup> kcal/mole	ΔH <sub>f298</sub> <sup>o</sup> (PuC <sub>1.5</sub> (s)) kcal/mole
1900	4.19 × 10 <sup>-7</sup>	21.17	95.7	-12.7
1800	1.05 × 10 <sup>-7</sup>	21.24	95.7	-12.7
1700	2.27 × 10 <sup>-8</sup>	21.32	95.7	-12.7
1600	4.02 × 10 <sup>-9</sup>	21.41	95.7	-12.7

The dicarbide decomposes in the range 1934 - 2140°K according to the reaction

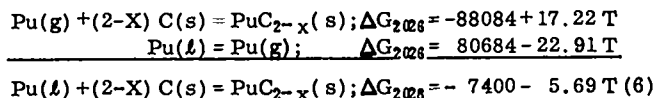


with the Pu(g) pressure given by

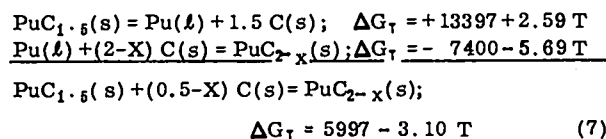
$$\log_{10} P_{\text{Pu}} \text{(atm)} = (3.764 \pm 0.143) - \frac{19250 \pm 289}{T^{\circ}\text{K}} \quad (5)$$

The composition limit of the dicarbide is not yet fixed, but is near PuC<sub>1.96</sub>. Again, a combination of the free energy expressions for the dicarbide decomposition and for the vaporization of Pu(l)<sup>(7)</sup> gives the free energy

of formation of the dicarbide:



If the free energy expressions for the formation of the sesquicarbide and the dicarbide are combined, one obtains the free energy of the sesquicarbide-dicarbide transition. This equation gives the transition temperature as 1662°K. Independent differential thermal analysis studies performed in this Laboratory indicate that the transition temperature is 1660 ± 10°K.<sup>(12)</sup>

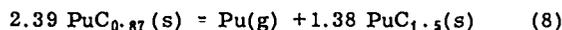


Monocarbide plus Sesquicarbide: A series of samples ranging from single phase PuC<sub>0.85</sub> to monocarbide-sesquicarbide mixtures were effused from tungsten Knudsen cells.

Figure 463-2 shows a plot of log Pu(g) pressure versus reciprocal temperature above monocarbide-sesquicarbide mixtures. Again the only vapor species observed was Pu(g), and the Pu<sup>+</sup> ion current data were converted to absolute pressure values, using Au as a standard and correcting for the relative ionization cross sections.

The decomposition process for the monocarbide is invariant, the Pu(g) pressure being independent of composition so long as the condensate consists of both mono- and sesquicarbide.

In the temperature range 1533-1799°K the monocarbide decomposes according to the reaction



with the Pu(g) pressure given by

$$\log_{10} P_{\text{Pu}} \text{(atm)} = (5.164 \pm 0.049) - \frac{18990 \pm 82}{T^{\circ}\text{K}} \quad (9)$$

A combination of the free energy expression for the monocarbide decomposition with those for the vaporization of plutonium metal,<sup>(7)</sup> and for the formation of the sesquicarbide yields the free energy of formation for the monocarbide.

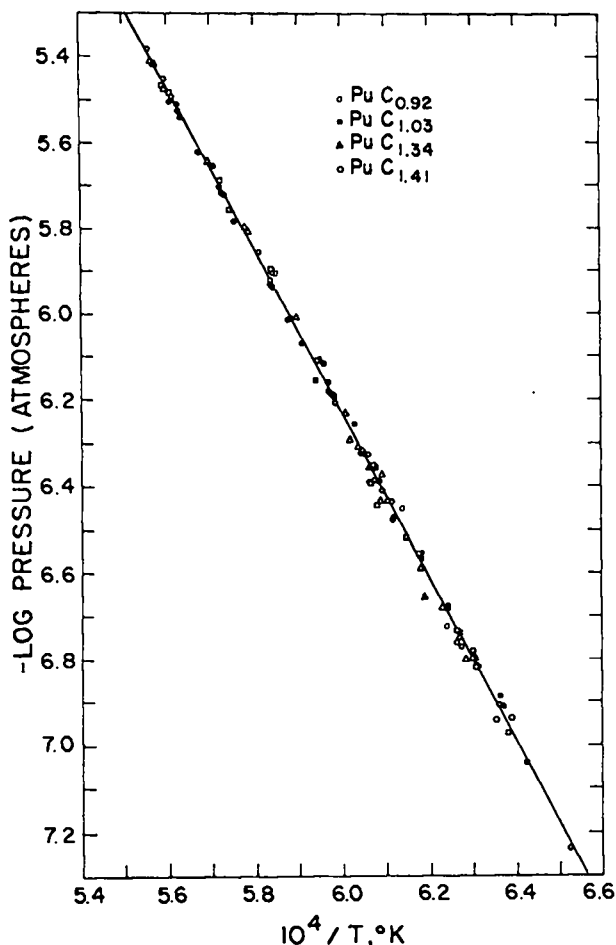
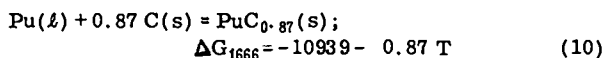
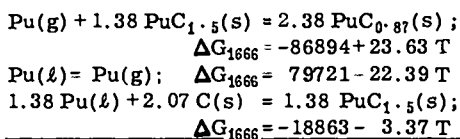


Figure 463-2. Plutonium Gas Pressure above Plutonium Monocarbide plus Plutonium Sesquicarbide



when equation (10) is reduced to 298°K using known thermodynamic functions for Pu, <sup>(7)</sup> C, <sup>(11)</sup> and PuC<sub>0.87</sub> <sup>(10)</sup> one obtains  $\Delta H_{f,298}^{\circ} = -10.5 \pm 2.5$  kcal/mole and  $\Delta S_{f,298}^{\circ} = +2.8 \pm 2.0$  eu for the monocarbide. The value of  $S_{298}^{\circ}$  is calculated to be +17.2 eu. The third law results are given in Table 463-IV.

Table 463-IV  
Third Law Results for the Decomposition of PuC<sub>0.87</sub>(s)

T, °K	P <sub>Pu</sub> (atm)	-Δ <sub>ref</sub> <sup>o</sup> eu	ΔH <sub>298</sub> <sup>o</sup> kcal/mole	ΔH <sub>298</sub> <sup>o</sup> (PuC <sub>0.87</sub> (s)) kcal/mole
1800	4.10 × 10 <sup>-6</sup>	25.37	90.0	-10.3
1700	9.86 × 10 <sup>-7</sup>	25.50	90.1	-10.3
1600	1.97 × 10 <sup>-7</sup>	25.63	90.1	-10.3
1500	3.19 × 10 <sup>-8</sup>	25.75	90.1	-10.3

Miscellaneous: Installation of the new Hitachi RM6-K magnetic mass spectrometer by factory personnel has been completed. Calibration and checkout procedures to be performed before the unit is to be enclosed in a glove box have been initiated. This unit employs an 8 in., 90° magnetic sector and has a theoretical resolution of  $(M/M + \Delta M) = 6,000$  with a 50% valley between peaks. So far the unit has proved capable of resolving to the baseline the mass 29 peak consisting of <sup>14</sup>N<sup>15</sup>N<sup>+</sup> and C<sub>2</sub>H<sub>5</sub><sup>+</sup>. The Knudsen cell has been heated to 2100°C using less than half of the rated power of the heater supply. The optical windows have been calibrated for use with an optical pyrometer.

In a rough calibration run, a sample of single crystal CaF<sub>2</sub> was effused from a Ta Knudsen cell. The appearance potential of the CaF<sup>+</sup> ion was found to be 5.5 ± 0.5 eV compared to the published value, 5.8 ± 0.3 eV. <sup>(13)</sup> Vapor pressure data obtained in the calibration experiment are compared with literature values in Table 463-V.

Some minor features of the new unit will be modified. The vacuum and water interlock systems will be changed and the Hitachi ion gauges will be replaced with standard Bayard-Alpert gauges. The original 10-stage electron multiplier will be replaced with a 16-stage unit.

## 6. High Temperature Calorimetry

### A. High Temperature Drop Calorimeter: (A. E. Ogard, G. Melton)

During this reporting period the heat content of W, Al<sub>2</sub>O<sub>3</sub>, and PuO<sub>2</sub> have been determined from 1055°C to 2070°C in a vacuum aneroid drop calorimeter. Results are shown in Table 463-VI. The results shown for W are "apparent" heat contents and are not corrected for

Table 463-V  
Experimental and Literature Vapor Pressure Values for CaF<sub>2</sub>

T °K	Pressure, (atm) (observed)	Pressure, (atm) (Ref)
1650	3.14 × 10 <sup>-6</sup>	2.98 × 10 <sup>-5</sup>
1588	1.01 × 10 <sup>-5</sup>	1.02 × 10 <sup>-6</sup>
1505	1.90 × 10 <sup>-6</sup>	2.07 × 10 <sup>-6</sup>
1635	2.41 × 10 <sup>-6</sup>	2.32 × 10 <sup>-5</sup>
1593	1.11 × 10 <sup>-5</sup>	1.11 × 10 <sup>-5</sup>
1565	6.47 × 10 <sup>-6</sup>	6.65 × 10 <sup>-6</sup>

Table 463-VI

Material	Temperature, °C	$H_T - H_{298}$ , kcal/mole
W	1055	6.4
W	1547	9.5
W	1625	10.2
W	1704	10.7
W	1832	11.9
W	1922	12.3
W	1984	12.7
W	2070	13.6
Al <sub>2</sub> O <sub>3</sub>	1077	27.9
Al <sub>2</sub> O <sub>3</sub>	1319	35.4
Al <sub>2</sub> O <sub>3</sub>	1423	38.7
Al <sub>2</sub> O <sub>3</sub>	1524	41.3
Al <sub>2</sub> O <sub>3</sub>	1626	45.4
Al <sub>2</sub> O <sub>3</sub>	1703	47.9
Al <sub>2</sub> O <sub>3</sub>	1837	51.2
Al <sub>2</sub> O <sub>3</sub>	1880	52.4
Al <sub>2</sub> O <sub>3</sub>	1990	57.1
PuO <sub>2</sub>	1225	24.4
PuO <sub>2</sub>	1440	28.3
PuO <sub>2</sub>	1537	31.6
PuO <sub>2</sub>	1620	33.1
PuO <sub>2</sub>	1714	36.6
PuO <sub>2</sub>	1780	37.8
PuO <sub>2</sub>	1885	40.2

heat loss during drop. The data for PuO<sub>2</sub> was corrected for the self-heating of the Pu before the heat contents were calculated. The self-heating of the Pu was determined by direct measurement in the calorimeter. A value of  $2.09 \times 10^{-3}$  watts/g Pu ( $\pm 4\%$ ) was calculated.

These results are somewhat lower than results reported in the literature. Curves will be fitted to the data when further data is available.

#### B. Adiabatic Calorimeter: (D. G. Clifton)

During this quarter further experiments were done with a sample of  $\alpha$ -Al<sub>2</sub>O<sub>3</sub> in the adiabatic calorimeter. These experiments consisted of following the temperature vs. time history of the sample as a function of equilibrium temperature, of heat addition to the sample, and of the temperature gradient,  $\Delta T$ , across the adiabatic shield. These experiments were extended to 1050°C.

It was found that at higher temperatures the "control signal" or temperature gradient ( $\Delta T$ ) across the radiation shield lost its true significance as a measure of the difference between the sample temperature

and the adiabatic shield temperature because of the physical arrangement of the couples and shield. Consequently, the calorimeter has been modified.

Now the thermocouple arrangement in the calorimeter is as follows. A total of nine thermocouples are installed. One thermocouple is in the sample in the same manner as previously. A second thermocouple extends up along the crucible support rod with its sensing junction just below the bottom "adiabatic" shield. A third thermocouple extends down along the sample heater insulating sheath with its sensing junction just above the top "adiabatic" shield. The other six couples are grouped into pairs spaced radially about the sample at 120°. One couple of each of these pairs is housed in a pod made of Ta sheet which is in turn in good thermal contact with the exterior of the sample crucible. The other couple of each pair is housed in a pod which is in good thermal contact with the exterior of the adiabatic shield. Each of the nine thermocouples have been extended out through the calorimeter housing and are connected to a switching system so that they can be read separately in comparison to a reference junction at 0°C. Also the six couples sensing  $\Delta T$  between the sample and "adiabatic" shield are wired such that they can be gauged in series as a thermocouple to give an average  $\Delta T$ .

The calorimeter is now reassembled in the above described mode. A series of tests are presently being conducted in which a thorough survey is being taken of the temperatures as they are sensed by the 9 thermocouples. This survey is made at a series of power settings, each of which has a corresponding steady state temperature and  $\Delta T$ .

#### 7. Transport Properties

(K. W. R. Johnson, J. F. Kerrisk)

A. Electrical Resistivity: A high temperature electrical resistivity system has been designed and is being built. The initial objective of the system is to make dc resistivity measurements on solid ceramic or metal systems containing plutonium between room temperature and 2500°C. Resistivities will be measured using a four point method. Samples will be

passively heated in a vacuum or inert gas furnace with a tungsten mesh heater.

The electrical equipment (potentiometer with its power supply, null detectors constant current dc supply, and standard resistors) purchased for the electrical resistivity apparatus has been received and installed in a rack. Preliminary tests on the potential measuring system are in progress. The high temperature furnace has been ordered and delivery is expected in December.

B. Thermal Diffusivity: A system for measuring the thermal diffusivity of plutonium ceramic materials between room temperature and 2500°C is being constructed. The diffusivity measurements will be made using a flash technique, in which a Korad Model K-2 125 joule laser pulse will heat the front surface of a disc sample while the back surface temperature is monitored with thermocouples or optically. The sample will be heated passively in a vacuum or inert gas furnace using a tungsten mesh heater.

The laser, with its associated auxiliary equipment, has been received and set up for preliminary operation. A circulating water system, which supplies cooled, constant temperature, distilled water to the laser head has been built. The initial tests on the laser indicate that it is functioning properly. The high temperature furnace has been ordered and is expected to arrive in November.

C. Thermal Conductivity: A thermal conductivity specimen was fabricated from LASL, "Round Robin", Armco Iron and measured between 71° and 674°C. Shown in Table 463-VII are the results of these measurements. Comparison with average values of BMI, "Round Robin", Armco Iron, and TPRC "most probable" values for Armco Iron indicate that the present measurements represent an accuracy of ± 1.5%.

The thermal conductivity of two U-15 w/o Pu-6.8 w/o Zr specimens was measured from 110° to 891°C using Inconel 702 meter bars. Measured conductivities are presented in Table 463-VIII. For the first specimen a normal pressure of 150 psi was applied to the top meter bar. On heating above 600°C, the temperature of

Table 463-VII  
Thermal Conductivity of Armco Iron

Temperature, °C	Thermal Conductivity cal./sec. cm. °C
71	0.168
220	0.143
325	0.121
477	0.103
674	0.082
589	0.090
321	0.124
322	0.124
190	0.144
110	0.162
75	0.166

a solid phase transformation, thermal conductivity values appeared unreasonably large. This trend persisted as the specimen was cooled. Examination of the specimen after the apparatus was disassembled revealed that appreciable deformation had occurred which altered the measurements by increasing the cross sectional area and decreasing the distance between thermocouples. The data in Table 463-VIII reflect these dimensional changes.

Although the second specimen was measured with only 10 psi pressure, deformation was still observed above 600°C. The average deviation of the values calculated from the upper and lower meter bars was 3.6%.

A new thermal conductivity apparatus baseplate and bell jar incorporating high vacuum principles was designed and fabricated. These components and a diffusion pump will be installed in the near future.

Table 463-VIII  
Thermal Conductivity of U-15 w/o Pu-6.8 w/o Zr

Specimen No.	Temperature, °C	Thermal Conductivity cal./sec. cm. °C
1	110	0.030
1	252	0.040
1	492	0.056
1	764	0.067*
1	891	0.080*
1	477	0.058*
2	111	0.030
2	342	0.046
2	769	0.073*

\*Value corrected for specimen deformation

8. Mechanical Properties  
(M. Tokar, A. Gonzales)

A. Hot Hardness: The hot hardness apparatus

currently in use has a maximum temperature capability of about 1000°C, but planned modifications will provide a capability of 1800°C. This will be achieved largely through the substitution of more refractory materials for those now in use. The radiation shields will be Ta instead of stainless steel and the indenter will be B<sub>4</sub>C rather than diamond or sapphire. A schematic diagram of the new design is shown in Figure 463-3.

Hot hardness measurements are being made with the original equipment on plutonium-uranium carbides at temperatures up to 1000°C. A diamond indenter is being used with a 200 g load. The hot hardness of a PuC specimen and a U<sub>0.5</sub>Pu<sub>0.5</sub>C specimen, each containing about 10 v/o sesquicarbide, are shown in Fig. 463-4. At least 5 indentations were made at each temperature and the mean values are plotted in the figure along with the highest and lowest values obtained at each temperature. As might be expected, the PuC is softer at elevated temperatures than the solid

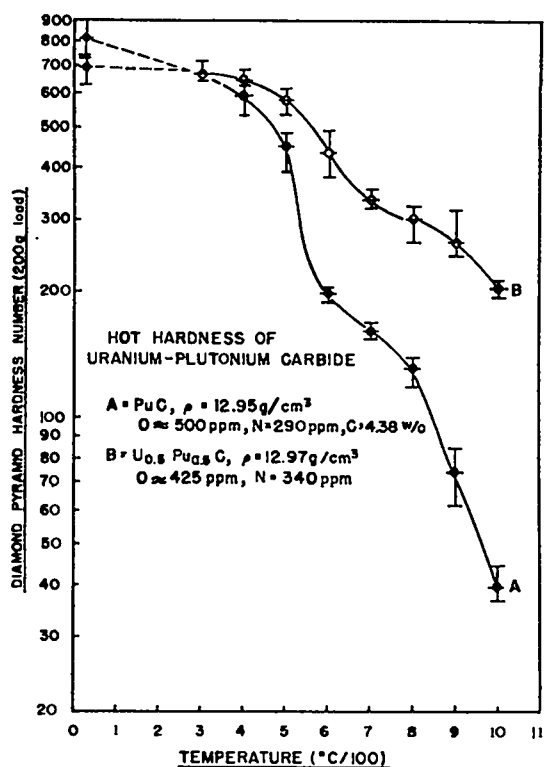


Figure 463-4. Hot Hardness of (U Pu)C

solution U<sub>0.5</sub>Pu<sub>0.5</sub>C, which at 1000°C still has a hardness of about 208 DPH. (As a comparison, 347 stainless steel has a hardness at room temperature of about 150 DPH and 25 DPH at 1000°C.) Since no information is available in the literature on the hot hardness of these materials, no comparison can be made with other data. The study is continuing with emphasis to be placed on the effect of carbon content (and secondary phases) on the hot hardness of PuC and U<sub>0.5</sub>Pu<sub>0.5</sub>C solid solutions.

B. Creep: The Optron extensometer is being installed to provide a means of measuring creep in situ.

#### IV. ANALYTICAL CHEMISTRY

##### 1. Determination of O<sub>2</sub> in Refractory Oxides, Carbides, and Nitrides

(M. E. Smith, J. E. Wilson, and C. S. MacDougall)

Modifications to the methods for determining O<sub>2</sub>, which greatly affects the properties of refractory oxides, carbides, and nitrides, are being investigated to improve the analyses of ceramic-type materials. One promising modification is impulse heating in which

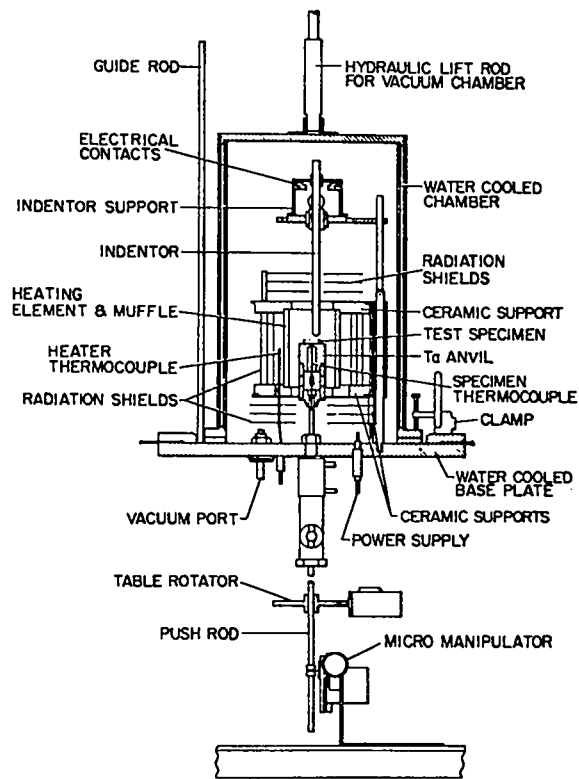


Figure 463-3. Hot Hardness Instrument

a high current of short duration is passed through a covered graphite crucible holding the sample. The sample is rapidly heated to about 3000°C and the O<sub>2</sub> evolved from the sample as CO is measured on a gas chromatograph. Apparent advantages of impulse heating over induction heating include: high sample temperatures rapidly attained, little outgassing from the small capsules, short analysis time, and elimination of sample loss by using covered capsules.

Initial tests of an impulse heater fabricated at LASL showed that some pitting occurred on the electrode surfaces contacting the graphite capsule. Changes made in the shapes of the electrode and capsules greatly reduced the amount of pitting and increased the temperature attained to slightly above 3400°C, as verified by the fact that tungsten melted in two test capsules. Analyses of test samples of CuO for O<sub>2</sub> were reproducible, and the chromatograph peak areas were a linear function of the quantities of O<sub>2</sub>. Further tests will be made using U<sub>3</sub>O<sub>8</sub> samples before Pu materials are analyzed.

A second modification being investigated is the use of a microwave-excited emissive detector system to measure the O<sub>2</sub> evolved as CO from the sample as it is heated to 2000°C in a graphite crucible. Microwave excitation of the CO causes a glow discharge that is photometrically monitored, and the O<sub>2</sub> concentration is calculated from the time-integrated signal from the photometer. Apparent advantages possible with this modification are rapidity of analysis, applicability to small (10- to 60-mg) samples, and continuous recording of CO evolved which aids greatly in selection of optimum operating conditions. Repeated analyses of U<sub>3</sub>O<sub>8</sub>, ThO<sub>2</sub>, Nb<sub>2</sub>O<sub>5</sub>, and Ta<sub>2</sub>O<sub>5</sub> test samples using this measurement system showed that the precision (1σ) of the method did not exceed 3 relative percent. More rigid control of operating conditions is being tried to improve the precision.

#### V. REFERENCES

1. Annual Status Report on the Advanced Plutonium Fuels Program for FY 1968, Report LA-3993-MS, p. 35.

2. A.L. Bowman, J. Inorg. Nucl. Chem. 19, 111 (1966).
3. J. T. Dalton, E. A. Harper, H. J. Hedger, and R. W. Starnard, AERE-R 5948 (1969).
4. F. Caligura, L. Maitinot, G. Diayckaerts, Bull. Soc. Chim. Belges 76, 5 (1967).
5. G.M. Campbell, J. Phys. Chem. 73, 350 (1969).
6. R. A. Kent and J. A. Leary, Los Alamos Scientific Laboratory Report LA-3902 (1968).
7. R. A. Kent, High Temperature Science 1, 169 (1969).
8. R. A. Kent and J. A. Leary, High Temperature Science 1, 176 (1969).
9. J. B. Mann, J. Chem. Phys. 46, 1646 (1967).
10. M. H. Rand, "A Thermochemical Assessment of the Plutonium-Carbon System," Presented at IAEA, Vienna, September 1968.
11. JANAF Thermochemical Tables, The Dow Chemical Co., Midland, Mich. (1965).
12. J. A. Leary, "Present Status of the Uranium-Plutonium-Carbon System," presented at the International Symposium on Ceramic Nuclear Fuels, Am. Ceram. Soc., Wash., D. C. (May 1968).
13. G. D. Blue, J. W. Green, R. G. Bautista, and J. L. Margrave, J. Phys. Chem. 67, 877 (1963).

#### VI. PUBLICATIONS

1. R. A. Kent, "Mass Spectrometric Studies of Plutonium Compounds at High Temperatures. III. The Vapor Pressure of Plutonium," High Temperature Science 1, 169 (1969).
2. R. A. Kent and J. A. Leary, "Mass Spectrometric Studies of Plutonium Compounds at High Temperatures. IV. The Vaporization of PuN," High Temperature Science 1, 176 (1969).
3. R. A. Kent, "Mass Spectrometric Studies of Plutonium Compounds at High Temperatures. V. The Plutonium-Carbon System," presented at the International Conference on Mass Spectroscopy, Kyoto, Japan, September 8-12, 1969.
4. J. A. Leary and R. A. Kent, "Ceramic Plutonium Fuel Materials Research at Los Alamos Scientific Laboratory," invited paper presented at the Japan Atomic Energy Research Institute, Tokai-Mura, Japan, September 17, 1969.

PROJECT 464

STUDIES OF Na-BONDED (U,Pu)C LMFBR FUELS

Person in Charge: D. B. Hall  
Principal Investigator: R. H. Perkins

---

I. INTRODUCTION

Mixed carbide is regarded as an attractive alternate to mixed oxide as fuel for commercial LMFBR application. The high heavy-atom density and thermal conductivity of the mixed carbide make it possible for this fuel to outperform mixed oxides. Full exploitation of carbides dictates the use of a gap between fuel and clad to accommodate fuel swelling (with minimal fuel-cladding mechanical interactions) and a high thermal conductivity path across the gap to limit fuel temperature. The conditions can be met by filling the annulus between fuel and clad with sodium.

Before a satisfactory sodium-bonded fuel element can be developed, however, information is required that will identify the number and severity of problems associated with sodium bonding and will suggest solutions to these problems. Problem areas that are being studied in this experimental program are:

1. The mechanisms and kinetics of carbon transfer to claddings through the sodium bond.
2. The significant fuel and sodium variables that affect compatibility.
3. The consequences of exposing fuel to coolant sodium.
4. The performance limitations of the sodium bond under high-heat-flux conditions.

High purity single-phase (U<sub>0.8</sub>Pu<sub>0.2</sub>)C is the principal fuel used in these investigations. Type 316 stainless steel is the base cladding material being studied, though vanadium alloys also are

being tested.

As prerequisites for this compatibility program, a number of developmental efforts have been undertaken. These include establishment of (1) techniques for the production of single-phase monocarbide pellets of known composition and dimensions, and (2) techniques and equipment for fuel pin loading, bonding, and inspection.

II. SYNTHESIS AND FABRICATION OF FUEL PELLETS  
(R. Honnell, S. McClanahan, R. Walker,  
G. Moore, C. Baker)

A. General

Standardized procedures for producing single-phase monocarbide pellets of known composition and dimensions have been developed. These pellets will be utilized in EBR-II irradiation experiments and compatibility testing. Basic process steps are:

1. Multiple arc melting of a 60-g mixture of <sup>235</sup>U, Pu, and C using a graphite electrode.
2. Solution treatment of the arc melted ingot for 24 h at 1600°C.
3. Crushing and grinding of the ingot in a WC vibratory mill, followed by screening of the resulting powder to a particle size range of  $\leq 62 \mu$ .
4. Elimination of higher carbides by reaction with H<sub>2</sub> at 850°C.
5. Cold compaction at 20 tsi into pellets without the use of binders or sintering aids.
6. Sintering the pellets in Ar at 1800°C for 4 h followed by heat treatment for 2 h at 1400°C.

7. Characterization of the pellets by linear dimensioning, weighing, metallography, x-ray diffraction analysis, chemical analysis for U, Pu, C, N, O, and trace impurities, radiography for determination of possible internal cracks, and isotopic analysis of uranium and plutonium.

#### B. Current Results

Pellets with varying carbon contents were prepared and characterized for the purpose of determining the compatibility of hyperstoichiometric (U,Pu)C material composed only of monocarbide (MC) and sesquicarbide ( $M_2C_3$ ) phases with potential fuel clad and metal coolant systems.

Weighed charges of plutonium, uranium, and carbon totaling approximately 65 g were alloyed by arc melting using 6 remelts to homogenize. The alloyed buttons were reduced to -325 mesh powder, and the powder pressed at 10 tsi into 0.283-in.-diam x 0.266-in.-long pellets. The green pellets were sintered in flowing Ar for the times and temperatures listed in Table 464-I. Dimensional shrinkage during

Table 464-I

Sintering Conditions and Densities of MC- $M_2C_3$  Pellets

Lot Number	Sintering Conditions		Immersion Density (g/cm <sup>3</sup> )
	Temp (°C)	Time (h)	
HNL8-36-1	1525	33	11.86
HNL8-36-2	1525	33	12.03
HNL8-38-1	1550	24	10.61
HNL8-38-2	1550	24	10.35
HNL8-40-1	1550	24	10.23

sintering decreased with increasing carbon-to-metal ratios and amounted to 7% for pellets with a C/M atomic ratio of 1.15.

The pellets were sampled by lot and subjected to chemical, x-ray radiographic, metallographic, and crystallographic analyses as well as density measurements. The results from these analyses are shown in Table 464-II.

Tungsten contamination varying from 40 to 300 ppm is apparent in four of the lots; this was probably introduced during the milling operation. The 2200 ppm N reported for HNL8-40-1 is undesirably high, apparently anomalous, and without explanation.

Table 464-II  
Chemical Composition of MC- $M_2C_3$  Pellets

Element	Chemical Composition* of Pellet Lots				
	HNL8-36-1	HNL8-36-2	HNL8-38-1	HNL8-38-2	HNL8-40-1
U	76.5 w/o	76.1 w/o	76.3 w/o	75.6 w/o	75.4 w/o
Pu	18.33 w/o	18.61 w/o	18.41 w/o	18.62 w/o	18.38 w/o
C	5.32 w/o	5.46 w/o	5.58 w/o	5.78 w/o	6.02 w/o
Al	--	10	--	--	--
Si	30	12	40	25	10
V	**	5	5	5	5
Cr	5	12	12	--	10
Fe	--	35	100	65	75
Cs	50	--	25	5	5
Cu	--	--	--	--	25
Zn	--	20	20	20	20
Ga	20	**	**	**	**
Mo	25	**	10	10	--
W	--	40	300	100	120
O	430	360	850	610	390
N	87	320	650	102	2200

\*ppm by weight, unless otherwise specified.

\*\*Not reported.

--Below detectable limits.

The reason for the 850 ppm O content of HNL8-38-1 also is unknown.

Metallographic examination of the sintered pellets indicates that they are quite porous and contain three phases. The two major phases appear to be MC and  $M_2C_3$ ; this is corroborated by x-ray diffraction measurements (Table 464-III). The third phase is very minor, acicular in shape, and of unknown chemistry. There is not enough of this phase to identify by either x-ray powder diffraction or microprobe examination.

Table 464-III  
Lattice Parameters, Å

Lot Number	MC	$M_2C_3$
HNL8-36-1	4.9643	8.0986
HNL8-36-2	4.9628	8.0970
HNL8-38-1	4.9619	8.0967
HNL8-38-2	4.9633	8.0953
HNL8-40-1	4.9555	8.0941

III. LOADING FACILITY FOR TEST CAPSULES  
(D. N. Dunning, J. O. Barner, J. A. Bridge)

#### A. General

A prerequisite to a compatibility program involving (U,Pu)C and sodium is a satisfactory

capsule loading and bonding facility. There is little point to obtaining well-characterized materials for testing if these materials are subject to contamination by impurities before they are placed in test. Sodium and (U,Pu)C are sufficiently reactive that all operations must be performed either in vacuum or in a high quality inert atmosphere. The loading facility for handling these materials has been constructed and is operational. The facility consists of inert-atmosphere gloveboxes equipped with inert-gas cleanup systems to provide an environment for handling fuel pellets and bonding sodium with a minimum of contamination.

#### B. Current Results

During this reporting period, four EBR-II irradiation test capsules were loaded and bonded. Capsule 37B was then shipped to EBR-II; 38B, 39B, and 40B, containing 90% dense (U,Pu)C pellets bonded with high purity sodium, have passed nondestructive tests and are ready for shipment. Problems encountered with bonding procedures, and from chips in the sodium annulus between the fuel pellets and the cladding, have been solved. A centrifuge was designed and built that provides proper forces to move chips to the bottom of the elements without producing new chips. There is also provision for heating so that the proper temperature gradient is available to give a bottom-to-top freezing pattern in the element during centrifugation. Certain parameters of the successful bonding procedure are given in Table 464-IV. The sodium quality in the

Table 464-IV

Operating Conditions for Bonding Centrifuge

Fuel Stack Region	Time to Freeze (min)	Temperature at Start of Centrifuging (°C)
Top	11	300
Middle	5	230
Bottom	1-1/2 to 2 (estimated)	150

Centrifuge speed 125 rpm

four completed elements is excellent; chief impurities are 7-16 ppm oxygen, < 10 ppm carbon, and < 1 ppm nitrogen.

Approximately 40 capsules for out-of-pile compatibility testing and metal fuel OWR experiments were also loaded during this quarter.

#### IV. CARBIDE FUEL COMPATIBILITY STUDIES (F. B. Litton, H. A. O'Brien, Jr., A. E. Morris, L. A. Geoffrion)

##### A. General

The objectives of this program are to study the interactions among single-phase mixed uranium-plutonium carbide, a sodium bond, and potential cladding materials, i.e., to investigate the technology related to sodium-bonded fuel elements. There are two approaches to the experimental work. The primary approach is to determine the reactions occurring between single-phase  $(U_{0.8}Pu_{0.2})C$  and potential cladding materials, using Type 316 stainless steel and a high strength vanadium-base alloy as the first and second choices of cladding material, respectively. (The experimental work on high strength vanadium-base alloys will be de-emphasized in the future and restricted to obtaining the data from specimens now in test.) The secondary approach is to study the fundamental aspects of the mechanism of carbon transport through sodium, the effect of impurities such as oxygen, and the carburizing potential of sodium in mutual contact with carbides and the preferred cladding materials.

Capsules containing sodium-bonded, single-phase (U,Pu)C are tested in sodium loops at 750°C for periods up to 10,000 h. High purity, thoroughly-characterized sodium is used for the studies. Fuels of known composition are used in the tests. Most of the testing is performed on single-phase (U,Pu)C fuel in which the Pu/U ratio is maintained at 0.25, but some experiments are being carried out on material containing a second phase (either metallic or carbon-rich). Of particular interest is mixed carbide fuel containing ~ 10 v/o sesquicarbide. Other experiments employ stoichiometric and hyperstoichiometric UC to determine the effect of plutonium addition on the behavior of carbide fuel.

##### B. Current Results

###### 1. Compatibility Studies

Experiments are being run to compare the compatibilities of (a) sodium-bonded, single-phase, mixed-carbide fuel prepared by LASL and (b) fuel prepared by United Nuclear Corporation containing ~ 10 v/o sesquicarbide with Type 316 stainless steel and V-15Cr-5Ti alloy capsules. This series of tests (750°C for 4000 h) will end during the next quarter.

Although sodium-bonded, single-phase, mixed-carbide fuel was previously shown to be compatible with Type 316 stainless steel under these test conditions, these additional capsules are being tested for statistical and comparative purposes.

## 2. Studies of Carbon Transfer in Sodium

Carburization of potential cladding alloys in sodium is thought to be a diffusion-controlled process in which the difference between chemical activity of carbon in the source and in the clad is the primary driving force. It is apparent that relatively long periods of time may be required to establish equilibrium in a given system, and that the activities of the carbon and metals in the source and the cladding alloy change during the carburizing process. This, of course, implies that the rate-controlling step also may change; but, in the case of sodium-bonded fuel capsules where the surface areas of the source and sink are nearly equivalent, carbon transfer appears to depend on the rate of carbon diffusion in the carbide source. Carbon is assumed to be soluble in sodium to some small but finite amount. While the transfer mechanism may be contingent on the formation of a particular species in the sodium, the end products of the reaction are independent of the transferring species. Carburization of cladding alloys using carbon sources of different chemical activities are being studied in an attempt to determine the rate-limiting step in the reaction. Current results from these studies are described below.

### Reaction of Sodium-Bonded UC<sub>1.07</sub> with Type 316 Stainless Steel

A series of Type 316 stainless steel capsules was loaded with ~ 5 g sodium, a Type 316L stainless steel tab, and UC<sub>1.07</sub> pellets. The UC<sub>1.07</sub>, containing 5.13 w/o carbon, 130 ppm oxygen, and 100 ppm nitrogen, was heat-treated for 100 h at 1350°C to convert the dicarbide phase in the cast material to sesquicarbide. The metallographic structure after heat treatment consisted of sesquicarbide distributed in a monocarbide matrix, with trace amounts of dicarbide phase generally associated with the sesquicarbide phase. The structure is shown in Fig. 464-1.

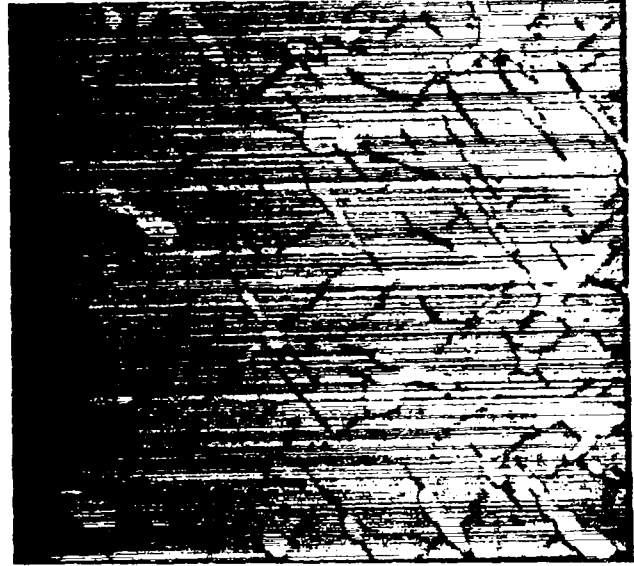


Fig. 464-1. Metallographic structure of UC<sub>1.07</sub> after heat-treating 100 h at 1350°C. Etched, 1000X.

The capsules were heated to 550, 650, and 750°C for 500 and 1000 h. The materials were then analyzed and examined metallographically for evidence of carbon transfer.

The capsule walls showed no carburized surface layer after heating at 650 and 750°C for 500- and 1000-h periods. However, carbide precipitation was observed in the grain boundaries and matrix of the stainless steel. As the base alloy contained ~ 500 ppm carbon, the observed precipitation was attributed to the rejection of carbon from solution during the heat-treating procedure. The tabs heated for 500 h at 650 and 750°C contained 140 and 90 ppm carbon, respectively. The original carbon content of the tabs was 175 ppm, so it appears that no significant carbon transfer occurred. The surface structure of the Type 316 stainless steel capsule after the 1000-h test at 750°C is shown in Fig. 464-2.

Metallographic examination of the UC<sub>1.07</sub> carbide source indicated that no reaction had occurred between the sodium and the monocarbide and sesquicarbide phases in the system during the 500- and 1000-h tests at 650 and 750°C. However, in the sodium contact area, the sources were depleted in the dicarbide phase to the following depths (Table 464-V).



Fig. 464-2. Type 316 stainless steel capsule wall after testing in sodium with  $UC_{1.07}$  for 1000 h at  $750^{\circ}C$ . Etched, 300X.

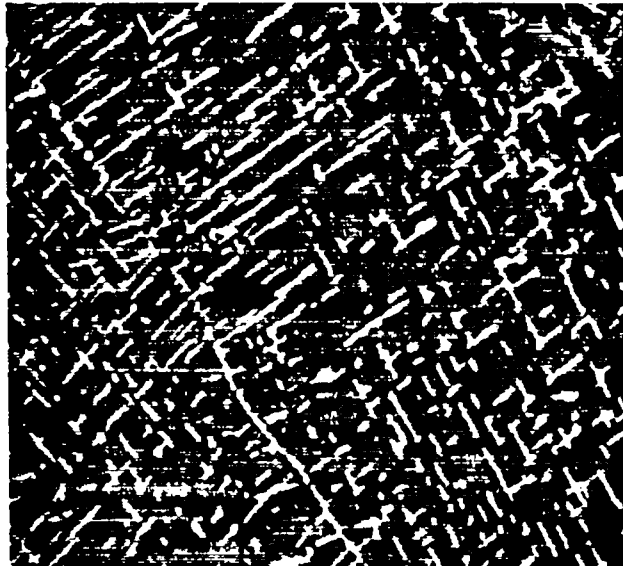


Fig. 464-3. Structure showing depletion of the dicarbide phase in sodium-bonded  $UC_{1.07}$  pellet heated 1000 h at  $750^{\circ}C$  in Type 316 stainless steel capsule. Etched, 300X.

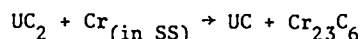
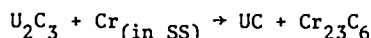
Table 464-V

Depths of Dicarbide Depletion in  $UC_{1.07}$  Sources

Test Time (h)	Temp ( $^{\circ}C$ )	Area of Carbide Source ( $cm^2$ )	Depth of Dicarbide Depletion (microns)
500	650	1.36	218
1000	650	1.08	283
500	750	1.33	385
1000	750	1.67	867

The metallographic structure in the dicarbide-depleted area of the source heated for 1000 h at  $750^{\circ}C$  is shown in Fig. 464-3. The extent of decarburization is shown by comparing Fig. 464-3 with Fig. 464-1.

Since the reactions:



involve negative free-energy changes, the carbon in a carbide fuel in excess of the monocarbide may be available to transfer to the cladding. Calculations were made to see how fast, within an order of magnitude, carbon would be expected to diffuse out of solid, crack-free UC. The calculations were based on the work of Lee and Barrett,<sup>1</sup> whose values of the diffusivity of carbon in UC are in generally

good agreement with earlier work. Their lowest experimental temperature was  $1200^{\circ}C$ , so an extrapolation of  $300-400^{\circ}C$  to reasonable fuel surface temperatures was required. This extrapolation, plus the predominance of grain boundary diffusion at lower temperatures, introduces considerable uncertainty into the calculations.

Assume fuel contains 5.1% carbon. Assume limits on stoichiometry of UC to be 4.82 and 4.92% carbon (i.e., composition can vary between these limits and still be single-phase). The times required to deplete the hyperstoichiometric carbon to a depth of  $10\ \mu m$  are then:  $650^{\circ}C$ ,  $1.5 \times 10^7$  h;  $750^{\circ}C$ ,  $5 \times 10^5$  h;  $850^{\circ}C$ ,  $3 \times 10^4$  h;  $950^{\circ}C$ ,  $3 \times 10^3$  h. These calculations show that carbon diffuses very slowly from a UC matrix below  $950^{\circ}C$ . Because the rate of diffusion of carbon in sodium is several orders of magnitude greater than the rate of diffusion of carbon in UC, the penetration of sodium into cracks or grain boundaries can result in much faster removal of carbon than would be calculated by diffusion of carbon in UC alone. Cracking of the carbide may explain the rapidity of carbon removal from the  $UC_{1.07}$  source in this experimental work.

The removal of carbon from the source without detectable carbon pickup by the Type 316 stainless steel was also observed during tests on the carburization of Type 316 stainless steel using  $Fe_3C$

sources. It is apparent that carbon in the sodium must reach a certain concentration (activity) prior to initiation of carburization of the fuel container. After the 500-h tests, the sodium contained 50 and 40 ppm carbon at 650 and 750°C, respectively.

#### Reaction of Sodium-Bonded $UC_{1.43}$ with Type 316 Stainless Steel

Arc-cast uranium carbide ingots were crushed to  $-1/4$  in. + 10 mesh under an argon atmosphere. The sized material was heat-treated for 100 h at 1350°C. Metallographic examination after heat treatment showed the structure was free of the di-carbide phase and consisted of uranium monocarbide dispersed in a sesquicarbide matrix. The structure is shown in Fig. 464-4. The material contained

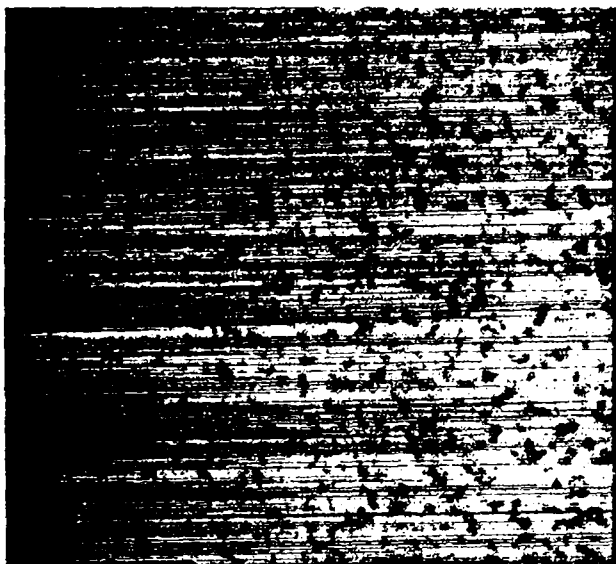


Fig. 464-4. Structure of  $UC_{1.43}$  after heating 100 h at 1350°C. Etched, 600X.

6.74 w/o C. Type 316 stainless steel and vanadium (V-15Cr-5Ti) alloy capsules are being loaded with the sesquicarbide material for compatibility. After nondestructive examination, they will be placed in test.

#### 3. Carburization of Type 316L Stainless Steel

The carburization of metallic chromium can result in the formation of one or more of the following carbides:  $Cr_{23}C_6$ ,  $Cr_7C_3$ , or  $Cr_3C_2$ . The  $Cr_{23}C_6$  phase is stable in equilibrium with metallic chromium, and the  $Cr_3C_2$  phase is stable in equilib-

rium with carbon.<sup>2</sup> The carburization of a chromium-containing alloy such as Type 316 stainless steel is more complicated than the carburizing of pure chromium for at least two reasons: (a) as carburization of the alloy proceeds, the amount and the activity of chromium in the metal phase decreases, and (b) the carbides that are formed are not simple chromium carbides; they are ternary or higher carbides containing other metals. (The carbides formed in Type 316 stainless steel contain mostly chromium, but also iron, molybdenum, and possibly manganese are present.)

In an attempt to determine experimentally the composition and crystal structure of the carbide and matrix phases in Type 316 stainless steel as a function of the extent of carburization, 60 specimens of Type 316L sheet were gas-carburized to various carbon contents up to about 1.7 w/o C. The experimental procedure was as follows:

1. Samples of 316L sheet, 0.030-in.-thick, 1/2-in.-wide, and 2-in.-long, were lightly sanded with 360 grit paper, washed in acetone, and identified. The samples were weighed to the nearest 0.1 mg (each sample weighed about 4.7 g) after dimpling the samples to keep them separated in the test fixture.
2. The samples were inserted into the hot zone of a tube furnace through which high purity  $H_2$  flowed. A few seconds after sample insertion, high purity  $CH_4$  was mixed with the  $H_2$  and admitted to the furnace. The carburizing temperature was  $970 \pm 15^\circ C$ .
3. The samples were left in the furnace for various times, up to several hours, depending on the amount of carbon pickup desired.
4. After removal from the furnace, the samples were reweighed.
5. The samples were then placed in nickel capsules (about 7 samples per capsule), and welded shut under argon. The nickel capsules were then placed in a tube furnace and heated to  $\sim 985^\circ C$  for 94 h.
6. The capsules were then cooled to 750°C and held at that temperature for 120 h. Subsequently the samples were furnace-cooled to room temperature.

7. The samples were removed from the nickel capsules and reweighed. They were then chemically analyzed for carbon.
8. The specimens were metallographically examined prior to carbide extraction and matrix analyses, which is in process at the present time.

Metallographic examination of the specimens showed that the carbides were uniformly distributed throughout the cross section. The specimens contained from 640 ppm to 1.65 w/o C; the lower amount of carbon was readily detected as a precipitate in the Type 316L structure, and the amount of carbide precipitation increased with increasing carbon content. The metallographic structures for the minimum and maximum carbon pickup are shown in Figs. 464-5 and 464-6, respectively.

4. Solubility of Uranium, Plutonium, and Mixed Carbides in Sodium

A delayed neutron counting procedure is to be used to determine the solubility of  $^{235}\text{U}$  and  $^{239}\text{Pu}$  in sodium, using metallic uranium and plutonium, as well as (U,Pu)C as sources. In these tests, it is planned to heat one pellet of the three materials with ~ 100 g sodium for 100 to 1000 h at 450, 550, and 650°C in Ta-10W alloy crucibles. After testing, ~ 2 g sodium will be trepanned from the crucible, the uranium and/or plutonium chemically separated, and the residue irradiated at ORNL. The test is designed to measure uranium and plutonium solubility in the parts per billion range.

During this period the basic equipment was assembled and tested. An isometric drawing of the basic equipment is shown in Fig. 464-7.

5. Behavior of Vanadium Alloys in Sodium

At the direction of AEC-DRDT, experimental work on this phase of the project is being discontinued. Vanadium alloy materials recently received from Westinghouse Astronuclear Laboratory and Argonne National Laboratory had been placed in hot-trapped sodium for 1000-h tests at 450 and 650°C just prior to receipt of the AEC directive. The objective of the work in process is to determine the stability of vanadium alloys in sodium containing < 5 ppm oxygen. The following alloy compositions are under test:

V-15Cr-5Ti  
 V-15Cr-5Nb  
 V-15Cr-10Nb  
 V-9.4Cr-3.3Fe-1.2Zr  
 V-8.4Cr-8.9Ta-1.1Zr  
 V-6.1Fe-5.2Nb-1.3Zr

It is planned to discontinue this program upon the completion of these tests.

V. SODIUM-BOND HEAT TRANSFER STUDIES  
 (K. L. Meier)

A. General

The purpose of this project is to evaluate the effects of fuel-pin defects on heat transfer properties of the sodium bond. Such defects could arise in a number of ways. For example, a void in the sodium bond could:

1. Be present before insertion in the reactor.
2. Come from dewetting of the pellet due to change in composition as fission products are formed.
3. Form from a hot spot on the pellet and consequent local vaporization of the sodium, and/or
4. Be produced from desorbed or fission-product gases.

Of these, probably the most serious defect would be the presence of fission gas bubbles in the bond region.

One method of obtaining the high heat fluxes necessary for "defect analysis" consists of utilizing a central, high-heat-flux heater. This method is being utilized at LASL in sodium-bond heat transfer studies.

B. Current Results

Much of the apparatus for out-of-pile testing of sodium bonds utilizing a central, high-heat-flux heater has been fabricated and tested. The completed portions include:

1. Graphite rod heater with boron nitride insulation.
2. UC cylinder.
3. Sodium test loop. Because this loop had a high pressure drop, portions of it were replaced during this reporting period. Tests indicate that the pressure drop has



Fig. 464-5. Carbide distribution in Type 316L stainless steel. Carburized to contain 640 ppm C. Electrolytic etch, 300X.

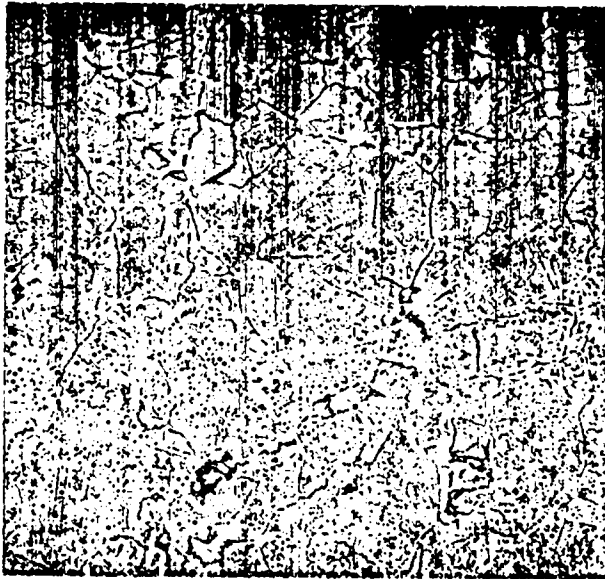


Fig. 464-6. Carbide distribution in Type 316L stainless steel. Carburized to contain 1.65 w/o C. Electrolytic etch, 300X.

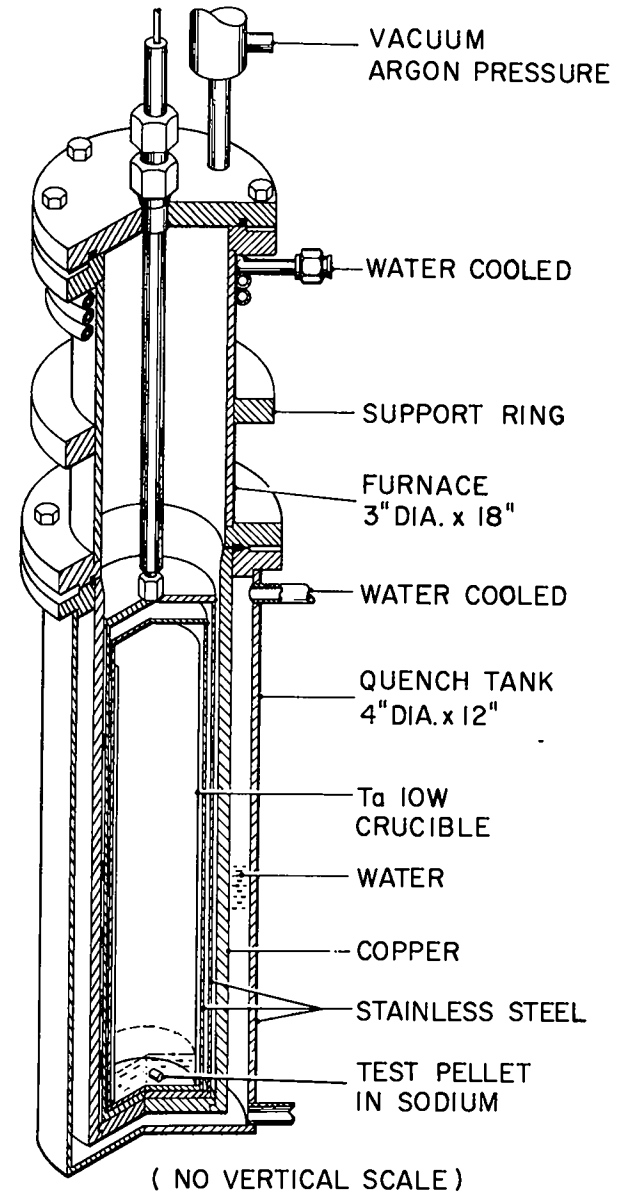


Fig. 464-7. Isometric drawing of equipment designed for determining the solubility of uranium and plutonium in sodium.

been reduced and the correct flowrate has been achieved.

Cladding temperatures during test will be measured with 40 thermocouples held in a fixture which can be rotated about the "fuel pin" so temperatures can be measured in 0.100-in. intervals horizontally and vertically on the cladding. The outer structure of this "thermal scanner" consists of three subassemblies. Drawings of these three subassemblies were made; fabrication of the outer structure is 30% complete and full completion is scheduled for December 15, 1969. Fabrication was completed on the motor mount, electrical connector plate, conductor shell, and sodium tube. All of the parts for the mounts which hold the 40 thermocouples have been fabricated. The stand for the thermal scanner was designed and drafting has begun.

A computer program was written to reduce the data obtained from the thermal scanner. The program takes the thermocouple readings from paper tape and prints out a temperature map of the cladding surface. When a bubble exists in the bond, temperatures deviate from the "normal," and the map shows the size and shape of the bubble. Subsequent maps plot the bubble movement.

A rigorous analysis of the heat transfer problem in the gas seal region was completed. The maximum O-ring temperature expected in the gas seal region is 210°F. The heat transfer analysis is being extended to the outer shell wall to determine the temperatures expected in the vicinity of the slip ring assembly.

## VI. ANALYTICAL CHEMISTRY (O. R. Simi, R. T. Phelps)

### A. General

Specific analytical techniques have been developed and evaluated to cope with the problems encountered in the investigation of fuel/clad compatibility. The results of many of these special analyses are given in several sections of the report in Project 464. A brief summary of some of the techniques, and the problems to which they were applied, is given below.

### B. Current Results

#### 1. Spectroanalysis of Sodium

A previously described spectrochemical method

for analyzing sodium for impurity elements was made more quantitative by including photometric measurement of the densities of the analytical lines. The reproducibility of the method for measuring six metals was determined by repeated analyses of two synthetic NaCl samples prepared to contain known concentrations of 23 added elements, and standard samples containing 27 elements in the concentration range between 0.3 and 300 ppm with each element at the nominal concentration of the standard. Each sample also contained 100 ppm of germanium as an internal standard. For initial tests, spectrographic exposures were made using a 2-meter ARL spectrograph in a glovebox system. Four spectrographic films were used with a total of four exposures of each of the standards, and twelve exposures of each of the synthetic samples. A computer program was used to calculate concentrations of the six elements from the optical density measurements of two analytical lines for four of the elements and one analytical line for two of the elements (Table 464-VI).

Table 464-VI  
Analysis of Prepared NaCl Samples

Element, and Wavelength (Å)	Sample	Concentration		Rel. Std. Dev. (1 $\sigma$ )
		Added (ppm)	Found (ppm)	
Al, 2575	1	150	129	13
	2	50	54	16
Al, 3082	1	150	133	15
	2	50	51	16
Ca, 3179	1	150	119	11
	2	50	38	17
Cr, 3021	1	50	51	16
	2	150	152	11
Fe, 2488	1	50	50	14
	2	150	134	11
Fe, 3021	1	50	49	14
	2	150	144	8
Mg, 2779	1	150	125	11
	2	50	44	8
Mg, 2782	1	150	130	9
	2	50	37	16
Ni, 3002	1	50	44	12
	2	150	126	10
Ni, 3050	1	50	46	9
	2	150	124	10

The two concentrations obtained by measuring two analytical lines for each element were not statistically different, indicating that either line

could be used. The relative standard deviation ( $1\sigma$ ) ranged between 8 and 17 percent. The fact that several measured concentrations are significantly lower than the known value probably is a result of the large number of elements in the standards and samples. The method will be tested using the hot cell spectrographic facility for repeated analyses of samples and standards having fewer added impurities.

#### VII. REFERENCES

1. A. M. Lee and L. R. Barrett, "Diffusion of Carbon and Uranium in Uranium Carbide," J. Nuc. Mat. 27, 275 (1968).
2. E. K. Storms, The Refractory Carbides, Academic Press, p. 105, 1967.

PROJECT 465

REACTOR PHYSICS

Person in Charge: D. B. Hall  
Principal Investigator: G. H. Best

---

I. INTRODUCTION

Basic to the evaluation of various fast breeder concepts and proposals are the analytical techniques and physical data used in the analyses. Valid comparisons between different concepts and proposals depend on minimization of differences in results due to methods of analyses. To this end, the Los Alamos Scientific Laboratory is cooperating with other AEC laboratories and contractors in the development of evaluated cross-section data and associated processing codes. In addition, the Laboratory is working on the development and maintenance of digital computer programs pertinent to the nuclear analysis of fast breeder concepts. The Laboratory is also adapting, modifying, and evaluating modular programming systems for comprehensive nuclear analysis. Finally, the Laboratory is evaluating the performance characteristics of various fast breeder reactor concepts.

II. CROSS-SECTION PROCUREMENT, EVALUATION, AND TESTING (M. E. Battat, D. J. Dudziak, R. J. LaBauve, R. E. Seamon)

A. General

Accurate predictions of reactor design parameters, such as critical mass, sodium worth, and spectral response, require the development and maintenance of up-to-date basic microscopic nuclear data files. To meet this end, a national cooperative program is in progress to prepare an evaluated nuclear data file (ENDF/B). The large amount of experimental data which is becoming available, together with the theoretical data, makes the maintenance of ENDF/B a continuing task. In addition, a large effort is needed in evaluating and testing the microscopic data prior to use in reactor calculations.

B. Revision of  ${}^6\text{Li}$  and  ${}^7\text{Li}$  Data Sets

A revised version of the ENDF/B library (Version 2) is planned for the fall of 1969. Hence, we are in the process of preparing revised  ${}^6\text{Li}$  and  ${}^7\text{Li}$  data sets for submission to the CSEWG. Minor changes made in 1967 and 1968 by the UKAEA will be incorporated in these data sets. The changes include: 1) extending the lower range of the data from 0.001 to 0.0001 eV, and 2) a slight change in the  ${}^6\text{Li}$  (n, $\alpha$ ) data below 1 keV. Major changes in the form used to describe the secondary neutron energy distributions are being made. Because of restrictions imposed by the ETOE-MC<sup>2</sup> processing codes, the secondary energy distributions in the ENDF/B must be expressed as a discrete energy loss ( $E' = E - \theta$ ) and/or a Maxwellian distribution. The present  ${}^6\text{Li}$  and  ${}^7\text{Li}$  files utilize the discrete energy loss form to describe the secondary energy distribution. It has been found that these distributions, except for the (n,n' $\gamma$ ) reaction, can be equally well approximated by Maxwellian distributions and at the same time reduce the size of the files by about 25%. For the revised sets, wherever possible, the Maxwellian form will be incorporated.

C. Data Testing

We have recently received from the National Neutron Cross Section Center at BNL tapes containing ENDF/B data for H<sub>2</sub>O, D<sub>2</sub>O, polyethylene, graphite, and ZrH. The information on the BNL tapes has been transferred to LASL tapes. Preparation of gallium data for ENDF/B is continuing. The smooth component of the capture cross section (MF = 3, MT = 102) has been altered to give the correct total when added to the resonance component.

#### D. Processing Codes

Work is continuing on the comparison of the three versions of the MC<sup>2</sup> code available at LASL. These three versions (BNLMC2, WAPMC2, and BAWMC2) were described in LA-4284-MS. For a test problem in which multigroup constants for <sup>239</sup>Pu and <sup>12</sup>C were generated, results using the three versions were in excellent agreement. The test problem was run using a P<sub>1</sub> fundamental mode calculation for both the fine- and ultrafine-group options. For the test problem (35 broad groups) using the ultrafine-group option, the central processor and peripheral processor execution times for WAPMC2 were 180 and 1800 sec, respectively; the corresponding figures for BAWMC2 were 160 and 600 sec. It appears that the Rensselaer Polytechnic Institute (RPI) modifications incorporated in BAWMC2 do indeed effect a considerable saving in peripheral processor time. However, the BAWMC2 version requires about 220,000<sub>8</sub> core storage locations as compared to 156,000<sub>8</sub> for WAPMC2. A problem has also been run using a consistent P<sub>1</sub> fundamental mode calculation (ultrafine-group option) for anisotropic neutronics with all three versions. Results obtained were in good agreement.

An unexplained difficulty in the MC<sup>2</sup> code has been that group-averaged self-scatter cross sections ( $\sigma_{g \rightarrow g}$ ) as output by the MC<sup>2</sup> code often occur as negative numbers in the resonance region for the heavy nuclides. In MC<sup>2</sup>,  $\sigma_{g \rightarrow g}$  is computed last and is taken as the broad-group transport cross section minus the sum of all other reaction and transfer broad-group cross sections. The reason that it is possible for the broad-group transport cross section to be less than the sum of cross sections for all other reactions and transfers, lies in the fact that, in the fine-group cross-section computation in MC<sup>2</sup>, the elastic scattering component is calculated using a reciprocal averaging  $\langle 1/\sigma_e \rangle^{-1}$ ; whereas all others, including the elastic downscatter, are calculated using a direct average  $\langle \sigma_e \rangle$ . Normally, if the cross section is a relatively slowly varying function of energy, the difference between the two methods is not very great. The elastic scatter cross sections for a heavy nuclide in the resonance region is certainly not in this category, however, as is shown in Fig. 465-1 for <sup>238</sup>U. For a

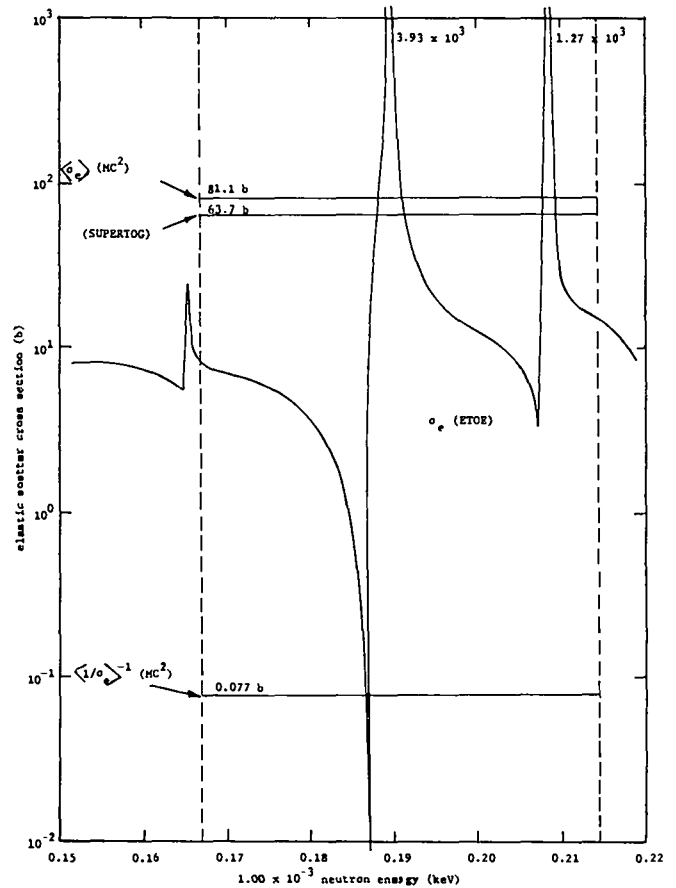


Fig. 465-1. Elastic scatter cross section for <sup>238</sup>U.

broad group in this region from 0.167 to 0.214 keV, reciprocal averaging  $\langle 1/\sigma_e \rangle^{-1}$  gives a value of 0.077 b, whereas direct averaging  $\langle \sigma_e \rangle$  gives 81.1 b. Also shown in the figure is a value of 63.7 b obtained using the SUPER TOG code<sup>1</sup> recently activated at LASL.

Figure 465-2 shows group-averaged elastic transport cross sections  $[\sigma_e(1 - \bar{v}_L)]$  as computed by: MC<sup>2</sup> using reciprocal averaging; MC<sup>2</sup> using direct averaging; and SUPER TOG for <sup>238</sup>U for an energy range from 50 eV to 10 keV. The energy intervals correspond to 0.25 lethargy increments.

An option will be put into MC<sup>2</sup> allowing the user to choose either direct or reciprocal averaging for the elastic transport cross section.

The WAPMC2 code has been used in other comparisons with the ENDF/B multigroup processing code, SUPER TOG. The SUPER TOG code is limited to an "all fine" treatment of the data (69, 99, or 299 groups)

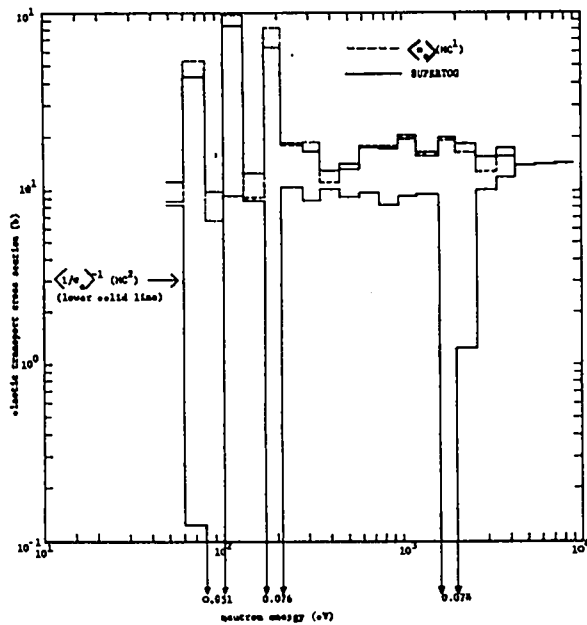


Fig. 465-2. Group averaging transport cross section for  $^{238}\text{U}$ .

but is capable of generating multigroup cross sections up to  $P_8$ , whereas only two tables ( $P_0$  and  $P_1$ ) are generated by  $\text{MC}^2$ . Comparative calculations were performed for two heavy nuclides,  $^{238}\text{U}$  and  $^{239}\text{Pu}$ , and two light nuclides,  $^{12}\text{C}$  and  $^{14}\text{N}$ . It can be seen from Table 465-I that for the heavy nuclides there is general agreement for all cross sections, except the elastic scatter for  $^{238}\text{U}$ , the reason for poor agreement in this case being noted in the table and discussed above. The agreement for the light nuclides is also good, as shown in Table 465-II, but there are some serious differences in the high-energy elastic components which need further investigation.

#### E. Shielding Methods

The Los Alamos Photon Production code (LAPH) retrieves data from the ENDF/B file and constructs a photon production matrix for  $N$  neutron-energy groups and  $G$  photon-energy groups. Work is now in progress toward calculating a photon source vector  $S(\vec{r})$  using the  $G \times N$  photon production matrices  $\sigma_{p1}$ , the atom number densities  $A_1$ , and the neutron broad-group flux vectors  $\phi(\vec{r})$ , where the subscript  $i$  refers to the  $i$ th material in the zone

corresponding to radius  $\vec{r}$ :

$$S(\vec{r}) = \left( \sum_1 A_1 \sigma_{p1} \right) \phi(\vec{r})$$

Flux vectors compatible with the test problem already in use have been obtained from the DTF-IV code for use in debugging.

An LA report describing the LAPH code is being drafted, and minor revisions (principally in output format) are being made in the code. The code will be checked in detail for conformance with the specifications originally outlined for it.

There has been a proposal made to the Shielding Subcommittee of the CSEWG to alter the format for gamma-ray production data in the ENDF/B file. Work is in progress to convert the sodium gamma-ray data into the proposed format in order to estimate the amount of work involved in the translation and to see what changes would be necessitated in the LAPH code.

### III. REACTOR ANALYSIS METHODS AND CONCEPT EVALUATION

#### A. General

A continuing task in fast reactor analysis and evaluation is the improvement of computer programs and the development of new computational methods. In addition to new methods, advances are constantly being made in computer technology which make possible the extension of existing calculational techniques.

#### B. Synthesis of Static Multigroup Transport Theory (R. E. Alcouffe)

As a continuing effort to account for two-dimensional transport leakage effects using one-dimensional transport calculations, the two-dimensional diffusion code 2DB has been modified to accept leakage information from transport calculations. This allows an effective two-dimensional synthesis from one-dimensional calculations. The procedure for doing this is:

1. One-dimensional  $S_n$  calculations are performed in each of the transverse directions on the system,
2. Leakage coefficients applicable to a two-dimensional diffusion theory are calculated from the above calculated fluxes and currents, and

TABLE 465-I  
CROSS SECTION DIFFERENCES BETWEEN MC<sup>2</sup> AND SUPERTO, HEAVY NUCLIDES

Cross Section	<sup>239</sup> Pu Energy Range 1 eV - 87 keV (resonance region only)				<sup>238</sup> U Energy Range 48 eV - 10 MeV			
	Difference		Energy at		Difference		Energy at	
	Average (%)	Maximum (%)	Maximum	Difference	Average (%)	Maximum (%)	Maximum	Difference
Unresolved capture	0.6	1.0	5.5	- 7.1 keV	1.2	2.9	41	- 52 keV
Unresolved fission	0.5	0.7	15	- 19 keV	-	-	-	-
Resolved capture	2.5	5.8	6.5	- 8.3 eV	3.6	8.1	79	- 100 eV
Resolved fission	2.5	9.4	8.3	- 11 eV	-	-	-	-
Total capture	1.4	5.8	6.5	- 8.3 eV	1.5	8.1	79	- 100 eV
Total fission	1.5	8.9	8.3	- 11 eV	1.4	3.4	0.64	- 0.82 MeV
Nu	-	-	-	-	3.1	5.7	6.1	- 7.8 MeV
Total inelastic	-	-	-	-	0.9	2.1	52	- 67 keV
N - 2N	-	-	-	-	3.1	5.7	6.1	- 7.8 MeV
Elastic transport <sup>1</sup>	-	-	-	-	0.2	0.4	15	- 19 keV
Elastic transport <sup>2</sup>	-	-	-	-	95.1	199.5	0.17	- 0.21 keV
Elastic transport <sup>3</sup>	-	-	-	-	13.3	39.2	79	- 100 eV

<sup>1</sup>At energies above the resolved resonance region (above 43 keV)

<sup>2</sup>Resolved resonance region with  $\langle 1/\sigma_e \rangle^{-1}$  averaging

<sup>3</sup>Resolved resonance region with  $\langle \sigma_e \rangle$  averaging

TABLE 465-II  
CROSS SECTION DIFFERENCES BETWEEN MC<sup>2</sup> AND SUPERTO, LIGHT NUCLIDES

Cross Section	<sup>14</sup> N Energy Range 48 eV - 10 MeV			<sup>12</sup> C Energy Range 0.45 keV - 10 MeV		
	Difference		Energy at	Difference		Energy at
	Average (%)	Maximum (%)	Maximum	Average (%)	Maximum (%)	Maximum
Capture	0.2	0.4	0.50 - 0.64 MeV	-	-	-
Total inelastic	1.8	2.3	4.7 - 6.1 MeV	1.9	5.1	4.7 - 6.1 MeV
N - P	0.9	8.9	0.39 - 0.50 MeV	-	-	-
N - α	1.2	2.8	1.1 - 1.4 MeV	5.7	9.3	4.7 - 6.1 MeV
Total elastic (P <sub>0</sub> )	6.5	14.6	6.1 - 7.8 MeV	6.1	20.1	6.1 - 7.8 MeV
Total elastic (P <sub>1</sub> )	11.0	21.0	6.1 - 7.8 MeV	9.1	26.0	6.1 - 7.8 MeV

3. The two-dimensional diffusion calculation is performed on the system to obtain the "synthesized" two-dimensional flux and eigenvalue.

In order to amplify Step 2, examine the leakage term from the two-dimensional cylindrical diffusion leakage expression around the mesh point (V<sub>i</sub>, Z<sub>j</sub>):

$$\begin{aligned}
 \mathcal{L}_{i,j} = & -2\pi \int_{z_{j-\frac{1}{2}}}^{z_{j+\frac{1}{2}}} dz \int_{r_{i-\frac{1}{2}}}^{r_{i+\frac{1}{2}}} r dr \left[ \frac{1}{r} \frac{\partial}{\partial r} \left( r D \frac{\partial \phi}{\partial r} \right) + \frac{\partial}{\partial z} \left( D \frac{\partial \phi}{\partial z} \right) \right] = -2\pi \left( z_{j+\frac{1}{2}} - z_{j-\frac{1}{2}} \right) \\
 & \cdot \left[ r_{i+\frac{1}{2}} D_{i+\frac{1}{2},j} \left( \frac{\phi_{i+1,j} - \phi_{i,j}}{r_{i+1} - r_i} \right) - r_{i-\frac{1}{2}} D_{i-\frac{1}{2},j} \left( \frac{\phi_{i,j} - \phi_{i-1,j}}{r_i - r_{i-1}} \right) \right] - \pi \left( r_{i+\frac{1}{2}}^2 - r_{i-\frac{1}{2}}^2 \right) \\
 & \cdot \left[ D_{i,j+\frac{1}{2}} \left( \frac{\phi_{i,j+1} - \phi_{i,j}}{z_{j+1} - z_j} \right) - D_{i,j-\frac{1}{2}} \left( \frac{\phi_{i,j} - \phi_{i,j-1}}{z_j - z_{j-1}} \right) \right] \quad (1)
 \end{aligned}$$

where the normal finite difference approximation

$$\left. \frac{\partial \phi}{\partial r} \right|_{r_{i+\frac{1}{2}}} \approx \frac{\phi_{i+1,j} - \phi_{i,j}}{r_{i+1} - r_i} \quad \text{etc.,}$$

has been made. Equation 1 is the term normally used to estimate two-dimensional leakage, with the diffusion coefficients being estimated by

$$D_{i,j} = \left( \frac{1}{3\Sigma_{Tr}} \right)_{i,j},$$

where  $\Sigma_{Tr}$  is the transport cross section. Equation 1 may be summarized as

$$\begin{aligned} \mathcal{L}_{i,j} = & R_{i,j}(\phi_{i+1,j} - \phi_{i,j}) - L_{i,j}(\phi_{i,j} - \phi_{i-1,j}) \\ & + T_{i,j}(\phi_{i,j+1} - \phi_{i,j}) - B_{i,j}(\phi_{i,j} - \phi_{i,j-1}). \end{aligned} \quad (2)$$

When currents and fluxes are available from a transport calculation, the equations

$$\begin{aligned} j_{r,i+\frac{1}{2},j} &= -D_{i+\frac{1}{2},j} \left. \frac{\partial \phi}{\partial r} \right|_{i+\frac{1}{2},j} \\ j_{z,i,j+\frac{1}{2}} &= -D_{i,j+\frac{1}{2}} \left. \frac{\partial \phi}{\partial z} \right|_{i,j+\frac{1}{2}} \end{aligned} \quad (3)$$

may be used to more adequately represent the diffusion coefficients appearing in the leakage term. The leakage coefficients of Eq. 2 then become:

$$\begin{aligned} R_{i,j} &= \frac{-2\pi \Delta z_j r_{i+\frac{1}{2}} j_{r,i+\frac{1}{2},j}}{\phi_{i+1,j} - \phi_{i,j}} \\ L_{i,j} &= \frac{-2\pi \Delta z_j r_{i-\frac{1}{2}} j_{r,i-\frac{1}{2},j}}{\phi_{i,j} - \phi_{i-1,j}} \\ T_{i,j} &= \frac{-\pi(r_{i+\frac{1}{2}}^2 - r_{i-\frac{1}{2}}^2) j_{z,i,j+\frac{1}{2}}}{\phi_{i,j+1} - \phi_{i,j}} \\ B_{i,j} &= \frac{-\pi(r_{i+\frac{1}{2}}^2 - r_{i-\frac{1}{2}}^2) j_{z,i,i-\frac{1}{2}}}{\phi_{i,j} - \phi_{i,j-1}}. \end{aligned} \quad (4)$$

This formulation is, therefore, consistent with the discrete two-dimensional diffusion leakage term.

The information supplied to Eq. 4 may be improved by also performing a source flux calculation in the reflector regions of the system. This is done by utilizing leakage information from Step 1.

The above procedure has been tested first by using the two-dimensional  $S_n$  code 2DF to calculate two-dimensional transport fluxes and currents. This information was formulated as leakage coefficients for the diffusion codes; the results of the subsequent diffusion calculation using these coefficients were virtually identical to the results from 2DF. The systems used as a test were described as examples #2 and #4 in Ref. 2. These are small fast, fully reflected cylindrical systems. The procedure described above was tested using one-dimensional transport calculations and using the resulting leakages in the diffusion code. The results of the eigenvalue calculations are shown in Table 465-III.

TABLE 465-III

EIGENVALUES FROM VARIOUS ESTIMATES OF THE TWO-DIMENSIONAL LEAKAGE

Method of Calculation	Eigenvalue	
	Case 2	Case 4
2DF	1.0425	1.0054
2DB <sup>a</sup>	1.1084	1.0226
2DB <sup>b</sup>	1.0412	1.0161
2DB unmodified	0.8782	0.9035
Contribution of leakage to neutron loss	52.5%	50.5%

<sup>a</sup>Using leakage coefficients calculated from core fluxes and currents.

<sup>b</sup>Using leakage coefficients calculated from both core and reflector fluxes and currents.

These preliminary results show that a significant improvement in the eigenvalue is obtained in this example, even though the leakage is more than 50% of the neutron losses.

#### C. Preparation and Maintenance of Code Packages

1. Improvement of Existing  $S_n$  Methods (B. M. Carmichael). The UPDATE program<sup>3</sup> and the CDC-6600 control cards provide facilities for linking free-standing codes. One advantage to UPDATE linking is that no modifications to the codes are required; consequently, the free-standing capabilities are

preserved. In the linking procedure, input and output data files, as well as program files, are stored on the UPDATE tape.

The DTF-IV  $S_n$  code and the DACI perturbation code have been linked by this method. The files on the UPDDATE tape for this case are:

- DTF-IV program
- DACI program
- Regular flux
- Adjoint flux
- Regular angular flux
- Adjoint angular flux
- DTF-IV input
- DACI perturbation input

The steps involved in solving a complete problem are:

1. Read DTF-IV input from regular input stream and store same on UPDATE tape.
2. Solve regular DTF-IV problem and store regular flux and regular angular flux on UPDATE tape.
3. Repeat Step 2 for adjoint problem.
4. Read DACI perturbation input from regular input stream and store same.
5. Recall all data files, except regular and adjoint total flux files from UPDATE tape for input to DACI.

The UPDATE facilities may be used to modify any of the input data files for subsequent runs. For example,  $n$  might be varied in successive DTF-IV runs or the convergence criterion might be varied. Where appropriate, the total flux, either regular or adjoint, would be recalled from the UPDATE tape to restart a problem. Once the DTF-IV problems for a given configuration are solved and the results are stored on tape, any number of different perturbation runs might be executed in which the same DTF-IV flux data are recalled from the UPDATE tape.

## 2. Modular Programming Systems (A. F. McGirt).

A modified version of the KAPL DATATRAM System<sup>4</sup> (renamed LAMPS for Los Alamos Modular Programming System) is now fully operational on the LASL CDC-6600 computers. All of the basic features of the KAPL system have been retained. Some examples of these features are:

1. Series of functional program units (modules) may be easily linked to perform a specific task,
2. Free-standing codes may be executed and linked in the environment of the LAMPS system with almost no additional user programming effort, and

3. Data lists generated by free-standing codes and modules (as well as the modules and free-standing codes themselves) may be saved on user-supplied tapes for later recall and use.

Experience gained through use of the LAMPS system should show that program units (modules) can easily be shared between groups, thus eliminating the need for costly duplicate programming. Better program documentation can also be promoted with simplified module input lists which are standardized.

The ARC system<sup>5</sup> is also being modified for use at LASL. Instead of trying to use the complete modular system as with DATATRAM, the one-dimensional transport theory computational module NU003 with LASL-supplied input and output routines is being loaded. Most of the problems encountered so far have been with the lack of compatibility between the IBM-360/75 and CDC-6600 FORTRAN-IV compilers. Once these differences are resolved, the loading of NU003 is expected to proceed without much difficulty.

3. Burnup Code (T. J. Hiron). The LA report on the burnup-refueling code PHENIX<sup>6</sup> has been written. PHENIX is a two-dimensional multigroup diffusion-burnup-refueling code for use in fast reactor criticality and burnup analysis. The code is designed primarily for fuel-cycle analysis of fast reactors and can be used to calculate the detailed burnup and refueling history of fast breeder reactor concepts having any generalized fuel management scheme. Either ordinary  $k_{eff}$  calculations or searches on material concentration or region dimensions can be performed at any time during the burnup history. The refueling option of the code accounts for the spatial flux shifts over the reactor lifetime. Effects of this flux shift were presented recently,<sup>7</sup> and are discussed in detail in Ref. 8. For each burnup interval in the fuel-cycle history, the code performs the following operations:

- a. Calculates, for each fuel isotope in each zone, both the atom density of the fuel fraction to be discharged and the atom density following the refueling,
- b. Calculates, for each fuel isotope, the total charge and discharge (in kg) of the entire reactor,
- c. Collapses the atom density data for any number of regions, e.g., all the radial or axial blanket regions, into a single total charge and discharge, and

- d. Punches on cards the charge-discharge mass balances for input to a reactor economics code (if desired).

All of these calculations reflect the spectral and spatial flux shifts from one burnup interval to another.

An abstract of this code has been submitted for publication to Nuclear Science and Engineering. It will also be submitted to the Argonne Code Center when the LA report is published.

D. Fast Reactor Design Analysis (T. J. Hirons and R. E. Alcouffe)

1. Heterogeneous and Resonance Self-Shielding Effects on Fast Breeder Calculations. In a typical LMFBR, the neutron flux spectra extend into the resolved resonance region of the fertile and fissile elements. As a result, the multigroup cross sections in the resonance region should include the effects of heterogeneity and resonance self-shielding. This section presents results of an investigation of these effects on fast breeder reactor physics and fuel-cycle parameters.

A large pancake mixed-oxide LMFBR<sup>9</sup> was used in the analysis. The core fuel consists of UO<sub>2</sub>-PuO<sub>2</sub>, and the clean blanket fuel contains only UO<sub>2</sub>. The <sup>238</sup>U atom density in a core fuel pin is 60% of the theoretical density of UO<sub>2</sub> and 16% of the theoretical density in the homogenized core mixture. The <sup>238</sup>U atom densities of the axial blanket are 90% and 24% of theoretical UO<sub>2</sub> density in the blanket fuel pin and homogenized blanket mixture, respectively.

The MC<sup>2</sup> code<sup>10</sup> was used to process ENDF/B cross sections into a 49-energy-group structure. The first 48 groups (10 MeV to 61 eV) are each of 0.25 lethargy width and correspond to the fine groups in MC<sup>2</sup>. The 49th group was a broad group covering the energy range 61 to 8 eV. Since the resonance self-shielding is mixture-dependent, four different MC<sup>2</sup> analyses were performed to determine the effects of heterogeneity and resonance self-shielding. These four runs consisted of both homogeneous and heterogeneous MC<sup>2</sup> calculations, using both core and axial blanket atom densities. The heterogeneous or cell calculation in MC<sup>2</sup> is limited to two regions, and

a modification of this cell model was required to include the effect of the beryllium oxide pins which are present in the mixed-oxide LMFBR being analyzed. The BeO pins have the same diameter as the fuel pins and are present in a ratio of approximately 1:3.5 (BeO to fuel). For the MC<sup>2</sup> cell runs, the appropriate volume fraction of BeO was smeared into the outer coolant region. Fine-energy mesh (49-group) MC<sup>2</sup> calculations were then performed for both core and axial blanket regions, using both the homogeneous and heterogeneous representations of the modified two-region cell described above.

In Table 465-IV, the total capture cross section of <sup>238</sup>U as calculated from these four MC<sup>2</sup> runs is shown for the latter 12 groups of the 49-group structure; these groups cover the majority of the resolved resonance region. This parameter is of

TABLE 465-IV

$\sigma_c$  FOR <sup>238</sup>U FROM HOMOGENEOUS AND HETEROGENEOUS MC<sup>2</sup> RUNS

Group	Core		Axial Blanket	
	Homog.	Heter.	Homog.	Heter.
38	1.94	1.85	1.57	1.48
39	1.78	1.68	1.35	1.26
40	1.85	1.75	1.40	1.31
41	1.65	1.58	1.30	1.21
42	1.76	1.63	1.21	1.11
43	2.38	2.19	1.59	1.44
44	2.57	2.34	1.70	1.54
45	1.61	1.54	1.35	1.27
46	5.45	4.96	3.41	3.10
47	2.85	2.71	2.02	1.88
48	4.19	3.83	3.06	2.78
49	1.11	1.07	1.36	1.27

considerable importance in the calculation of breeding ratio and other fuel-cycle parameters. The results indicate that the heterogeneous shielding effects lower the <sup>238</sup>U  $\sigma_c$  by anywhere from 4 to 10% in both the core and axial blanket regions. The cross section values given are lower in the axial blanket because of the greater resonance self-shielding caused by the higher <sup>238</sup>U content in the blanket. Using cross sections from both the homogeneous and heterogeneous MC<sup>2</sup> runs, 49-group two-dimensional diffusion theory calculations were performed on the pancake LMFBR. The breeding ratios for the clean reactor are given in Table 465-V. For the homogeneous and heterogeneous MC<sup>2</sup> analyses, criticality calculations were performed using two sets of cross sections (both core and axial blanket), and core cross sections alone. The effect of

heterogeneity decreases the reactor breeding ratio by 1.4% for the two-set cross-section case (about a 1.2% decrease when core cross sections only are used). The effect of resonance self-shielding on the breeding ratio can be seen by comparing either heterogeneous or homogeneous calculations for the one- and two-set cross-section cases (2.2% error for heterogeneous, 2.0% error for homogeneous).

A Monte Carlo calculation of the actual reactor cell is presently being formulated. Results of this calculation will provide a check on the validity of the modified two-region cell used in the MC<sup>2</sup> runs.

2. Development of a Space-Energy Collapsing Scheme Applicable to Fast Reactor Burnup and Fuel-Cycle Analysis. In a recent report,<sup>11</sup> the initial development of a space-energy collapsing scheme applicable to fast reactor fuel-cycle analysis was discussed, and some preliminary results were given for the energy collapse.

Discussed in this section are 1) the effects on fast reactor parameters of different methods of energy collapsing the leakage and 2) the differences in fuel-cycle parameters obtained from using space-dependent and fundamental-mode collapsing spectra.

a. Effects on Fast Reactor Parameters of Various Leakage Collapsing Methods. The treatment of spectral differences in the calculation of group constants can be improved by first performing a fine energy-mesh reference calculation at some representative state of the system (for example, beginning of life). This fine-group space-dependent spectrum is then used to derive broad-group diffusion equation parameters. The group constants for the fine-group problem are obtained from a multi-group cross-section preparation code<sup>10</sup> such as MC<sup>2</sup> and are assumed insensitive to the averaging procedure used to derive them from the fundamental cross-section data. A collapsing technique to derive the broad-group parameters has been developed which preserves, exactly, the eigenvalue, energy-averaged flux, and reaction rates in each broad group. This procedure includes a consistent treatment of the leakage which insures that the

TABLE 465-V  
BREEDING RATIOS FOR CLEAN REACTOR

	Two Cross-Section Sets <sup>a</sup>		One Cross-Section Set	
	Heter.	Homog.	Heter.	Homog.
Initial Breeding Ratio	1.100	1.115	1.124	1.137
% Error		1.4	2.2	3.4

<sup>a</sup>Reference case

leakage information contained in a reference fine-group calculation is preserved in a calculation using the condensed parameters. However, a penalty is imposed by using this method in that the storage requirement is increased. In order to justify this penalty, the consequences of using various approximations for the collapsing of the leakage are examined here.

Three leakage-collapse approximations commonly used or proposed for neutron diffusion codes have been formulated and applied to a large mixed-oxide LMFBR.<sup>9</sup> The methods may be described as:

1. Flux averaged transport cross section,

$$D_{g,I}^1 = \frac{\bar{\phi}_{g,I}}{\sum_{k \in g} \Sigma_{k,I} \phi_{k,I}}$$

2. Flux-averaged diffusion coefficient

$$D_{g,I}^2 = \sum_{k \in g} \frac{\bar{\phi}_{k,I}}{\Sigma_{k,I}} / \bar{\phi}_{g,I}$$

3. Flux gradient-averaged diffusion coefficient

$$D_{g,I}^3 = \sum_{k \in g} \frac{\int_{S_I} \hat{n} \cdot \nabla \phi_{k,I} dS}{\Sigma_{k,I}} / \int_{S_I} \hat{n} \cdot \nabla \phi_{k,I} dS$$

where  $\Sigma_{k,I}$  is the fine-group transport cross section, and  $D_{g,I}$  is the appropriate broad-group diffusion coefficient in region I, a region being defined by the spatial area in which the cross sections are spatially constant. The gradient term on the surfaces is approximated by a first-order finite difference formula.

TABLE 465-VI

EFFECT OF LEAKAGE COLLAPSE  
UPON FAST BREEDER PARAMETERS

Parameter	Reference	Group	Consistent	Approximate		
				Case 1	Case 2	Case 3
Initial $k_{eff}$	1.0109	8	1.0112	1.0129	1.0111	1.0137
		4	1.0105	1.0191	1.0135	---
Final $k_{eff}$	0.9836	8	0.9840	0.9848	0.9834	0.9858
		4	0.9836	0.9905	0.9857	---
Initial BR	1.1472	8	1.1463	1.1426	1.1454	1.1420
		4	1.1466	1.1302	1.1396	---
Final BR	1.1795	8	1.1794	1.1757	1.1777	1.1750
		4	1.1788	1.1632	1.1717	---
Pu discharge	160.1	8	160.1	159.1	159.5	159.4
		4	160.3	154.8	158.3	---

These approximate formulas were tested in calculations in which a 49-group reference set of cross sections is reduced to 8 and 4 groups, respectively, using the two-dimensional spectrum. The parameters resulting from the calculations using the 8- and 4-group data are listed along with those resulting from the reference calculation in Table 465-VI. Also included are the parameters resulting from the consistent treatment of the leakage reduced to 8 and 4 groups.

This table of data shows that the consequences of using any of the three approximations for the 8-group calculation are not very severe in that all parameters are calculated within 0.5% of the reference case. There is a marked deterioration in the 4-group calculation for case 1, in which the breeding ratio is underestimated by 1.5%. The 4-group calculation in case 2 is still satisfactory with a maximum error of less than -0.7%. However, in case 3, the 4-group calculation fails because of a spectral effect on the gradient term. In the lower groups, the current changes sign frequently across a region boundary introducing the possibility of a negative diffusion coefficient in the collapse. This effect is manifested in the 4-group case. For this reason, this type of averaging is unsatisfactory since it requires a careful combination of groups in order to ensure against negative diffusion coefficients.

In conclusion, if one performs only spectral collapse of the cross-section data, the method of case 2 is probably a satisfactory method of estimating the leakage. However, this method cannot be extended to spatial collapse (as can the consistent method) and still retain this accuracy.

b. Comparison of Fuel-Cycle Parameters Obtained from Using Space-Dependent and Fundamental-Mode Collapsing Spectra. This comparison of fuel-cycle parameters was performed using the LMFBR design<sup>9</sup> mentioned in Section 1. The collapsing technique includes the consistent treatment of the leakage and the use of a separate set of broad-group microscopic cross sections appropriate for each burnable isotope in each reactor zone.

The use of the initial two-dimensional fine spectrum is profitable, if the changes in the spatial and energy distribution of the flux in time are such that the resultant spectrum is not very different from the reference calculation. If these changes are small or if the group structure is chosen to be consistent with the expected changes, the initial investment in the reference calculation will yield fuel-cycle results which are accurate throughout the burnup history of the reactor. This is verified below for the reactor system chosen.

To begin the calculation, a 49-fine-group reference calculation was performed using ENDF/B cross-section data processed by MC<sup>2</sup>, but with no broad-group collapsing performed by MC<sup>2</sup>. The fine-group

cross sections and leakage coefficients were condensed to 8 and 4 broad groups, using the two-dimensional space-dependent spectrum. Burnup analyses, using these broad-group structures, were then carried out over the first six burnup intervals. Refueling was performed between burnup intervals according to the prescribed fuel management schedule. The 49-group reference calculation was performed through the first burnup interval. Parallel burnup analyses, using 8- and 4-group cross sections generated directly from MC<sup>2</sup>, were also performed to compare the effects of using space-dependent and fundamental-mode collapsing spectra. All fine- and broad-group criticality and fuel-cycle calculations were performed using two-dimensional diffusion theory.

The results of the collapsed analyses (8 from 49 and 4 from 49) were virtually identical and differed from the 49-group calculation by less than 0.2% in  $k_{eff}$ , breeding ratio, and plutonium content in the blankets at the end of the first burnup interval. A 2-from-49 analysis was also performed, resulting in less than 1% error in all parameters. The 49-fine-group calculation was rerun at the beginning of the fifth burnup interval, but the resultant collapse yielded no significant changes from the broad-group cross sections calculated at beginning-of-life. This indicates that the changes in the time-dependent spectrum have been adequately accounted for by both the 8- and 4-group structures.

For the 8-group analysis using cross sections averaged over a fundamental core spectrum generated by MC<sup>2</sup>, errors in the breeding ratio (compared with the collapsed analyses) over the first six burnup intervals ranged from -2.9 to -1.6%, while for the 4-group case, this range was -11.1 to -8.3%. The errors in the <sup>239</sup>Pu discharge from the axial blankets for the 8-group analysis ranged from -4.1 to -2.2%, while for the 4-group case the range was -16.4 to -11.8%. The error decreases in time due to a compensation of larger errors in effective <sup>238</sup>U and <sup>239</sup>Pu cross sections used for the burnup equations. All of the results given above are based on a single set of cross sections from MC<sup>2</sup> calculated using core atom densities only. The burnup analyses were also performed using two sets of cross sections from MC<sup>2</sup>, one based on the core

and the other on the axial blanket atom densities and spectrum. Results of these fuel-cycle analyses showed a slight reduction in the range of errors incurred relative to the use of core cross sections only. For example, errors in the breeding ratio using 4-group cross sections generated directly from MC<sup>2</sup> ranged from -10.3 to -7.1% with two sets as compared with -11.1 to -8.3% when one cross-section set was used.

The main conclusion to be drawn from these results is that, when cross-section data is averaged over a representative two-dimensional fine-group spectrum, the fuel-cycle parameters are relatively insensitive to the number and distribution of energy groups used. This success is due to the fact that the neutron spectrum changes very little from the beginning-of-life spectrum during the entire reactor lifetime. This is not true of the same analysis performed on the same system using parameters derived from fundamental-mode or infinite-medium spectra. The results are very sensitive to the number of groups and their distribution in the energy domain. Confidence in the results can be obtained only by increasing the number of groups to show that the results have not changed. Therefore, before performing a fuel-cycle analysis on a given system, it is recommended that as detailed a calculation as is possible be performed at the beginning-of-life and from this few-group parameters appropriate for the time-dependent analysis be derived.

#### E. Computational Techniques for Repetitively Pulsed Reactors (G. C. Hopkins)

In a repetitively pulsed reactor excited by some form of accelerator and synchronously pulsed reactivity, a problem arises in determining the neutronic response in a computationally efficient manner. The quasi-stabilized time-dependent solution to the monoenergetic point kinetics equations is sought with equal, but unknown, initial and final boundary conditions. Pulse characteristics and typical system parameters have been described previously.<sup>12</sup>

To date, studies of this problem have involved: approximating the precursor density as a constant;<sup>13</sup> computationally long asymptotic approaches to the

quasi-stabilized state;<sup>14</sup> and considering the power pulse as a delta function.<sup>15</sup> None of these restrictions are contained in the present formulation.

Two basic cases are being investigated: 1) the linear problem associated with either constant or a priori known time-dependent reactivities and sources, both during the pulse and off-pulse; and 2) the nonlinear problem arising from consideration of feedback-dependent reactivity.

For the first of these cases, then, the problem is to obtain the neutronic response over the cycle  $t = 0 \rightarrow T$ , starting from the point kinetic equations:

$$\frac{dN(t)}{dt} = \frac{\rho(t) - \beta}{\Lambda} N(t) + \lambda C(t) + S(t)$$

$$\frac{dC(t)}{dt} = \frac{\beta}{\Lambda} N(t) - \lambda C(t),$$

where

$$S(t) = \bar{S} \quad t = 0 \rightarrow t = t_p$$

$$= 0 \quad t = t_p \rightarrow t = T$$

and, for illustrative purposes

$$\rho(t) = \rho_0 + \rho_1 \sin\left(\frac{\pi}{t_p} t\right) \quad t = 0 \rightarrow t = t_p$$

$$= \rho_0 \quad t = t_p \rightarrow t = T$$

Most numerical techniques for solving this equation set are iterative, based on dividing the entire cycle into many time intervals, during each one of which two approximations are made:

1) approximating the derivatives and 2) approximating the reactivity, as constants during the interval. The size of the time interval is then dependent upon how well both approximations are satisfied. For a problem such as this, with rapidly varying neutron behavior, the derivative approximation leads to a much more stringent time-interval determination than does the reactivity approximation.

The Laplace transform-residue method, however, is not only noniterative but also involves only one approximation--that for the reactivity from  $t = 0 \rightarrow t = t_p$ , which is only a thousandth of the entire cycle. The portion of the cycle from  $t = t_p \rightarrow t = T$  can be treated as one time interval without any approximation, in contrast to most other techniques.

The solution is obtained by starting with the Laplace transform of Eqs. 1 and 2, treating  $\rho(t)$  and  $S(t)$  as constants. After some algebraic manipulations and inverse transforming, the equation set reappears in the form:

$$N_0 = N_n \quad (5)$$

$$C_0 = C_n$$

$$N_{i+1} = a_{1i} N_i + a_{2i} C_i + a_{3i} \bar{S}_i$$

$$C_{i+1} = b_{1i} N_i + b_{2i} C_i + b_{3i} \bar{S}_i \quad i = 1, n-1 \quad (6)$$

In matrix form, this is

$$\underline{MN} = \underline{S}, \quad (7)$$

where

$$\underline{N} = \begin{bmatrix} N_0 \\ C_0 \\ N_1 \\ C_1 \\ \vdots \\ \vdots \\ N_n \\ C_n \end{bmatrix} \quad \underline{S} = \begin{bmatrix} 0 \\ 0 \\ a_{31} \bar{S}_1 \\ b_{31} \bar{S}_1 \\ \vdots \\ \vdots \\ a_{3n} \bar{S}_n \\ b_{3n} \bar{S}_n \end{bmatrix} \quad (8)$$

and

$$M = \begin{bmatrix} 1 & 0 & \dots & \dots & 0 & -1 & 0 \\ 0 & 1 & & & & & -1 \\ a_{11} & a_{21} & 1 & & & & \\ b_{11} & b_{21} & & 1 & & & \\ 0 & & & & & & \\ \vdots & & & & & & \\ \vdots & & & & & & \\ \vdots & & & & a_{1n} & a_{2n} & 1 & 0 \\ 0 & \dots & \dots & b_{1n} & b_{2n} & 0 & 1 \end{bmatrix} \quad (9)$$

The solution,  $\underline{N} = M^{-1}\underline{S}$ , is going to depend, either explicitly or implicitly, on some form of inversion of the matrix  $M$ . But for 1000 time intervals, typical for the reactivity approximation, and the two variables  $N(t)$  and  $C(t)$ , the matrix  $M$  is  $2000 \times 2000$ , too bulky for efficient manipulation as such. However, a quick examination reveals that no row contains more than three elements, thereby reducing the matrix to two  $2000 \times 3$  arrays: one for the coefficients and one for the indices. The straight inversion is still out of the question, however, because each row of the inverse would contain many more than three elements.

A method well suited to this matrix, though, is Gaussian elimination. Because of the nature of the method and the matrix, plus the fact that the diagonal already consists of only 1's, a single array of 2000 x 2 and 2 sec of central processor time are all that is required to effect a solution.

The results of this method can be used as an initial iteration in solving the other nonlinear problem associated with feedback reactivity. This is currently being investigated.

#### REFERENCES

1. R. Q. Wright et al., "SUPERTO: A Program to Generate Fine Group Constants and  $P_n$  Scattering Matrices from ENDF/B," ORNL-RSIC-27 (to be published).
2. "Quarterly Status Report on the Advanced Plutonium Fuels Program, October 1 to December 31, 1968," LA-4114-MS, Los Alamos Scientific Laboratory (1968).
3. "Control Data Scope 3 Reference Manual," Publication No. 60189400, Control Data Corporation (1969).
4. H. J. Kopp, J. D. Morris, and W. E. Schilling, "DATATRAM Modular Programming System for Digital Computers," KAPL-M-6997, Knolls Atomic Power Laboratory (1968).
5. B. J. Toppel, "The Argonne Reactor Computation (ARC) System," ANL-7332, Argonne National Laboratory (1967).
6. R. Douglas O'Dell and Thomas J. Hiron, "PHENIX, A Two-Dimensional Diffusion-Burnup-Refueling Code," LA-4231, Los Alamos Scientific Laboratory (in press).
7. Thomas J. Hiron and R. Douglas O'Dell, "Models for Fuel-Cycle Analysis in Large Fast Breeders," Trans. Am. Nucl. Soc. **12**, 38 (1969).
8. Thomas J. Hiron and R. Douglas O'Dell, "Calculational Modeling Effects on Fast Breeder Fuel-Cycle Analysis," LA-4187, Los Alamos Scientific Laboratory (1969).
9. "Liquid Metal Fast Breeder Reactor Design Study (1000 MWe UO<sub>2</sub>-PuO<sub>2</sub> Fueled Plant)," GEAP-4418, General Electric Company (1963).
10. B. J. Toppel, A. L. Rago, and D. M. O'Shea, "MC<sup>2</sup>, A Code to Calculate Multigroup Cross Sections," ANL-7318, Argonne National Laboratory (1967).
11. "Quarterly Status Report on the Advanced Plutonium Fuels Program, April 1 to June 30, 1969 and Third Annual Report, FY 1969," LA-4284-MS, Los Alamos Scientific Laboratory.
12. "Quarterly Status Report on the Advanced Plutonium Fuels Program, January 1 to March 31, 1969," LA-4193-MS, Los Alamos Scientific Laboratory.
13. Ing. T. Trombetti, "Cinetica di un Reattore Veloce Pulsato in Regime Periodico o Quasi Periodico," ARV(65)43, Comitato Nazionale Per L'Energia Nucleare, Bologna (1965).
14. M. S. Trasi, "Integration of the Point-Reactor Kinetic Equations with a Periodic Reactivity Input by Use of Quasi-Periodic Vector Solutions," B.A.R.C.-371, Bhabha Atomic Research Center, Bombay (1968).
15. G. Blaesser and J. A. Larrimore, Nucl. Sci. Eng. **37**, 186 (1969).

PROJECT 467

FUEL IRRADIATION EXPERIMENTS

Person in Charge: D. B. Hall  
 Principal Investigators: R. H. Perkins  
 J. C. Clifford

I. INTRODUCTION

The goal of this program is to examine the irradiation behavior of advanced fuels for LMFBRs. At present the two fuel concepts under study are sodium-bonded mixed carbides and metals.

The principal effort with carbides centers on the irradiation performance of high purity, single-phase  $(U_{0.8}Pu_{0.2})C$  produced and characterized under LASL Program 463. Fast flux irradiation of this material, sodium-bonded to Type 316 stainless steel cladding, at lineal heat ratings of interest to fast reactor designers is the principal activity. The experiments are designed to determine the degree of fuel swelling, gas release, fuel-sodium-clad interaction, and the migration of fissionable material and fission products as a function of burn-up and fuel density. Thermal flux irradiations of LASL-produced carbides also are included to augment determination of the effects of high burnup on fuel-bond-clad compatibility.

Because of a shift of interest from metal alloys as LMFBR fuels, metal fuel work has been reduced and reoriented. Thermal irradiations are being conducted to evaluate the behavior of a U-Pu-Zr alloy produced at LASL during a previously completed alloy development program.<sup>1</sup> No fast reactor irradiations of metal fuels are planned. Supporting out-of-pile effort is directed toward evaluating fuel-cladding interactions.

II. EBR-II IRRADIATION TESTING  
 (J. O. Barner)

A. General

The purpose of the EBR-II irradiations is to

evaluate candidate fuel/sodium/clad fuel element systems for the LMFBR program. In the reference design, fuel pellets of single-phase (U,Pu)C are separated by a sodium bond from a cladding of Type 316 stainless steel. Three series of experiments are planned and approval-in-principle has been received from the AEC.

The capsules are to be irradiated under the following conditions:

Condition	Series 1	Series 2	Series 3
1. Lineal power, kW/ft	~ 30	~ 45	~ 30
2. Fuel composition	$(U_{0.8}Pu_{0.2})C$ , single-phase, sintered		
3. Fuel uranium	$^{235}U$	$^{233}U$	$^{235}U$
4. Fuel density	90%	95%	95%
5. Sinter density	80%	80%	80%
6. Clad size	0.300-in. i.d. x 0.010-in. wall		
7. Clad type	316 SS	316 SS	316 SS
8. Max clad temp, °F	1250	1275	1250
9. Max fuel center-line temp, °F	2130	2550	2100
10. Burnup	3 a/o to 8 a/o		

The capsules are doubly contained.

B. Current Results

A capsule from Series 1, designated K-(LASL)-42B, has operated in EBR-II to a maximum burnup of 1.5 a/o. The capsule is at EBR-II for reinsertion in the X070 subassembly for a burnup to 4.5 a/o (total).

A second capsule from Series 1, K-36B, is also at EBR-II for insertion in the X070 subassembly. Irradiation of X070 is tentatively scheduled to start in mid-December.

Three additional capsules, K-37B, K-38B, and K-39B, have been loaded and are available for irradiation. There is no definite schedule for their irradiation at this time.

Part of the fuel for Series 3 has been fabricated. Loading of some of the capsules for Series 3 will start during the next quarter.

The  $^{233}\text{U}$  for Series 2 has been received. Fabrication of this fuel will start during the next quarter. Until completion of the fabrication of Series 2 fuel, fabrication of the Series 3 fuel will be interrupted.

### III. THERMAL IRRADIATIONS OF SODIUM-BONDED MIXED CARBIDES (J. C. Clifford, R. L. Cubitt, D. C. Kirkpatrick)

#### A. General

Mixed carbides, sodium-bonded to Type 316 stainless steel cladding, will be irradiated in the LASL Omega West Reactor (OWR), an 8 mW MTR type facility. The purpose of the experiments is to determine whether fuel, clad, and sodium remain mutually compatible as burnups of interest in the LMFBR program are approached. While fast spectrum irradiations are preferred in order to produce the power densities and radial temperature gradients anticipated in LMFBRs, thermal irradiations appear acceptable in this instance because the fuel regions of prime interest (those in contact with sodium) for compatibility studies can be maintained at realistic temperatures. Because of the high  $^{235}\text{U}$  content of the fuel for thermal flux experiments, power density at the surface of the fuel will be significantly higher (a factor of three) than that at the surface of an LMFBR fuel. Whether this difference in power densities will be significant in terms of compatibility among fuel, sodium, and clad remains to be seen.

Experiments will be conducted in one of two instrumented environmental cells installed semi-permanently in the OWR. The principal features of these cells, which have been described in detail elsewhere,<sup>2</sup> are: (1) a heat removal and temperature control system consisting of a natural convection sodium loop, electrical heaters, and a variable conductivity heat leak, and (2) a sweep gas system for the rapid detection of leaking fuel capsules. Since the cells had been idle for three years,

considerable refurbishing of control, alarm, and gas systems was necessary before irradiation experiments were started. One cell was refurbished for use with metal fuels (Section 467-IV) and the other was removed for destructive examination.

#### B. Current Results

A replacement cell has been fabricated and operated satisfactorily for several weeks at elevated temperatures. The alarm system for this cell has been reworked and modifications and checkout of the gas and control systems are in progress. The first carbide experiment is being assembled for insertion in the reactor during the next quarter.

### IV. THERMAL IRRADIATIONS OF SODIUM-BONDED U-Pu-Zr (J. C. Clifford, R. L. Cubitt, D. C. Kirkpatrick)

#### A. General

Thermal irradiations are being conducted to evaluate the behavior (intrinsic swelling, migration of fuel constituents, fission gas release, fuel-sodium-clad compatibility) of U-Pu-Zr alloys produced by LASL. Irradiations are conducted at the Omega West Reactor in an environmental cell in which temperature changes accompanying reactor power level changes are minimized with electrical heat and with a variable conductivity heat leak. Using this cell, it is possible to minimize thermal cycling of the fuel through phase transformations that affect its swelling behavior.

Complementary to the irradiations is an out-of-pile investigation of the compatibility of LASL-produced U-Pu-Zr alloys with Type 316 stainless steel and with a vanadium alloy. Of prime interest is the effect of zirconium and oxygen content of the fuel on reactions between fuel and stainless steel in the temperature range 550 to 750°C.

#### B. Current Results

##### 1. Irradiation Experiments

OWREX-12, a U-15Pu-12Zr fuel experiment which released fission gas four days after startup, has been disassembled and examined visually. Radiographic inspection of the assembly showed that fuel relocation had occurred in the top capsule. No abnormalities were detected in the remaining capsules. Figure 467-1 shows the failed pin and a portion of a normal pin, the secondary containment for the



Fig. 467-1. Radiograph of a portion of the OWREX-12 insert after failure of the top pin. Fuel apparently has reacted with the clad and with the fuel slug centering device. Thermocouples and their positioning wires and fuel capsule spacer disks are visible.

experiment, and a transport container. The stainless steel piece immediately above the fuel (near the mid-plane of each capsule) is a cruciform device for centering the fuel slug in the capsule. In the failed pin, some fuel is adhering to the centering device, which appears to be fixed in its original location. The remainder of the fuel has moved downward and outward, apparently penetrating the capsule wall.

The capsule was cut open above the centering

device. No sodium, except for a residue, was visible in this region which pre-test radiographs had shown to be filled. A circumferential crack extending one-third of the way around the capsule was visible in the capsule wall immediately above the lower closure weld (Fig. 467-2). Several small pits were

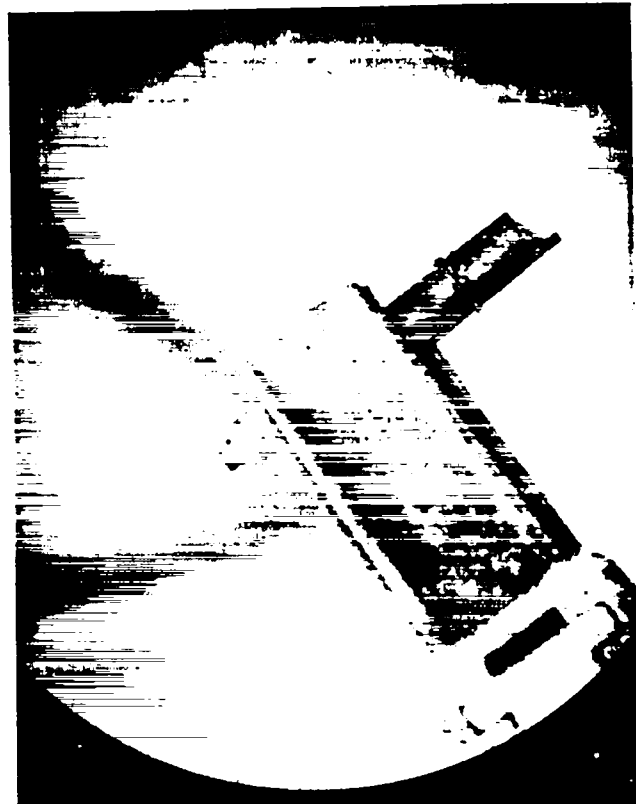


Fig. 467-2. Fueled half of the failed capsule from OWREX-12. A crack is visible above the lower closure weld (lower left hand corner of the figure). Also visible are sodium residues, a thermocouple and its positioning wire, and a portion of the manipulator.

visible in the lower closure weld opposite the crack. No other abnormalities were noted in this capsule and none were visible in the other three. The failed capsule will be examined further as time permits.

The evidence of fuel movement throughout the length of the fuel column, the crack in the capsule wall, and the partial or complete loss of sodium from the capsule suggest that sodium was expelled from a cladding failure located in the heat-affected zone of the lower closure weld. Loss of sodium caused fuel overheat and slumping. The crack is

thought to be peculiar to the nickel-to-stainless steel closure weld of this capsule.

Assembly and inspection of OWREX-13, another U-15Pu-12Zr experiment, was completed and the experiment was placed in the reactor at the end of September. The experiment contains three fuel capsules stacked end on end at the axis of the secondary container. Fuel material is LASL-cast and extruded (570°C) U-Pu-Zr and the container material is Type 304 stainless steel.

During this irradiation, the environmental cell is being operated to maintain all fuel slugs in a single-phase region requiring a minimum fuel temperature of approximately 650°C. The radial and axial temperature gradients calculated for this case do not appear excessive in terms of fuel strength or fuel/clad and sodium/stainless steel compatibilities. It is planned to irradiate this assembly to 1 a/o burnup, average, requiring approximately three months.

## 2. Compatibility Experiments

Experiments conducted to date have been restricted to evaluating the effects of specimen surface conditions and contact pressures on the extent and rapidity of reaction. The test specimens are sandwiches of Type 316 stainless steel, fuel, and vanadium alloy held together in presses of stainless steel or molybdenum. Partial analyses of the fuel and vanadium alloy are shown in Table 467-I.

Table 467-I  
Impurities in Materials for Compatibility Experiments

Species	Concentration*	
	U-15Pu-12.7Zr	V-15Cr-5.1Ti
O	180	815
C	190	234
N	--	138
H	--	47
Fe	80	--
Si	35	--
Cu	200	--
Cr	10	(15.0 w/o)

\*Concentration expressed in ppm unless stated otherwise.

Specimens of the individual alloys are prepared by grinding the flat surfaces of cylindrical blanks on 320- and 600-grit paper. The specimens are trans-

ferred to a high purity inert gas glovebox train (Section 464-III) where final polishing is done by hand immediately before assembly of the sandwiches. The assembled sandwiches are wrapped in zirconium foil and sealed into stainless steel capsules, using the glovebox atmosphere as the cover gas.

Eight assemblies have been heated at 750°C; two for a period of 250 h, four for 500 h, and two for 1000 h. Presses of molybdenum and of stainless steel were used in each time period to apply different compressive loadings to the sandwiches during test. The 250- and 500-h sandwiches have been examined metallographically and the 1000-h sandwiches are available for examination. At the relatively short times of 250 and 500 h, any difference in depth of penetration resulting from differences in compressive loading were masked by variations in initial surface conditions. (This ignores the possibility that the fuel was creeping under load and that the two types of presses were applying the same load over the majority of the test period.)

The qualitative behavior in these sandwiches is illustrated in Figs. 467-3 and 467-4. At the

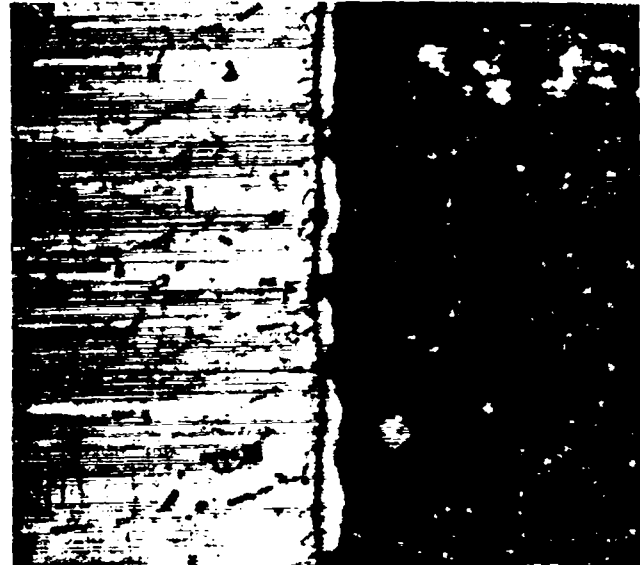
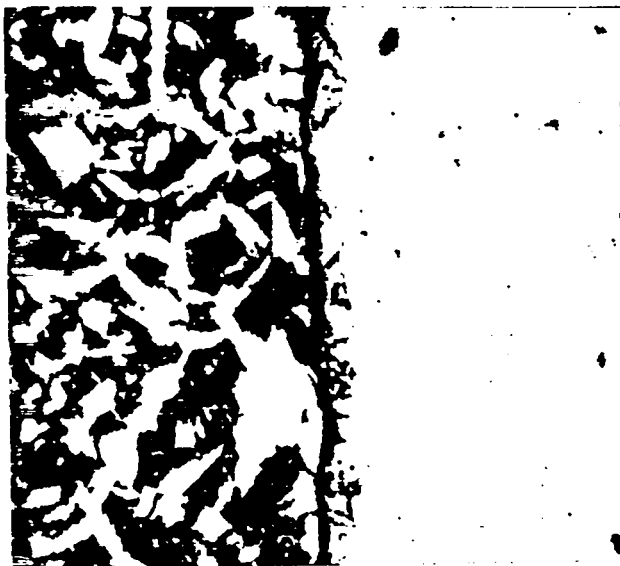


Fig. 467-3. Interface between U-15Pu-12.7Zr and Type 316 stainless steel alloys after 500 h at 750°C. Etched for stainless steel microstructure. Pu has penetrated the stainless steel and a Zr-rich layer has formed at the fuel surface. 600X.



Fuel

Vanadium Alloy

Fig. 467-4. Interface between U-15Pu-12.7Zr and V-15Cr-5.1Ti alloys after 250 h at 750°C. Etched for fuel microstructure. The vanadium alloy has been attacked by the fuel, and vanadium and chromium have moved to the fuel, resulting in the mottled appearance of the fuel. 300X.

stainless steel/fuel interface of a 500-h sandwich (Fig. 467-3) plutonium had penetrated the stainless steel to a depth of approximately 1  $\mu$ , and microprobe analysis indicated that some enrichment of chromium and depletion of nickel had taken place to this depth. On the fuel alloy side of the interface, a narrow band was visible in which only zirconium could be detected. The zone was too narrow to permit hardness measurements.

Figure 467-4 shows the interface between the fuel and vanadium alloy after 250 h at 750°C. Microprobe traverses on this region revealed zirconium, with smaller amounts of vanadium and chromium, in the irregularly-shaped layer on the vanadium alloy side of the interface. The depth of zirconium penetration varied from 1/2 to 3  $\mu$ . The dark areas visible within this zone contained all three fuel constituents. The fuel adjacent to the vanadium alloy consisted of large amounts of a light-colored, irregularly-shaped "phase" dispersed in a darker "matrix." The matrix was similar in composition and appearance to the original U-15Pu-12.7Zr alloy. At increasing distances from the vanadium alloy/fuel interface, the amount of the second phase in the fuel decreased, finally disappearing.

With respect to the matrix, the second phase was harder, was enriched in plutonium and depleted in uranium and zirconium, and contained some vanadium and chromium. The amounts of vanadium and chromium present are estimated as 0.8 and 0.4 w/o maximum, respectively, decreasing with increasing distance from the interface. Both vanadium and titanium were detected in the fuel matrix adjacent to the interface. Also present in the fuel, but not visible in Fig. 467-4, were small amounts of alpha zirconium. Alpha zirconium also was observed in the as-fabricated fuel.

Although the depth and uniformity of interactions among the three materials have varied from test to test, the qualitative or microstructural features of the specimens are similar. There is evidence of plutonium migration from the fuel into both the stainless steel and the vanadium alloy. The appearance of a zirconium-rich layer in the fuel adjacent to the stainless steel interface raises the question whether this layer can act as a barrier to the diffusion of plutonium outward from the fuel. The fact that oxygen stabilizes alpha zirconium in this alloy system<sup>3</sup> suggests that the layer may contain oxygen. If this is the case, the source is of concern.

The relatively rapid movement of chromium and vanadium from the vanadium alloy into the fuel, together with the beginning of penetration of the vanadium alloy by plutonium, uranium, and zirconium, suggest that vanadium alloys of this general composition probably would not be suitable containers for U-Pu-Zr at 750°C. This was not unexpected in view of results obtained at the Argonne National Laboratory.<sup>4,5</sup>

#### V. REFERENCES

1. "Quarterly Status Report on the Advanced Plutonium Fuels Program, April 1 to June 30, 1969, and Third Annual Report, FY 1969," Report LA-4284-MS, Los Alamos Scientific Laboratory, Oct. 15, 1969.
2. R. L. Cubitt, G. L. Ragan, D. C. Kirkpatrick, "Thermal Irradiation of Liquid Plutonium Alloy Fuels," Report LA-3832, Los Alamos Scientific Laboratory, June 1968.
3. W. N. Beck, R. J. Fousek, J. H. Kittel, "The Irradiation Behavior of High-Burnup Uranium-Plutonium Alloy Prototype Fuel Elements," Report ANL-7388, Argonne National Laboratory, May 1968.

4. "Annual Progress Report for 1965, Metallurgy Division," Report ANL-7155, Argonne National Laboratory, 1966.
5. S. T. Zegler and C. M. Walter, "Compatibility Between Metallic U-Pu-Base Fuels and Potential Cladding Materials," pp. 335-344 in K. E. Horton et al., editors, Proceedings of the 1967 International Symposium on Plutonium Fuels Technology held in Scottsdale, Arizona on October 4-6, 1967.

PROJECT 471

OTHER ADVANCED SYSTEMS  
RESEARCH AND DEVELOPMENT

Person in Charge: D. B. Hall  
Principal Investigator: G. H. Best

---

I. MEASUREMENT OF DELAYED GAMMA-RAY YIELDS (B. M. Moore)

The short-lived delayed gamma spectra from fast neutron fission of plutonium was experimentally measured by using a Ge(Li) detector. The half-lives and energies of the more prominent gamma rays in the spectra were determined for half-lives in the range  $1 \text{ min} \leq t_{1/2} \leq 60 \text{ min}$  and for energies in the range  $170 \text{ keV} \leq E \leq 1800 \text{ keV}$ .

From the delayed gamma spectra, yields were determined for the short-lived fission products  $^{89}\text{Rb}$ ,  $^{90}\text{Rb}$ ,  $^{94}\text{Sr}$ ,  $^{94}\text{Y}$ ,  $^{101}\text{Mo}$ ,  $^{101}\text{Tc}$ ,  $^{131}\text{Sb}$ ,  $^{135\text{m}}\text{Xe}$ ,  $^{136}\text{I}$ ,  $^{137}\text{Xe}$ ,  $^{138}\text{Xe}$ ,  $^{140}\text{Cs}$ , and  $^{145}\text{Ce}$ .

Some of these yields are shown in Table 471-I. The errors shown include just experimental standard deviations and do not include errors in  $f_Y$  or  $\lambda$ . The table also shows the value of  $f_Y$  and  $t_{1/2}$  used in the determination of the yield. In cases where the maximum possible value of  $f_Y$  could only be estimated from nuclear level schemes and relative intensities, the minimum estimate in yield is given. These yields are compared with calculated yields from the literature and with experimental yields closer to stability on the isobaric chain. These experimental yields are given the notations th for thermal and FS for fission spectrum yields. There were no experimental yields in the literature to compare directly with those obtained.

The delayed gamma spectra from fast fission of  $^{239}\text{Pu}$  was compared to that obtained from  $^{235}\text{U}$ . Figure 471-1 shows a comparison of a portion of the two spectra in the first counting interval. It can be seen from the figure that the spectra are quite similar. The major difference is in the peak at 832 keV. This peak is from  $^{90}\text{Rb}$ , and the

difference is caused by the greater probability of creation with the fission of  $^{235}\text{U}$  than  $^{239}\text{Pu}$ .

Table 471-II shows a comparison of intensity ratios for the first four counting intervals. The ratios taken are  $I(E)/I(975)$  where  $I(E)$  is the intensity of the peak at energy  $E$  and  $I(975)$  is the intensity of the peak at 975 keV. From this data, it can be seen that there is a measurable difference in the two spectra. Although there are similar differences in the low-energy part of the spectra, the higher-energy part of the spectra was used here. This is because the higher-energy gamma rays are more useful when observing bulk fuel (i.e., less self-absorption effects).

From the results obtained, conclusions could be reached on what fission products would produce the largest differences in the two spectra at high energy. This particular information is needed to help keep fuel inventory in reactors. This will protect against the unwarranted use of nuclear fuels that are produced in reactors (safeguards).

The full report of this work is contained in Ref. 15.

II. CODES (B. K. Barnes)

A computer code has been written to present two-dimensional gamma scanning data as a density plot, in which the intensity at some point  $(x,y)$  is represented by the density of the plotting dots around that point; Fig. 471-2 is an example of this form of presentation. This presentation is more sensitive than either contour plots or isometric projection views, as details of the data were observed which had not been seen in either of the other presentations. Work is under way to make these

TABLE 471-I

## FISSION PRODUCT YIELDS

Fission Product	Gamma-Ray Energy (keV)	Gamma Emission per Decay $f_Y$	Half-Life $t_{1/2}$ (min)	Percent Cumulative Yield (this work)	Other Experimental Cumulative Yields(14)	Calculated Cumulative Yields(13)
$^{139}\text{Xe}$	174.1	$\leq 0.27$ (1)	0.69 (2)	$\geq 4.4 \pm 0.5$	$5.78 \pm 0.55$ (th), $^{139}\text{Ba}$	2.99
$^{101}\text{Tc}$	305.6	0.91 (3)	14.0 (3)	$5.6 \pm 0.7$	$5.86 \pm 0.44$ (th), $^{101}\text{Ru}$	6.00
$^{104}\text{Tc}$	356.5	$\leq 0.78$ (4)	18.0 (3)	$\geq 6.4 \pm 0.5$	$5.88 \pm 0.45$ (th), $^{104}\text{Ru}$	5.59
$^{137}\text{Xe}$	454.4	0.33 (3)	3.8 (2)	$4.2 \pm 0.3$	5.6 (FS), $^{137}\text{Cs}$	6.50
$^{135\text{m}}\text{Xe}$	526.4	0.80 (3)	15.6 (3)	$0.79 \pm 0.07^{\text{a}}$		0.55 <sup>a</sup>
$^{140}\text{Cs}$	602.1	$\leq 1.0$ (1)	1.09 (1)	$\geq 1.8 \pm 0.1$	4.97 (FS), $^{140}\text{Ba}$	4.43
$^{145}\text{Ce}$	723.7	$\leq 0.68$ (5)	3.0 (5)	$\geq 2.1 \pm 0.1$	$3.12 \pm 0.21$ (th), $^{145}\text{Nd}$	3.53
$^{90}\text{Rb}$	831.2	0.61 (6,7)	4.30 (8)	$1.5 \pm 0.1^{\text{b}}$	2.26 (FS), $^{90}\text{Sr}$	2.09
$^{101}\text{Mo}$	893.8	0.15 (3)	14.6 (3)	$5.3 \pm 0.5$	$5.86 \pm 0.44$ (th), $^{101}\text{Ru}$	5.99
$^{94}\text{Y}$	918.4	0.43 (3,9)	20.3 (3)	$4.4 \pm 0.2$	$4.45 \pm 0.35$ (th), $^{94}\text{Zr}$	4.58
$^{131}\text{Sb}$	943.0	0.48 (10)	25.5 (10)	$2.4 \pm 0.2$	$3.8 \pm 0.14$ (th), $^{131}\text{I}$	2.20
$^{95}\text{Y}$	953.5	$\leq 0.15$ (11)	10.7 (11)	$\geq 4.4 \pm 0.4$	5.3 (FS), $^{95}\text{Zr}$	5.18
$^{89}\text{Rb}$	1031.5	0.60 (12)	14.9 (12)	$1.6 \pm 0.1$	1.8 (FS), $^{89}\text{Sr}$	1.60
$^{136}\text{I}$	1313.0	0.70 (3)	1.38 (3)	$1.2 \pm 0.1$	2.1 (13) (th), $^{136}\text{I}$	5.20
$^{94}\text{Sr}$	1428.0	1.0 (3)	1.28 (8)	$2.6 \pm 0.2$	$4.45 \pm 0.35$ (th), $^{94}\text{Zr}$	3.88
$^{138}\text{Xe}$	1435.8 (Cs)	0.73 (3)	17.0 (3)	$3.2 \pm 0.8$	$6.28 \pm 0.54$ (th), $^{138}\text{Ba}$	4.97
$^{138}\text{Cs}$	1435.8	0.73 (3)	32.2 (3)	$5.0 \pm 0.9$	$6.28 \pm 0.54$ (th), $^{138}\text{Ba}$	6.07

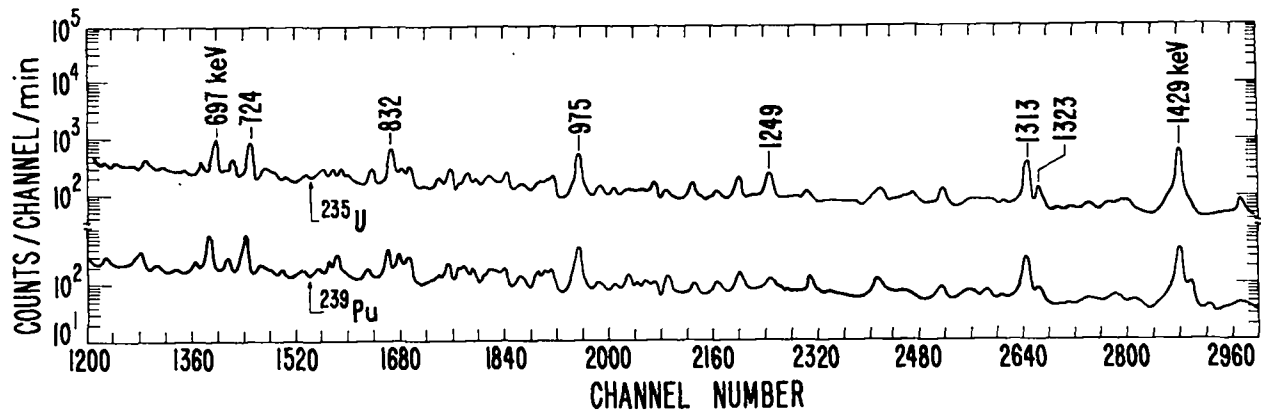
<sup>a</sup>Independent yield<sup>b</sup>There is an isometric state reported in Ref. 8.Fig. 471-1. Comparison of the delayed gamma-ray spectra from fast fission of  $^{239}\text{Pu}$  and  $^{235}\text{U}$ .

TABLE 471-II

COMPARISON OF RELATIVE GAMMA-RAY INTENSITIES  
OBTAINED FOR  $^{239}\text{Pu}$  AND  $^{235}\text{U}$ 

Energy (keV) & Element	I(E)/I(975) for Count Interval After Fission			
	0.035-3.37 min	3.44-6.77 min	6.84-10.17 min	10.24-13.58 min
E = 1436, Pu			0.679 $\pm$ 0.051	1.48 $\pm$ 0.13
E = 1436, U			0.480 $\pm$ 0.036	1.06 $\pm$ 0.09
E = 1428, Pu	1.16 $\pm$ 0.06	0.404 $\pm$ 0.025		
E = 1428, U	1.29 $\pm$ 0.06	0.429 $\pm$ 0.024		
E = 1313, Pu	0.785 $\pm$ 0.043	0.209 $\pm$ 0.030		
E = 1313, U	0.720 $\pm$ 0.051	0.228 $\pm$ 0.022		
E = 839, Pu	0.451 $\pm$ 0.044	0.941 $\pm$ 0.047	1.66 $\pm$ 0.09	2.95 $\pm$ 0.24
E = 839, U	0.393 $\pm$ 0.027	0.806 $\pm$ 0.039	1.61 $\pm$ 0.09	2.56 $\pm$ 0.22
E = 832, Pu	0.602 $\pm$ 0.084	0.909 $\pm$ 0.046	0.998 $\pm$ 0.066	1.246 $\pm$ 0.133
E = 832, U	1.184 $\pm$ 0.053	1.329 $\pm$ 0.050	1.623 $\pm$ 0.091	1.796 $\pm$ 0.167

density plots in color, allowing plots for different gamma rays to be overlapped for direct comparison.

The isometric projection still provides the best way of showing what a distribution looks like for anyone unfamiliar with the distribution. The subroutine for plotting three dimensional data in isometric projection views has been modified to suppress the plotting of portions of the data which are shielded from view. Figure 471-3 shows  $^{137}\text{Cs}$  plotted in this manner.

## REFERENCES

1. T. Alvager et al., Phys. Rev. **167**, 1105 (1968).
2. N. P. Archer and G. L. Keech, Can. J. Phys. **44**, 1823 (1966).
3. C. M. Lederer, J. M. Hollander, and I. Perlman, Table of Isotopes, Sixth Edition, John Wiley and Sons, Inc. (1968).
4. A. R. Zander, P. R. Gray, and T. G. Ebrey, Nucl. Phys. **75**, 209 (1966).
5. Nuclear Data, Section B, Academic Press, Inc., (1965 through 1968).
6. E. A. Zherebin et al., Soviet J. Nucl. Phys. **5**, 1 (1967).

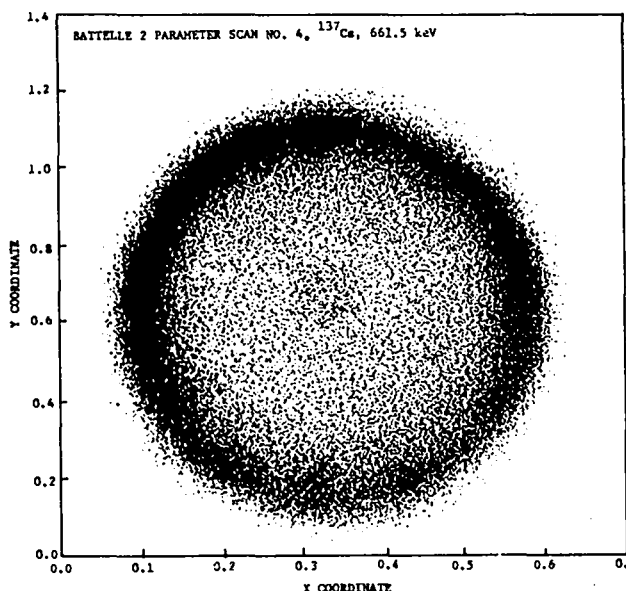


Fig. 471-2. Density plot of  $^{137}\text{Cs}$  distribution in Battelle fuel element section.

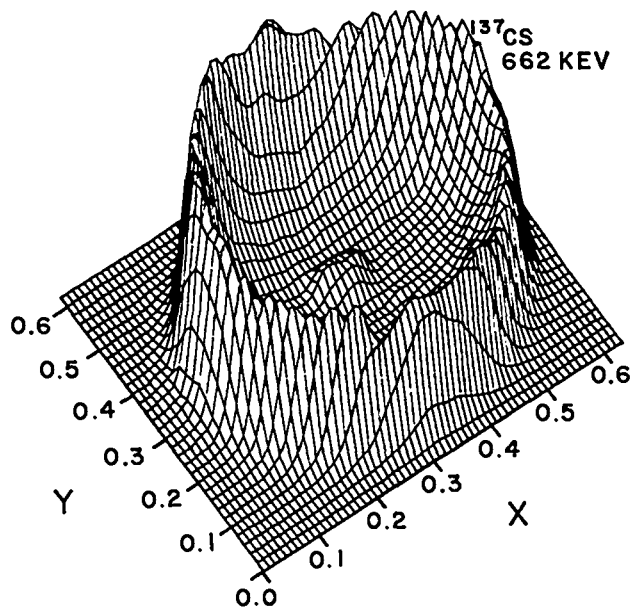


Fig. 471-3.  $^{137}\text{Cs}$  distribution.

7. Nuclear Data Sheets, National Academy of Sciences (1964).
8. I. Amarel et al., Phys. Rev. Letters **24B**, 402 (1967).
9. H. J. Fiedler and T. J. Kennett, J. Inorg. Nucl. Chem. **28**, 1129 (1966).
10. J. A. Cooper et al., J. Inorg. Nucl. Chem. **26**, 2041 (1964).
11. J. Van Klinken et al., Phys. Rev. **154**, 1116 (1967).
12. J. E. Kitching and M. W. Johns, Can. J. Phys. **44**, 2661 (1966).
13. M. E. Meek and B. F. Rider, "Summary of Fission Product Yields for U<sup>235</sup>, U<sup>238</sup>, Pu<sup>239</sup>, and Pu<sup>241</sup> at Thermal, Fission Spectrum, and 14 MeV Neutron Energies," APED 5398 (1968).
14. I. F. Croall, "Yields from Neutron Induced Fission," N68-23543 (1968).
15. B. M. Moore, "Short-Lived Delayed Gamma-Ray Emission from Fast Fission of Plutonium," LA-4257 (1969).

## PROJECT 501

### STANDARDS, QUALITY CONTROL, AND INSPECTION OF PRODUCTS

Person in Charge: R. D. Baker  
Principal Investigator: C. F. Metz

---

#### I. INTRODUCTION

A major factor in the development of a successful reactor fuel is a high degree of technical competence for doing the required chemical analysis and related measurements necessary to characterize thoroughly the raw materials, the manufactured fuel, and the irradiated fuel. This project is identified with the mixed oxide fuel development phase of the LMFBR/FFTF Program.

This project is directed toward (1) developing an analytical chemistry and measurements program, thereby ensuring high quality and uniformity of raw materials, (2) establishing and conducting a statistically designed quality control program of chemical analyses and other measurements that can be used to assure continuing adequate analytical competence of the fuel producers during the fuel fabrication stage, and (3) doing correlated chemical analyses and related measurements on irradiated fuel as a means of studying fuel behavior during core life; specifically involved will be burnup studies correlated with microprobe and metallography studies, gas release studies as related to cladding corrosion, and gas retention studies as related to porosity, particle size, and other properties of the fuel.

#### II. FFTF ANALYTICAL CHEMISTRY PROGRAM

Phase I of the LMFBR/FFTF Fuels Development Quality Control and Assurance Analytical Chemistry Program was completed and a progress report, identified as CMB-1-861, was issued previously.

Phase II is continuing to progress with AI, B&W, GE, LASL, NUMEC, PNL and UNC participating in the

analytical program as outlined in LASL Document CMB-1-870. B&W and NUMEC have not reported the results of their work. As soon as all of the data are received, a statistical analysis will be made and a LASL Report will be issued.

#### III. INVESTIGATION OF METHODS

An important part of the analytical chemistry program is the investigation and improvement of analytical methods, and development of new methods. The following analyses of sintered (U,Pu)O<sub>2</sub> were investigated:

1. Determination of F in Sintered (U,Pu)O<sub>2</sub>  
(T. K. Marshall)

Measurement of trace concentrations of F with a fluoride ion specific electrode following pyrohydrolytic separation from a sintered oxide was shown previously to be reliable by repeated determinations of 1 to 10 µg of F added to 1-g portions of U<sub>3</sub>O<sub>8</sub>, used as a standard for (U,Pu)O<sub>2</sub>. The pyrohydrolysis was carried out in an all-Ni apparatus to obtain optimum recovery of F. Under these conditions the recovery of F was 97% and the precision (1 σ) was 4 relative percent.

In preparing to test the method using (U,Pu)O<sub>2</sub> samples, the equipment was inspected and transferred to a gloved box. Deterioration and splitting of the plastic sheath of the calibrated fluoride ion electrode was observed, and a new electrode having a different-type plastic sheath was obtained. The electrode was calibrated in the gloved box, and samples of (U,Pu)O<sub>2</sub> were prepared for use in testing the method.

2. O/M Atom Ratios in Sintered (U, Pu)O<sub>2</sub>  
(J. W. Dahlby, T. K. Marshall, G. C. Swanson, and G. R. Waterbury)

One of the probable specifications for FFTF fuel is O/M ratio. In one of the proposed thermogravimetric methods<sup>(1)</sup> for determining the O/M ratio of mixed oxide fuel, the sample is heated at 750°C in air to form a slightly super stoichiometric mixed dioxide, and then reduced in He-6% H<sub>2</sub> at 700°C to the stoichiometric dioxide. The O/M ratio is calculated from the initial and final weights of the sample and is based on the assumption that the final dioxide is exactly stoichiometric. To test this assumption, unsintered UO<sub>2</sub>, PuO<sub>2</sub>, and a mixture of UO<sub>2</sub> and PuO<sub>2</sub> in a ratio of 3 to 1 were prepared from very high purity metals (> 99.99% pure) and carried through the recommended procedure with the exception that the temperature of reduction was varied between 700 and 1000°C. Reduction at 700°C produced oxides having O/M ratios between 2.010 and 2.019, but at 1000°C the final oxides were reduced to stoichiometric dioxides.

An investigation was begun to determine optimum operating conditions for analyzing sintered mixed oxide pellets by a modified method in which the reduction temperature was 1000° to 1015°C. Analyses of whole and crushed (< 0.06-in. diam pieces) sintered pellets from the same lot showed that crushing the sample did not affect the results. Increasing the length of the reduction period from 9 to 18 h likewise had no effect. Shorter reductions and various flow rates for the reducing gas are being tried.

In another proposed thermogravimetric method<sup>(2)</sup> the sample is reacted at 800°C with Ar-8% H<sub>2</sub> containing 4 mm partial pressure of H<sub>2</sub>O to form the stoichiometric dioxide. Under these conditions, the final oxides produced from the unsintered UO<sub>2</sub>, PuO<sub>2</sub>, or UO<sub>2</sub>-PuO<sub>2</sub> mixture prepared from the pure metals, were superstoichiometric, having O/M ratios between 2.016 and 2.019. When the reaction temperature was increased to 1000°C, the average O/M ratio for the mixed oxide (3 UO<sub>2</sub> to 1 PuO<sub>2</sub>) was reduced to 2.008. Although this result indicated that this method should give higher results than the method described above when the reaction

temperature was 1000°C in each case, there was no significant difference in the O/M ratios obtained by each method for repeated analyses of two lots of sintered substoichiometric (U<sub>0.25</sub>Pu<sub>0.25</sub>)O<sub>2</sub> pellets. Crushing the sintered mixed oxide pellets into pieces no larger than 0.06 in. diam, and increasing the reaction period at 1000°C from 6 to 12 h, did not change the O/M ratio obtained for the sintered oxides. To determine if this apparent anomaly was a result of incomplete oxidation of the substoichiometric oxide by the Ar-8% H<sub>2</sub> containing 4 mm partial pressure of H<sub>2</sub>O, four samples each of high purity U and Pu metal were heated individually in the gas mixture at 1000°C. The averages of the O/M ratios were 2.008 for the UO<sub>2</sub> and 2.000 for the PuO<sub>2</sub> produced. These results indicate that the gas mixture does oxidize unsintered substoichiometric dioxides. Planned investigations include determining the effects on the method of higher reaction temperatures, shorter reaction periods, and various gas flow rates.

3. Gas Evolution from Sintered (U, Pu)O<sub>2</sub>  
(D. E. Vance and M. E. Smith)

A property of mixed oxides important to their use as fuels is the quantity of gas evolved, including water vapor, at reactor operating temperatures. An apparatus was constructed for measuring the water vapor evolved from a sintered mixed-oxide pellet as it was heated in a fused-silica tube to 800°C. The evolved H<sub>2</sub>O was swept by an Ar gas flow to a moisture monitor, and the monitor signal was integrated electronically to obtain a quantitative measure of the H<sub>2</sub>O. Calibration of the apparatus consisted of injection measured volumes of air having a known moisture content into the furnace tube and correlating each quantity of H<sub>2</sub>O with the integrated signal. The moisture content of the air was measured with a calibrated humidity indicator. The apparatus was used successfully in measuring H<sub>2</sub>O at low ppm concentrations in several sintered mixed oxide pellets.

Frequent calibrations of the apparatus to detect malfunctions or a decrease in sensitivity showed that the sensor cell of the moisture monitor had a useful life of only 3 to 4 wk. A new moisture monitor was installed and a positive pressure was maintained in the sensor cell

to extend the cell life. The success of these changes will be evaluated by continued calibration checks.

Another apparatus was constructed for measuring independently the gases other than  $H_2O$  vapor evolved from a sintered mixed oxide pellet heated inductively in a W crucible to  $1600^\circ C$ . The gases were pumped from the furnace through an anhydrous  $Mg(ClO_4)_2$  trap to remove  $H_2O$  and then collected using a Toeppler pump. The total volume of the gases under standard conditions was calculated from the measured volume, temperature, and pressure. The original apparatus was improved by several modifications including the substitution of water cooling for the liquid  $N_2$  coolant in the diffusion pumps to prevent trapping of some of the easily-condensed gases evolved from the sample. The modified apparatus performed satisfactorily in measuring small quantities (0.02 to 0.06 cc/g) of gases evolved from several sintered mixed oxide pellets. An investigation was started to determine on a mass spectrometer the main components of the evolved gas.

4. Measurement of  $N_2$  in  $(U, Pu)O_2$   
(G. C. Swanson, N. L. Koski, T. K. Marshall, and G. R. Waterbury)

Some type of Kjeldahl method generally is used in analyzing mixed oxides for  $N_2$ , one of the impurity elements in FFTF fuels for which a specification is under consideration. The most tedious part of the analysis is the dissolution of the sintered mixed oxide. This can be done in about 2 h in  $12M$  HCl at 3000 to 4000 lb/sq in. pressure and  $300^\circ C$  by a sealed tube method.<sup>(3)</sup> As facilities for this dissolution method are not available in many laboratories dissolutions at lower temperatures were tried by refluxing the sample in various solvents, including  $H_2SiF_6-CuSeO_4$ ,  $HCl-HNO_3-HF$ ,  $HNO_3-HF$ ,  $H_2SO_4$ ,  $H_2SO_4-H_3PO_4$ ,  $H_3PO_4-HF$ , and  $H_3PO_4$ . The samples were finely ground sintered  $(U, Pu)O_2$  to which trace amounts of NaF, NaCl, C, and UN had been added. The various acid mixtures containing  $HNO_3$  or  $H_2SO_4$  did not dissolve the sample completely. The results for  $N_2$  following dissolution in  $H_2SiF_6-CuSeO_4$  lacked the desired precision. Complete dissolution of 1 g of  $(U, Pu)O_2$  was accomplished in 4 to 6 h by refluxing in 5 ml of concentrated  $H_3PO_4$ , or in 2 h by refluxing in 5 ml of

concentrated  $H_3PO_4$  containing 3 drops of 48% HF.

Two sets of samples were dissolved in  $H_3PO_4-HF$  and one set in  $H_3PO_4$ . Devarda's alloy was added to each solution, NaOH was added to make the solution strongly alkaline, and the  $N_2$  was distilled as  $NH_3$  into a boric acid trap. A colored  $N_2$  complex was formed with Nessler's reagent in the distillate, measured spectrophotometrically at  $410 \mu$ , and the concentration of  $N_2$  determined from a calibration curve. The results (Table 501-I) showed that  $H_3PO_4$  or  $H_3PO_4-HF$  was a satisfactory solvent. The recovery of  $N_2$  was 85 to 90%, and the standard deviation ( $1 \sigma$ ) was no greater than 10 ppm. The HF, while not necessary for complete dissolution of the sample, reduced the digestion time and apparently was not deleterious.

Table 501-I  
Determination of  $N_2$  in  $(U, Pu)O_2$

Number of Determinations	Solvent	N Present, ppm	N Found, ppm
4	$H_3PO_4$	54	$47 \pm 4^a$
6	$H_3PO_4-HF$	49	$45 \pm 10^a$
4	$H_3PO_4-HF$	47	$39 \pm 3^a$

<sup>a</sup>Standard deviation ( $1 \sigma$ )

Dissolution by the sealed tube method is preferred because it is faster, and the results for  $N_2$  in the HCl solutions are more precise. Previous results show that the standard deviation ( $1 \sigma$ ) is 1 to 2 ppm in measuring 35 ppm of added  $N_2$  following dissolution in  $12M$  HCl in a sealed tube.

A LECO Nitrox-6 analyzer also is being investigated for measuring  $N_2$  in  $(U, Pu)O_2$ . One advantage of this instrument is that dissolution of the sample is not required. The solid sample is heated inductively in a C crucible to a temperature between  $1900$  and  $2100^\circ C$  to free the  $N_2$  which is measured in a simple gas chromatographic system. Oxygen in the sample reacts with the C crucible to form CO which also can be measured in the gas chromatographic system. Following successful tests in measuring N added to  $U_3O_8$  samples, the analyzer was moved to a gloved box assemblage for tests with  $(U, Pu)O_2$  samples. Initial results showed that the lower limit of

reliable measurement of  $N_2$  in oxide samples was 120 ppm because of interference from the large quantity of CO generated from the  $O_2$  in the sample. To remove the CO, a heated tube containing CuO to oxidize the CO and an Ascarite trap for  $CO_2$  was connected into the analyzer system immediately before the gas chromatographic column. Optimum operating conditions for the modified analyzer in the gloved box are being determined before calibration is started.

5. Determination of Burn-up  
(R. G. Hurley, E. A. Hakkila, and  
J. W. Dahlby)

Measuring the concentrations of fission product Nd by x-ray fluorescence offers promise as a method of determining burn-up. A proposed method was tested previously by analyzing solutions prepared from normal U, Ru, Rh, Mo, Zr, Nb, and Nd at relative concentrations found in a U fuel having undergone 10% burn-up. The Nd, with Y carrier and Tb internal standard, was separated by fluoride precipitation and purified further by adsorption from HCl-butanol onto cation exchange resin filter paper. The intensities of the  $L\beta_1$  x-ray for Nd and the  $L\alpha_1$  x-ray for Tb on the paper were compared to x-ray intensities measured from discs having known concentration of each rare earth. The relative standard deviation ( $1\sigma$ ) was 0.7% in measuring 20 to 50  $\mu g$  of Nd in 200 mg of U and increased to 5% and 16%, respectively, in measuring 5 and 1  $\mu g$  of Nd. Expected quantities of other rare earth elements and stainless steel did not interfere.

An equation was derived for calculating percent burn-up from the total Nd found. It was assumed that fission of  $^{238}U$  was negligible compared to fission of  $^{235}U$ , and a correction was included for the amount of Nd formed by decay of  $^{144}Ce$ . A sample of irradiated U fission was dissolved and the Nd separated by fluoride precipitation as described above. The radioactivity of the rare earth fluorides was at a low level that permitted removal of the precipitate from the hot cell for the cation exchange resin purification and x-ray fluorescence measurements. Data from this initial determination are being processed.

#### 6. Papers Presented

"The Determination of Oxygen to Metal Atom Ratios in Sintered Oxides," by J. W. Dahlby, G. R. Waterbury, and C. F. Metz, 13th Conference on Analytical Chemistry in Nuclear Technology, September 30 to October 2, 1969, Gatlinburg, Tennessee.

#### IV. REFERENCES

1. W. L. Lyon, GEAP-4271, 1963.
2. T. D. Chikalla, "Quarterly Progress Report, October-December 1966," F. W. Albaugh et al, pp 4.1, BNWL-CC-957, 1967.
3. C. F. Metz and G. R. Waterbury, LA Report 3559, Los Alamos Scientific Laboratory, 1966.

SPECIAL DISTRIBUTION

Atomic Energy Commission, Washington

Division of Research

D. K. Stevens

Division of Naval Reactors

R. H. Steele

Division of Reactor Development and Technology

L. J. Colby  
G. W. Cunningham  
D. E. Erb  
Nicholas Grossman  
W. H. Hannum (2)  
K. E. Horton  
J. R. Humphreys  
R. E. Pahler  
J. M. Simmons (2)  
E. E. Sinclair  
Bernard Singer  
C. E. Weber  
G. W. Wensch  
M. J. Whitman

Division of Space Nuclear Systems

G. K. Dicker  
F. C. Schwenk

Safeguards & Materials Management

J. M. Williams

Idaho Operations Office

DeWitt Moss

Ames Laboratory, ISU

O. N. Carlson  
W. L. Larsen  
M. Smutz

Argonne National Laboratory

F. G. Foote  
Sherman Greenberg  
J. H. Kittel  
W. B. Loewenstein  
R. E. Macherey  
M. V. Nevitt

Idaho Falls, Idaho

D. W. Cissel  
R. C. Robertson

Atomics International

R. W. Dickinson, Director (2)  
Liquid Metals Information Center

J. L. Ballif

Babcock & Wilcox Co.

C. Baroch  
J. H. MacMillan

Battelle Memorial Institute

D. L. Keller  
S. J. Paprocki

Brookhaven National Laboratory

D. H. Gurinsky  
C. Klamut

Combustion Engineering, Inc.

S. Christopher

Donald W. Douglas Laboratories

R. W. Andelin

General Electric Co., Cincinnati, Ohio

V. P. Calkins

General Electric Co., Sunnyvale, California

R. E. Skavdahl

Gulf General Atomic, Inc.

E. C. Creutz

Idaho Nuclear Corporation

W. C. Francis

IIT Research Institute

R. Van Tyne

Lawrence Radiation Laboratory

Leo Brewer  
J. S. Kane  
A. J. Rothman

LMFBR Program Office

Alfred Amorosi  
D. K. Butler (Physics)  
L. R. Kelman (Fuels & Materials)  
J. M. McKee (Sodium Technology)

Mound Laboratory

R. G. Grove

NASA, Lewis Research Center

J. J. Lombardo

Naval Research Laboratory

L. E. Steele

Oak Ridge National Laboratory

G. M. Adamson  
J. E. Cunningham  
J. H. Frye, Jr.  
C. J. McHargue  
P. Patriarca  
O. Sisman  
M. S. Wechsler  
J. R. Weir

Pacific Northwest Laboratory

F. W. Albaugh  
E. A. Evans  
V. J. Rutkauskas  
W. R. Wykoff

FFTF Project

E. R. Astley  
B. M. Johnson  
D. W. Shannon (2)

U. S. Department of Interior

Bureau of Mines, Albany, Oregon

H. Kato

United Nuclear Corporation

A. Strasser

Westinghouse, Advanced Research Division

E. C. Bishop